A COMPARISON OF COMPUTATIONAL
ELECTROMAGNETIC METHODS FOR THE
PREDICTION OF RADAR CROSS SECTION

THESIS

Ulice J. Macias
Second Lieutenant, USAF

AFIT/GE/ENG/86D-13

DEPARTMENT OF THE AIR FORCE
AIR UNIVERSITY
AIR FORCE INSTITUTE OF TECHNOLOGY

87 3 12 087

AFIT/GE/ENG/86

A COMPARISON OF COMPUTATIONAL
ELECTROMAGNETIC METHODS FOR THE
PREDICTION OF RADAR CROSS SECTION

THESIS

Ulice J. Macias
Second Lieutenant, USAF

AFIT/GE/ENG/86D-13

MAR 1 6 1987

AFIT/GE/ENG/86D-13

A COMPARISON OF COMPUTATIONAL ELECTROMAGNETIC MEHTODS

FOR THE PREDICTION OF RADAR CROSS SECTION

THESIS

Presented to the Faculty of the School of Engineering

of the Air Force Institute of Technology

Air University

In Partial Fulfillment of the

Requirements for the Degree of

Master of Science in Electrical Engineering

Ulice J. Macias, B.S.

Second Lieutenant, USAF

December 1986

Accession For

NTIS GRA&I	☒
DTIC TAB	☐
Unannounced	☐
Justification	

By_____
Distribution/
Availability Codes
Avail and/or
Dist Special

A-1

Approved for public release; distribution unlimited

Acknowledgements

I would like to thank the personnel at AFWAL/AAWP-3, particularly my sponsor, Lt Paul Skinner, who helped me learn to use their RCS measurement facilities and provided all the computer support necessary to perform the investigations. Without their help there would be no thesis. I would especially like to thank David Liang who created the plotting routine used to plot the RCS results.

Also, I want to thank my thesis advisor, Dr. A. J. Terzuoli for all his support to the project. I am also indebted to my committee members, Capt Randy Jost and Dr. Alan Lair.

I would also like to thank my parents for their continued support and inspiration.

Finally, I would like to thank my best friend and fiancee, Marcia, for editing the thesis, writing the equations, and for being there when I needed inspiration.

Contents

List of Figures

List of Tables

Abstract

The effectiveness of the various Radar Cross Section
(RCS) prediction techniques was investigated. The RCS of
square flat plates was analyzed using the Physical Optics
approximation, the Physical Theory of Diffraction, the
Geometrical Theory of Diffraction, the Uniform Theory of
Diffraction, and the Moment Method or Method of Moments. The
RCS predicted by the computational methods was compared to
measurements performed in an anechoic RCS measurement
chamber. Also, the five computational methods were compared
in terms of plate size (in wavelengths), computer (CPU) time
for each computation, and angular regions of computational
integrity.

It was found that although the Moment Method is the most
accurate RCS prediction method, it takes too much CPU time
for large plates (over 2.5 wavelengths). The Uniform Theory
of Diffraction, on the other hand, is accurate for large
plates and takes less CPU time than the Moment Method. The
Geometric Theory of Diffraction is also accurate but fails
near the edge of the plate. Finally, the Physical Theory of
Diffraction and the Physical Optics approximation are
relatively inaccurate.

A COMPARISON OF COMPUTATIONAL ELECTROMAGNETIC METHODS FOR THE PREDICTION OF RADAR CROSS SECTION

I.   Introduction

Background

Since World War II, the prediction of radar cross section (RCS) for different targets has been a priority (Knott, 1985:252), although, the history of RCS goes back even further than WW II. The development of RCS has its roots in the investigations on the nature of light. Thus, the development of RCS goes back to the works of Pythagoras, Aristotle, Ptolemy, and others (Kouycumjian, 1985:1). These men investigated the nature of light and its propagation.

Geometrical Optics was developed in the early seventeenth century (Young, 1976:84) and modeled the propagation of light in terms of rays. According to the theory of Geometrical Optics, light travels in straight lines in a homogeneous medium (Young, 1976:84). In 1801, Thomas Young was the first person to try to explain the nature of diffraction by the use of rays (Kouyoumjian, 1985:2). He demonstrated that light consists of waves whose wavelengths are small (Young, 1976:84). In 1862, Maxwell predicted the existence of electromagnetic waves and stated that light is an electromagnetic wave (Kouyoumjian, 1985:7; Young, 1976:84-85).

In 1880, Kirchhoff postulated what is now known as the Physical Optics approximation. The Physical Optics

approximation predicts the scattering of electromagnetic
waves from a perfect conductor (more on that later). In
1887, Hertz conducted experiments concerning on the
reflection of radio waves from metallic and dielectric
objects (Blacksmith, 1985:902; Skolnik, 1980:8). Hertz
demonstrated that radio waves and light waves operate on a
similar principle (Skolnik, 1980:8). Also, Hertz verified
Maxwell's equations experimentally (Kouyoumjian, 1985:7).

In 1894, Sommerfeld calculated the diffraction of a
conducting infinite half-plane (Kouyoumjian, 1965:867) (see
Fig 1.1).
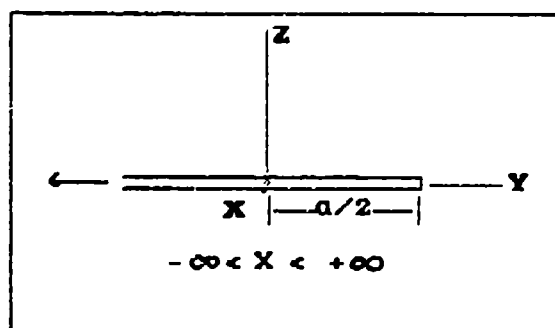
Fig 1.1.   Infinite Half-Plane
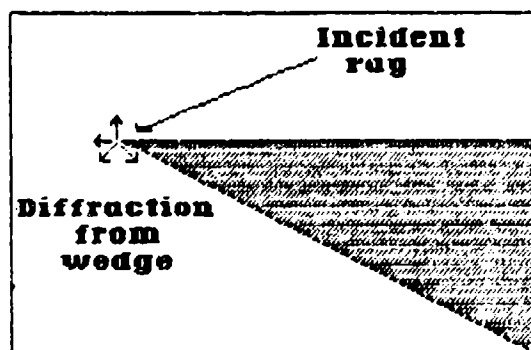
Fig 1.2.   Perfectly Conducting Wedge

In 1912, McDonald produced an asymptotic solution for the

diffraction from a perfectly conducting infinite wedge
(Kouyoumjian, 1965:867) (see Fig 1.2). In 1953, Keller
developed the Geometrical Theory of Diffraction (Kouyoumjian,
1985:12). He introduced the concept of diffracted rays which
are added to the rays obtained from the Geometrical Optics
model to obtain the total scattering from an object
(Kouyoumjian, 1985:12). Also in the fifties, Braunbek (in
the U.S.) and Ufimstev (in the U.S.S.R.) developed the
Physical Theory of Diffraction (Kouyoumjian, 1985:12). This
method was similar to the Geometrical Theory of Diffraction,
but, it sought to improve the Physical Optics result instead
of the Geometrical Optics result (Kouyoumjian, 1985:12). As
will be discussed later, the Geometrical Theory of
Diffraction failed at the shadow and reflection boundary,
where it predicted an infinite result (Kouyoumjian, 1985:7).
To overcome this problem and others which the Geometrical
Theory of Diffraction presented, the Uniform Theory of
Diffraction (due to Kouyoumjian and Pathak) and the Uniform
Asymptotic Theory (due to Lee and Deschamps) were developed
(Knott and others, 1985:134). In the late sixties, the
Moment Method, which is a numerical solution to an exact
equation, was implemented thanks to the availability of
high-speed computers (Stutzman, 1981:307). Other
computational methods have been developed after these such as
the Equivalent Current Method, and others (Knott and others,
1985:136).

Each computational method differs in its approach to a

1-3

particular problem. Also, each method has some advantages
and disadvantages when compared to the others (Skinner,
1985:2-3). The purpose of this investigation is to explore
to what extent each method is reasonable to use in terms of
RCS pattern prediction and CPU time. Each method will be
compared in terms of frequency of operation, angle of
incidence of the target to the radar, polarization of the
incident wave, and computer (CPU) time.

Problem

The problem is to decide how effective and time consuming
are the computational methods used when analyzing the total
scattering behavior from square flat plates.

Basic Theory

RCS describes the "electromagnetic size" of an object
detected by a radar system. The radar emits electromagnetic
(EM) waves.
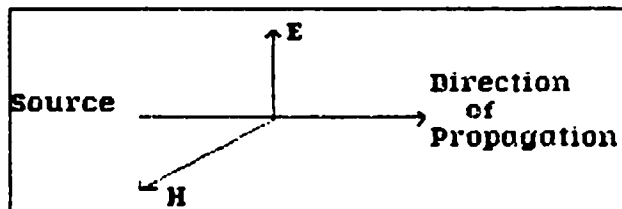
Fig 1.3. Electromagnetic Wave

These waves are composed of an electric ($\bar{E}$) field and a
magnetic ($\bar{H}$) field. These fields are perpendicular to each

1-4

other and to the direction of propagation (see Fig 1.3). The direction of the E-field determines the polarization of the electromagnetic wave (Knott and others, 1985:70-71). (See Fig 1.4).
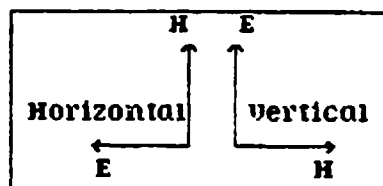
Fig 1.4.   E-field Polarizations

The RCS is a function of the target's shape, the frequency or wavelength of operation, the polarization of the transmitter and receiver, the angle of incidence of the incident wave with respect to the target, and the materials composing the target (Knott and others, 1985:48).

When making RCS measurements, it is very useful to classify the target's dimensions in terms of the operating wavelength of the radar (Johnson, 1982:2). The wavelength is obtained by dividing the speed of light (3.0×10^8 m/s) by the radar's frequency of operation.

Scope

In this thesis, the computational methods will be compared in terms of their accuracy using different angles between the incident EM wave and the target, the size of the target compared to the wavelength of operation, and the CPU time they require.

The investigation covers five computational methods. The

methods applied are the Physical Optics approximation, the Geometrical Theory of Diffraction, the Uniform Theory of Diffraction, the Physical Theory of Diffraction, and the Method of Moments.

Square flat plates were used as the targets in this investigation. The size of the plates varies from half a wavelength (on one side) to six and a half wavelengths in 0.5 wavelength increments. Also, 0.75 wavelength plate was used. The plates were measured in the Avionics Laboratory Far-Field RCS Measurement Facility. The measurements were compared against the results obtained by the computational methods. These comparisons provide a good standard on how accurate each method is as the electrical length of the plates change. Also, it is possible to predict where each method fails to produce good results as the aspect angle changes. Finally, each method was compared in terms of CPU time. These guidelines will be useful in the case where the RCS of a more complex target is desired .

Summary of Current Knowledge

The Physical Optics Approach (PO) is often a preferred method because it is easy to use for any geometry (Skinner, 1985:6). This method assumes that electrical currents are induced by the EM waves on the area that is "seen" by the radar (illuminated region). It also assumes that no currents exist in the shadow region (the region that EM waves do not illuminate directly). (See Fig 1.5).
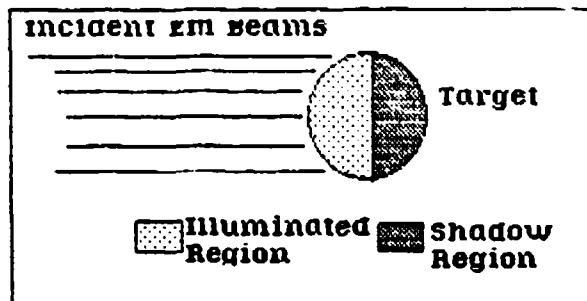
Fig 1.5. EM wave illumination

Some of PO's advantages are: it is easy to use, the user does not need an extensive background in electromagnetics, and the PO computer codes require a small amount of CPU time (Skinner, 1985:6). Unfortunately, PO also has some disadvantages. Some of these disadvantages are: the target can only be a good electrical conductor, the target's area must be much greater than the wavelength, and higher order scattering effects are neglected (Knott and others, 1985:59). Higher order scattering effects are effects that are due to the particular shape or surface characteristics of the target. Some examples are effects that occur at sharp spots such as edges, tips, corners, and curved surfaces. The EM waves from the radar hit these sharp discontinuities and are re-radiated in all directions. Thus, the radar sees a different RCS than the PO method would predict on some targets (Stutzman, 1981:458).

The Geometrical Theory of Diffraction (GTD) is a ray tracing method developed by Keller (Keller, 1962). Ray

tracing methods assume that electromagnetic waves propagate in "line-of-sight" directions. Ray tracing methods are more dependent on exact geometrical description than PO and provide a better insight of what is happening as the EM waves bounce off the target (Skinner, 1985:2). GTD provides fast computations. Its results are good for almost all large targets. It takes into account higher order effects such as tip, corner, and edge scattering. Also, GTD takes into account the RCS contribution of the shadow region. Unfortunately, GTD predicts an infinite result on the shadow and the reflection boundaries (Knott and others, 1985:133).

The Uniform Theory of Diffraction (UTD) is an extension of GTD. The first version of UTD was developed by Kouyoumjian and Pathak of Ohio State University (Knott and others, 1985:134). UTD solves the problems that GTD has at shadow boundaries. It prevents the RCS from approaching infinity at the shadow boundary. Except for this, UTD is practically identical to GTD. The CPU time it requires is almost the same as that required by GTD. However, the UTD calculations are more complex (Skinner, 1985:10).

The Physical Theory of Diffraction (PTD) was developed by Ufimstev of the U.S.S.R. and Braunbek of the U.S. almost at the same time (Skinner, 1985:12). PTD is an extension of PO which adds "a correction factor without any physical significance" (Skinner, 1985:12). This correction factor increases the accuracy of PO. Otherwise, the advantages and disadvantages of PTD are the same as those for PO (Skinner,

1985:12).

The Moment Method (MM) is also known as the Method of Moments. It is a technique that is very accurate in producing results for targets whose dimensions in wavelengths are very small (Stutzman, 1981:370). MM presents the solution to an integral equation which models a particular target "exactly" (Stutzman, 1981:306-307). The limits of the integral equation depend on the particular target used. MM has some advantages which make it very useful in some applications. Among these advantages are: it can produce an almost exact solution, it can be used to find all the electromagnetic properties of the target, and it can accurately predict all the scattering properties of the target (Skinner, 1985:16). One of its disadvantages is that it takes too much CPU time to calculate the RCS if the target's size is greater than 2 to 3 wavelengths (Skinner, 1985:16). Another disadvantage is it does not give much insight on the scattering mechanisms of the target (Skinner, 1985:17).

Approach

1. Computations were performed to predict the RCS of different sizes of square flat plates using PO, GTD, UTD, PTD, and MM. The size of the plates ranged from .5 wavelengths to 6.5 wavelengths in .5 wavelength increments. First, the computations were performed using a vertically polarized incident wave vs the angle of incidence of the

1-9

transmitter. Then, a horizontally polarized wave was used.

2. Measurements were performed on the square flat plates given by the Avionics Laboratory. Again, the sizes of the plates ranged from .5 wavelengths per side to 6.5 wavelengths in .5 wavelength increments.

3. Comparisons were made between the results of the computations and measurements for each square flat plate.

4. General conclusions were obtained from the comparisons mentioned above. These conclusions will be helpful in deciding which of these RCS computational methods is more useful for a target consisting of perfectly conducting flat elements.

Materials and Equipment

A VAX 11/780 mainframe computer is available for the implementation of the computational methods. The targets were provided by the sponsor. The Avionics Laboratory Measurement Facility was used for the measurements of the targets.

The RCSBSC computer code developed at Ohio State University by Marhefka (Marhefka, 1981) was used to calculate the RCS of different targets using PO, PTD, and UTD. The ESP computer code (Newman, 1985) was used to calculate the RCS of the targets using MM. Both computer codes were available in the VAX computer.

The GTD calculations were obtained from a program that was developed for this thesis from formulations developed by

Ross (Ross, 1966).

In Chapter II, the theory used for the computational methods is discussed in more detail. In Chapter III, the measurement procedure is explained. In Chapter IV, the measurements are compared to the RCS computational methods. Finally, Chapter V offers conclusions and recommendations.

II. Theory

General Theory

Sets of small polygonal flat plates can be used to model almost any target. This is one reason why flat plates were used in this investigation as targets. Also, flat plates are cheap and easy to construct. In this chapter, square flat plates will be discussed in general. Also, each computational method will be used to see how it calculates the RCS from the flat plates.

Note, $\underline{A}$ is a general complex scalar, $\bar{B}$ is a general real vector, and $\bar{\underline{C}}$ is a general complex vector.

RCS is defined by

$$\sigma = 4\pi \lim_{R \to \infty} R^2 \frac{|\bar{E}^s|^2}{|\bar{E}^i|^2} \qquad (2.1)$$

where $\underline{\bar{E}}^s$ and $\underline{\bar{E}}^i$ are the scattered and incident electric fields respectively (Knott and others, 1985:48) and R is the distance between the target and the radar. Since R approaches infinity and $\bar{E}^s$ decays as 1/R, the RCS does not depend on the distance of the target from the radar, as long as the distance is large (Knott, 1985:252). Typically, the RCS measurements are made using this approximation (far-field approximation), although it is possible to measure the RCS when the target is in the near field. From Eq (2.1), it can be shown that RCS has dimensions of area. Usually these

2-1

dimensions are given in square meters. Furthermore, the units of RCS are converted to decibels relative to a square meter (dBsm) to provide a standard for comparison purposes.

The targets used in the investigation are square flat plates. Flat plates exhibit three different scattering behaviors (Knott and others, 1985:6-7). The first one is specular or broadside scattering. In this case, the plate's broadside is parallel to the radar antenna's aperture. This RCS is "proportional to the square of the area of the plate and the square of the frequency" (Knott and others, 1985:6).

The second type of scattering possible for a flat plate is when the plate is oriented out of the specular angle, and having two edges perpendicular to the "line-of-sight" with the receiver. Now the RCS is proportional to the square of the length of the edge (Knott and others, 1985:6). This RCS is independent of frequency, which is similar to the case of a large sphere or a spheroid (Knott and others, 1985:6-7).

The third type of scattering occurs when the flat plate is oriented such that the receiver only "sees" the RCS from the four corners (Knott and others, 1985:7). This occurs at all other angular positions. These returns are inversely proportional to square of the frequency of operation (Knott and others, 1985:7).

Each computational method used in the investigation is good for approximating the specular scattering from the plates, as long as the plates are large. Only the Moment Method is good for calculating the specular behavior of

plates which are small when compared to wavelength. This is
because the other computational methods are good only when
the target's size is greater than the operating wavelength.
The purpose of the investigation is to see how effective and
time consuming each of the computational methods is when
analyzing the total scattering behavior from square flat
plates.

The coordinate system which was used to define the target
is as shown on Fig 2.1.
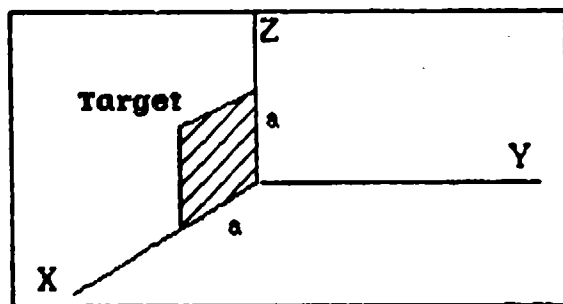
Fig 2.1. Coordinate system used

In the following sections each of the computational
methods used in the investigation will be discussed in
reference to the square flat plate.

Physical Optics (PO)

The basic premise assumed by PO is that the incident
field on the target will produce a current given by

$$\overline{J}_{po} = \begin{cases} \hat{n} \times \overline{H}_{total} = 2\hat{n} \times \overline{H}_i & \text{in illuminated region} \\ O & \text{in shadow region} \end{cases} \qquad (2.2)$$

2-3

where $\hat{n}$ is the unit vector perpendicular to the target's surface (see Fig 2.2).
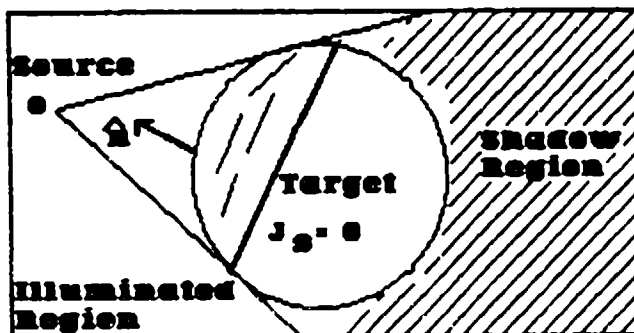
Fig 2.2.   PO current on a target

Assuming a monostatic case (the radar transmitter and receiver are co-located), the RCS will always be measured in the illuminated region. The vector potential is used to obtain an expression for the field scattered by the target (Stutzman, 1981:455).   The vector potential is given by

$$\overline{A} = \iint_{s} \frac{\overline{J}_{po}\, exp(-jkR)}{4\pi R}\, ds \qquad (2.3)$$

where R is the distance between the incremental surface patch and the radar, and k is the wave number. Assuming that the target is far away (far-field), the scattered field is given by

$$\overline{E}^S = -j w \mu \overline{A}$$

$$(2.4)$$

where μ is the permeability constant (in free space $\mu = 4\pi \times 10^{-7}$).

Using the definition of RCS (Eq (2.1)) and evaluating A for a rectangular flat plate the following expression is obtained:

$$\sigma_{Po} = \frac{64 a^2 b^2 \pi}{\lambda^2} \cos^2 \theta \left[\frac{\sin(2ka \sin\theta)}{(2ka \sin\theta)} \right]^2$$

$$(2.5)$$

where λ is the wavelength, $k = 2\pi/\lambda$, is the aspect angle, and b=a for a square flat plate (Ross, 1966:330). This equation is independent of polarization, because the result is the same in either polarization (Ross, 1966:330).

Geometrical Theory of Diffraction (GTD)

The GTD approach has its roots in the Geometrical Optics (GO) theory. GO assumes that EM waves travel along ray paths (Ruck, 1970:39-40). Unfortunately, GO fails to account for diffraction. Diffraction occurs when the incident wave hits tips, corners, edges, tangent points, or any discontinuity (Ruck, 1970:44). The following example will illustrate the

concept of diffraction.
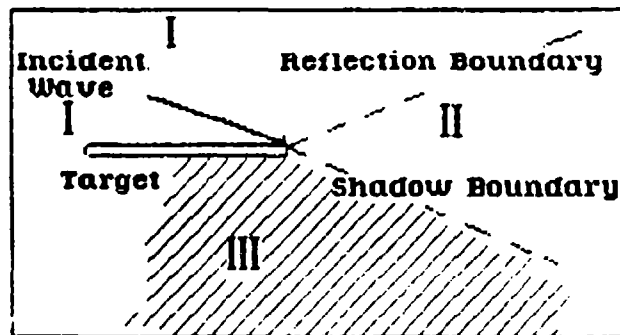
Fig 2.3.   Diffraction Example.

Consider the case of a semi-infinite plane which is perfectly conducting. A radar transmitter emits EM waves which hit the plane. The transmitter is far away from the half plane so that the EM waves reaching the plane can be considered plane waves. Region I is where all reflected rays exist. Region II is composed of all rays which don't reach the plane. The last region is denoted as the shadow region.

GO would only predict a return if the receiver was located in Regions I or II. In all regions, GTD predicts a more realistic return than GO (Stutzman, 1981:458). Thus, GTD is more accurate in computing the RCS of a target than PO, which predicts no return in the shadow region.

To calculate the RCS of a target caused by a point of diffraction, the diffracted field ($\bar{E}_d$) must be calculated in the desired direction leaving the diffraction point. The diffracted field is proportional to the value of the incident field ($\bar{E}_i$) multiplied by a diffraction coefficient at the point of diffraction (Stutzman, 1981:459). The diffraction

2-6

coefficients are a local phenomena which depend on the local
point of diffraction (Keller, 1962:117). Diffraction
coefficients have been obtained for canonical problems such
as wedges, half planes, and infinite strips.
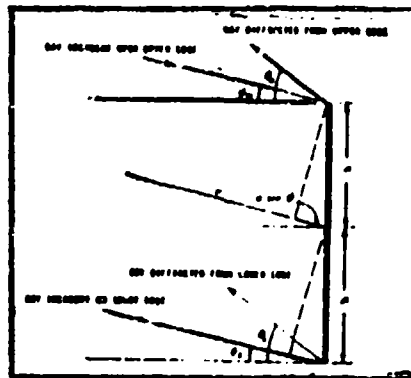
Fig 2.4.   Edge diffraction from an infinite strip of width 2a
(Ross, 1966:331)

Ross used infinite strips to derive the GTD Monostatic
RCS from a rectangular plate (Ross, 1966:331). He obtained
the backscatter fields from an infinite strip in the X-Y
plane of width 2a (in X) and infinite height (in Y). The
following formulas are the expressions Ross computed for the
backscatter field of the infinite strip. The expressions
derived by Ross are given in the next pages.

For vertical polarization:

$$M_{Total\ V} = \frac{A\ exp\left(j[kr + \pi/4]\right)}{2\ (2\pi kr)^{1/2}}$$

$$\times \left\{\left[1 + \frac{1}{\sin\theta}\right] exp(-j2ka\ \sin\theta)\right.$$

$$\left. + \left[1 - \frac{1}{\sin\theta}\right] exp(j2ka\ \sin\theta)\right\}$$

$$+ \left\{\frac{A\ exp\left(jk[r+2a]\right)}{2\pi\ (kr)^{1/2}\ (2ka)^{3/2}\ \cos\theta}\right. \tag{2.6}$$

$$+ \frac{A\ exp\left(j[k(r+4a) - \pi/4]\right)}{8\pi\ (2\pi kr)^{1/2}\ (2ka)^3}$$

$$\times \left[\frac{(1+\sin\theta)}{(1-\sin\theta)^2}\ exp(-j2ka\ \sin\theta)\right.$$

$$\left. + \frac{(1-\sin\theta)}{(1+\sin\theta)^2}\ exp(j2ka\ \sin\theta)\right]\right\}$$

$$\times \left\{\frac{1}{1 - \dfrac{exp\left(j[4ka - \pi/2]\right)}{8\pi\ (2ka)^3}}\right\}$$

and, for horizontal polarization the expression is

$$M_{\text{Total H}} = \frac{-A\,\exp\left(j\left[kr+\frac{\pi}{4}\right]\right)}{2(2\pi kr)^{1/2}}\left\{\left[1-\frac{1}{\sin\theta}\right]\right.$$

$$\times\,\exp\left(-j\left[ka\,\sin\theta\right]\right)+\left[1+\frac{1}{\sin\theta}\right]$$

$$\times\,\exp\left(j\left[2ka\,\sin\theta\right]\right)\Bigg\}$$

$$-\left\{\frac{2A\,\exp\left(j\left[kr+\pi/4\right]\right)}{\pi\,(kr\,2ka)^{1/2}\,\cos\theta}\right.$$

$$-\frac{2A\,\exp\left(j\left[k(r+4a)+3\pi/4\right]\right)}{2\pi(2\pi kr)^{1/2}\,(2ka)}\tag{2.7}$$

$$\left[\frac{\exp(-j2ka\,\sin\theta)}{1-\sin\theta}\right.$$

$$\left.\left.+\frac{\exp(j2ka\,\sin\theta)}{1+\sin\theta}\right]\right\}$$

$$\times\left\{\frac{1}{1-\dfrac{\exp\left(j\left[4a+\frac{\pi}{2}\right]\right)}{2\pi(2ka)}}\right\}$$

where θ is the azimuth angle measured from broadside to edge
(Ross, 1966:331). The RCS per unit length of the strip is

obtained by

$$\sigma = \lim_{r \to \infty} 2\pi r \frac{|\mu|^2}{|A|^2} \tag{2.8}$$

where μ is the backscatter field from the strip. To obtain
the RCS from a rectangular flat plate, the following
relationship is used:

$$\sigma(area) = \frac{8b^2}{\lambda^2} \sigma(length) \tag{2.9}$$

where 2b is the length of the plate (in Y) (Ross, 1966:331).
Simplification of (2.6) and (2.7) produces the following
formulas:

$$
\sigma_{V,GTD} = \frac{4b^2}{\pi} \left| \left[\cos(2Ka\ \sin\theta) - j\frac{\sin(2Ka\ \sin\theta)}{\sin\theta} \right] \right.
$$

$$
- \frac{\exp\left(j\left[2Ka - \frac{\pi}{4}\right]\right)}{(2\pi)^{1/2}(2Ka)^{3/2}} \left[\frac{1}{\cos\theta} + \frac{\exp\left(j\left[2Ka - \frac{\pi}{4}\right]\right)}{4(2\pi)^{1/2}(2Ka)^{3/2}} \right.
$$

$$
\times \left(\frac{[1+\sin\theta]\exp(-j2Ka\ \sin\theta)}{(1-\sin\theta)^2} \right.
$$

$$
\left. \left. \frac{(1-\sin\theta)\exp[j2Ka\ \sin\theta]}{(1+\sin\theta)^2} \right) \right] \tag{2.10}
$$

$$
\times \left. \left| 1 - \left[\frac{\exp\left(j\left[4Ka - \frac{\pi}{2}\right]\right)}{8\pi(2Ka)^3} \right]^{-1} \right| \right|^2
$$

$$\sigma_{H,GTD} = \frac{4b^2}{\pi} \left| \left[\cos(2Ka\ \sin\theta) + j\ \frac{\sin(2Ka\ \sin\theta)}{\sin\theta} \right] \right.$$

$$- \frac{4\exp\left(j\left[2Ka + \frac{\pi}{4}\right]\right)}{(2\pi)^{1/2}(2Ka)^{1/2}} \left[\frac{1}{\cos\theta} - \frac{\exp\left(j\left[2Ka + \frac{\pi}{4}\right]\right)}{2(2\pi)^{1/2}(2Ka)^{1/2}} \right.$$

(2.11)

$$\times \left(\frac{\exp(-j2Ka\ \sin\theta)}{1 - \sin\theta} + \frac{\exp[j2Ka\ \sin\theta]}{1 + \sin\theta} \right)$$

$$\left. \times \left[1 - \frac{\exp\left(j\left[2Ka + \frac{\pi}{2}\right]\right)}{2\pi(2Ka)} \right]^{-1} \right|^2$$

which gives us the GTD RCS of a rectangular flat plate of an area of 2a by 2b (Ross, 1966:332). To obtain the RCS of a square flat plate assume that a=b. Note that if θ is equal to 90° (grazing incidence) the expression for the RCS becomes infinite. The expression is still very good when near grazing incidence is avoided. Note that the singularity occurs in the second and third order terms, i.e., the first and second term in the second bracket, respectively.

Physical Theory of Diffraction (PTD)

PTD was developed in its original form by Ufimstev (Knott and others, 1985:140). He worked on a way of improving the

Physical Optics approximation as opposed to Keller who worked on improving the Geometrical Optics approximation.

The PTD solution was applied in the investigation thru the use of the frill equivalent current solution (Marhefka, 1981:Ch 2, 11). The diffraction coefficients used in this method are obtained by subtracting Keller's diffraction coefficient and the physical optics diffraction coefficient in the following (Marhefka, 1981:Ch 2, 3,11):

$$G_f^{e,m} = G^{e,m} - G_{PO}^{e,m} \qquad (2.12)$$

where

$$G_{PO}^{e,m} = -\left[\mathrm{Tan}\left(\theta-\theta'\right)/2 \pm \mathrm{Tan}\left(\theta+\theta'\right)/2 \right] \qquad (2.13)$$

and

$$G^{e,m} = \frac{1}{2}\left[\left(-\sec\left[\theta-\theta'\right]\right)/2 \pm \sec\left(\theta+\theta'\right)/2 \right] \qquad (2.14)$$

The PO diffraction coefficient is defined only for a wedge angle of zero. This method is used in the same fashion as GTD (see Geometrical Theory of Diffraction). However, the PO results must be calculated explicitly and added to this solution (Marhefka, 1981:Ch 2, 11).

Uniform Theory of Diffraction (UTD)

UTD was first developed by Kouyoumjian and Pathak to

solve some problems presented by the GTD diffraction
coefficient on the shadow and illumination boundaries. UTD
provides a continuous solution on the transition boundaries
(Kouyoumjian, 1974:1) unlike GTD, which predicts an infinite
RCS on those boundaries. The form of UTD used in the
investigation is based on the Equivalent Current Method.
This method is an extension to the original form of UTD.

The Equivalent Current method was first used by Millar
(Knott and others, 1985:136). Eventually, it was introduced
into a GTD solution by Ryan and Rudduck (Peters, 1985:2). The
Equivalent Current method is essential when a finite edge or
corner is part of the target (Peters, 1985:1) as in the case
of a flat plate. These currents can be found by finding a
line source that produces the same fields at the observation
point as is diffracted to that point by an infinite straight
edge (Peters, 1985:3) (see Fig 2.5).
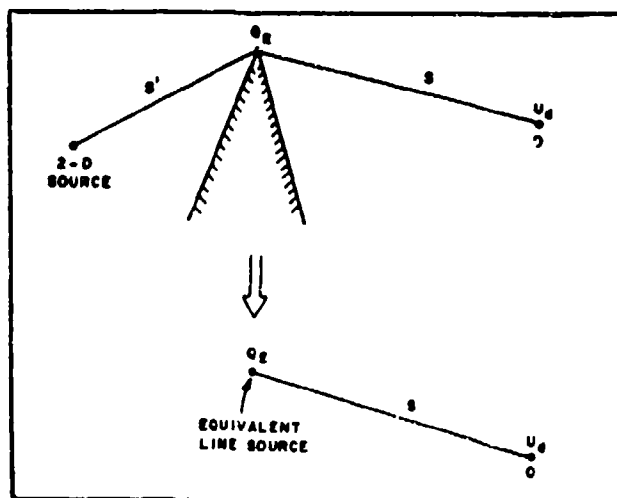
Fig 2.5.   Illustration of Equivalent Current Concept
(Peters, 1985:17)

For the geometry in Fig 2.5, assume that the incident electric field is given by

$$\bar{E}^i = \bar{E}_o^i \exp(jk\hat{r}^i \cdot \bar{r})$$ (2.15)

where

$$\bar{E}_o^i = \frac{[(\hat{r} + \hat{r}^i)] \times \hat{n}]}{\left| (\hat{r} + \hat{r}^i) \times \hat{n} \right|} \left\{ \frac{[(\hat{r} + \hat{r}^i) \times \hat{n}]}{\left| (\hat{r} + \hat{r}^i) \times \hat{n} \right|} \cdot \hat{e}^i E_o^i \right\}$$ (2.16)

and $\hat{n}$ is the unit vector normal to the surface. From this, the following expression for the equivalent electric current is obtained:

$$\bar{I}_e = \frac{2jG^e}{z_0 K \sin\beta_o \sin\beta_o} \left(\hat{e} \cdot \bar{E}_o^i \right) \exp(jk\hat{r}^i \cdot \bar{r}')$$ (2.17)

where G^e is the soft form (the incident ray polarization is parallel to the edge) of Keller's Diffraction coefficient (see Eq (2.13)). In the monostatic case, β_0 is equal to β_d (Marhefka, 1981:Ch 2, 3). $\bar{I}_e$ is an equivalent current because it is a function of the observation direction (Marhefka, 1981:Ch 2, 3). The edge diffracted field will then be given by

$$\bar{E}_\beta = \frac{-G^e}{\sin\beta_0}\left(\hat{e}\cdot\bar{E}_o^i\right)\frac{\exp(-jks)}{2\pi s}\int_{-\ell/2}^{\ell/2}\exp\left(jk\left[\hat{r}+\hat{r}^i\right]\cdot\hat{e}z'\right)dz' \tag{2.18}$$

which in turn is

$$\bar{E}_\beta = \frac{-\ell G^e}{\sin\beta_0}\left(\hat{e}\cdot\bar{E}_o^i\right)\frac{\exp(-jks)}{2\pi s}\frac{\sin\left[k\ell/2(\hat{r}\times\hat{r}^i)\cdot\hat{e}\right]}{\left[k\ell/2(\hat{r}\times\hat{r}^i)\cdot\hat{e}\right]} \tag{2.19}$$

Note this result is only the diffraction caused by one of the edges of the target. Thus, this is only a single diffraction result for one edge. There is another point in the plate

that diffracts the wave.

Another important diffraction contribution to the total RCS of the plate is the corners. Marhefka also includes a corner solution to its RCSBSC computer code which enables the code to model multiple plate structures (Marhefka, 1981:Ch 2,8). For a perfectly conducting plate, the Equivalent Current corner solution is obtained by adding the edge diffracted fields that come together at that corner (Marhefka, 1981:Ch 2, 8). In the far-field, the corner diffracted field is given by (Marhefka, 1981:Ch 2, 8-9)

$$\begin{bmatrix} \overline{E}_v^c \\ \overline{E}_H^c \end{bmatrix} = - \begin{bmatrix} D_S^c(\phi,\phi';\beta_o,\beta_d) & O \\ O & D_H^c(\phi,\phi';\beta_o,\beta_d) \end{bmatrix} \begin{bmatrix} E_v^i(Q_c) \\ E_H^i(Q_c) \end{bmatrix} \quad (2.20)$$

where

$$\begin{bmatrix} D_S^c \\ D_h^c \end{bmatrix} = \begin{Bmatrix} C_S(Q_E) \\ C_h(Q_E) \end{Bmatrix} \frac{(\sin\beta_o \sin\beta_d)^{1/2}}{(\mp 1)(\cos\beta_d + \cos\beta_o)} \left(\frac{8\pi}{K}\right)^{1/2} \frac{\exp(-j\pi/4)}{4\pi} \quad (2.21)$$

and

$$C_{S,h}(Q_E) = \left[D_o^c(\phi-\phi') + D_n^c(\phi-\phi') \right] \mp \left[D_o^c(\phi+\phi') + D_n^c(\phi+\phi') \right] \quad (2.22)$$

2-16

and

$$D_{o,n}^{c}(\Psi) = D_{o,n}(\Psi)\left|F\left[\frac{\sin\beta_o\, a(\Psi)}{2\pi a(\beta_d+\beta_o)}\right]\right| \qquad (2.23)$$

and

$$a(\beta) = 2\cos^2(\beta/2) \qquad (2.24)$$

and

$$D_{o,n}(\Psi) = \frac{-\exp(-j\pi/4)}{2n\,(2\pi K)^{1/2}\sin\beta_o}\cot\left[\frac{1}{2n}(\pi\mp\Psi)\right] \qquad (2.25)$$

where

$$F(x) = 2j\left|(x)^{1/2}\right|e^{jx}\int_{|x^{1/2}|}^{\infty}e^{-j\gamma^2}\,d\gamma \qquad (2.26)$$

$F(x)$ "is a heuristic function which insures that the diffraction coefficient will not change sign abruptly when it passes thru the shadow boundaries of the edge " (Peters, 1985:14). This solution (Eq (2.20)) is self-contained by a flat plate (Marhefka, 1981:Ch 2, 9). In other words, at the limit of (Eq(2.20)), the specular scattered field will be obtained for the appropriate region.

Diffractions from edge to corner, corner to edge, and

corner to corner are known as double diffraction terms (see Fig 2.6). The UTD solution used for this investigation has a double diffraction solution built into it.

a. Edge to Corner Diffraction

b. Corner to corner diffraction
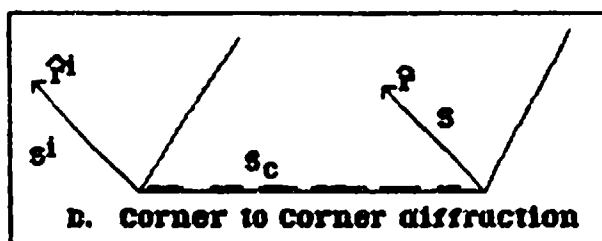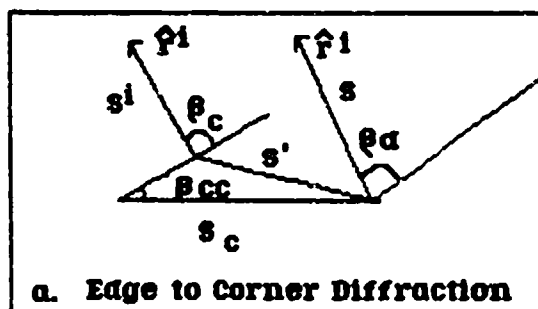
Fig 2.6. Examples of Double Diffraction

The double diffraction solution only calculates the component perpendicular to the edge. In other words, only the double diffraction solution for the horizontally polarized case is computed. For vertical polarization, the double diffraction solution is practically the same (because of surface boundary conditions) as the single diffraction solution for the same case (Marhefka, 1981:Ch 2, 15). The doubly diffracted fields are given by (Marhefka, 1981:Ch 2, 15)

a. corner to edge:

$$\underline{E}_H^{cd} = (\hat{e}^i \cdot \hat{\phi}^i) \underline{E}_c^i D_n^c(\infty, \beta_d, \beta_c, S'' \sin^2 \beta_c, \beta_c, 0, \phi^i)$$

$$\times \tfrac{1}{2} D_n(S' \sin^2 \beta_0, \phi, 0)(S'')^{-\frac{1}{2}} e^{-jkS^i} e^{-jkS'} \frac{e^{-jkS}}{S} \quad (2.27)$$

b. corner to corner:

$$\underline{E}_H^{cc_d} = (\hat{e}^i \cdot \hat{\phi}^i) E_0^i D_n^c(\infty, \beta_d, \beta_c, S'' \sin^2 \beta_0, 0, \phi^i)$$

$$\times \tfrac{1}{2} D_n^c(S_c \sin^2 \beta_{cc}, \beta_{cc}, \beta_0, S' \sin^2 \beta_0, \beta_0, \phi, 0) \quad (2.28)$$

$$\times \frac{1}{(S'' S_c)^{\frac{1}{2}}} e^{-jkS^i} e^{-jkS'} \frac{e^{-jkS}}{S}$$

c. edge to corner:

$$\underline{E}_H^{dc} = (\hat{e}^i \cdot \hat{\phi}^i) E_0^i D_n(S' \sin^2 \beta_0, \beta_0, 0, \phi^i)$$

$$\times \tfrac{1}{2} D_n^c(\infty, \beta_d, \beta_c, S'' \sin^2 \beta_d, \beta_d, \phi, 0) \quad (2.29)$$

$$\times (S''/S') e^{-jkS^i} e^{-jkS'} \frac{e^{-jkS}}{S}$$

where the edge and corner diffraction coefficients are given
respectively by

$$D_n(L, \beta_c, \phi, \phi') = \left[D_0(L, \beta_0, \phi - \phi') + D_n(L, \beta_0, \phi - \phi') \right]$$

$$+ \left[D_0(L, \beta_0, \phi + \phi') + D_n(L, \beta_0, \phi + \phi') \right] \quad (2.30)$$

$$D_n^c(L_c, \beta_d, \beta_c, L, \beta_o, \phi, \phi') = \frac{(\sin\beta_d \sin\beta_c)^{1/2}}{(\mp 1)(\cos\beta_d + \cos\beta_c)}\left(\frac{8\pi}{K}\right)^{1/2}$$

$$\frac{e^{-j\pi/4}}{4\pi} F\left[KL_c a(\beta_d + \beta_c) \times D_n(L, \beta_c, \phi, \phi')\right] \tag{2.31}$$

where

$$D_{o,n}(L, \beta_c, \psi) = \frac{-e^{-j\frac{\pi}{4}}}{2(2\pi K)^{1/2}\sin\beta_o} \cot\left[\frac{1}{2\pi}(\pi \mp \psi)\right] F\left[KLa(\psi)\right] \tag{2.32}$$

To get the total RCS, all the contributions of the diffracted field are added together. Using equation (2.1), the RCS of the target is obtained.

Moment Method (MM)

The Method of Moments or Moment Method is a numerical technique used to solve the following integral equation:

$$\int \overline{J}(r') K(r,r') dr' = -\overset{i}{E}(r) \tag{2.33}$$

in terms of the current $\overline{J}(r')$ (Stutzman, 1981:306). This equation is known as an electric field integral equation (EFIE). The current is used to obtain the fields. Then the RCS is obtained from the fields. In Fig 2.7, S is the surface of the plate and n is the unit vector perpendicular

to the surface (Newman, 1985:4). The unit vector in this particular example is $-\hat{y}$. Let $(\bar{\underline{J}}_i)$ be a source that produces the incident fields $(\bar{\underline{E}}_i)$.
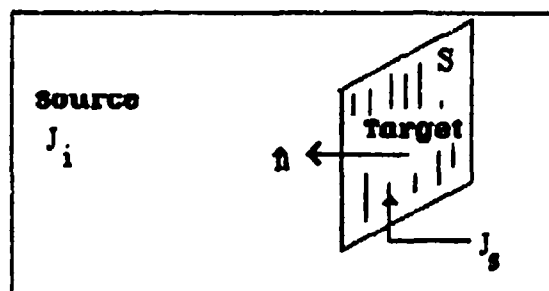
Fig 2.7. Scattering from a flat plate

The fields scattered by the plates are given by

$$\bar{\underline{E}}_s = \bar{\underline{E}} - \bar{\underline{E}}_i \qquad (2.34)$$

where $\underline{E}$ is the field in the presence of the target (Newman, 1985:4-5).

To solve for the unknown current, MM assumes that $\bar{\underline{J}}(r')$ can be approximated as a linear combination of known functions, which are known as expansion functions. Usually, the unknown current is given by

$$\overline{\overline{J}}(r') = \sum_{n=1}^{N} I_n \overline{\overline{F}}_n(r') \qquad (2.35)$$

where r' is a general position vector to any point on a scattering source, I_n is the nth expansion coefficient, and $\overline{F}_n$ is the expansion function (Newman, 1985:8). The simplest type of expansion function is the pulse function. The target's scattering surface is broken into N pieces. The expansion function can then be generally described by

$$\overline{F}_n(r') = \begin{cases} 1 & \text{for the nth piece} \\ 0 & \text{otherwise} \end{cases} \qquad (2.36)$$

The pulse expansion function is not very accurate if the N pulses are too big as can be seen in Fig 2.8.
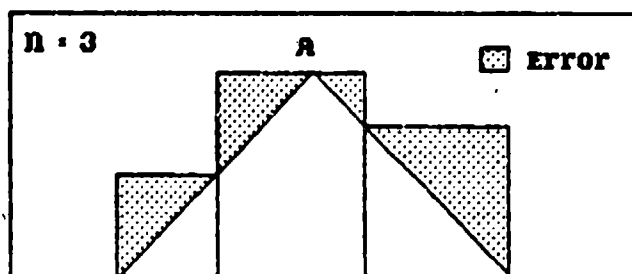
Fig 2.8. Expansion of a triangular distribution current

The solution to this problem is to choose a larger N, or choose another expansion function. The ESP computer code was used to calculate the RCS of the targets using MM. It offers three expansion modes. These are the wire-grid, surface patch, and attachment dipole modes (Newman, 1985:9).

Either the surface patch mode or the wire mode can be used to model a rectangular flat plate with ESP. The wire-grid model is easy to implement and produces good results at the far-field (Wilton, 1981:70). Unfortunately, its results are not good in the near-field. Also, Wilton states that the wire-grid models accuracy has been put in doubt (Wilton, 1981:70). The surface patch code is more accurate than the wire-grid model at the near field. Also, it is easier to model a flat plate with the surface patch model than with the wire-grid model. For these reasons, the surface patch model was used to model the square flat plates.

The surface patch mode is implemented by assuming that the currents on the rectangular flat plate are expanded in terms of rectangular piecewise sinusoidal (PWS) surface patch dipole modes (Newman, 1985:11) (see Fig 2.9). The current density for Fig 2.9 is (Newman, 1985:7)

$$\overline{J_s} = \hat{z}\, \frac{\overline{P_1}\, \sin K(z-z_1)}{2w \sin K(z_2-z_1)} + \hat{z}\, \frac{\overline{P_2}\, \sin K(z_3-z)}{2w \sin K(z_3-z_2)}$$

(2.37)

here $\bar{P}_1$ and $\bar{P}_2$ are pulse functions given by

$$\bar{P}_1 = \begin{cases} 1 & Z_1 < Z < Z_2 \\ 0 & \text{elsewhere} \end{cases} \tag{2.38}$$

$$\bar{P}_2 = \begin{cases} 1 & Z_2 < Z < Z_3 \\ 0 & \text{elsewhere} \end{cases} \tag{2.39}$$
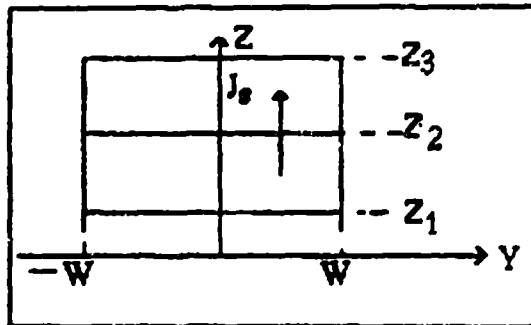
Fig 2.9. A PWS rectangular surface patch dipole mode.

It is time to solve for $\bar{J}_s$ or $\bar{J}(r')$. This is accomplished by using testing or weighting functions (Wilton, 1981:80). Assume that a test source with ($\bar{J}_m$) is placed on the target (Newman, 1985:6). This test source will produce the electric field, ($\bar{E}_m$). Because of boundary conditions, the fields inside the target must be zero. Then the following is true:

$$-\iint_S \left(\overline{J}_s \cdot \underline{E}_M \right) ds = \iiint_V \left(\overline{J}_i \cdot \underline{E}_M \right) dv \qquad (2.40)$$

where V is the volume of the source (Newman, 1985:6). Using Eq (2.35) and (2.40), the following is obtained (Newman, 1985:8):

$$\underline{V}_m = \sum_{n=1}^{N} I_n \underline{Z}_{m,n} \; ; \quad m = 1, 2, 3, \ldots, N \qquad (2.41)$$

where

$$\underline{Z}_{m,n} = -\iint_n \overline{E}_m \cdot \overline{F}_n \, ds \qquad (2.42)$$

and

$$\underline{V}_m = \iiint_V \overline{J}_m \cdot \overline{E}_i \, dV \qquad (2.43)$$

are the mutual impedance between the mth and nth mode and the modal excitation voltage for the mth mode, respectively. Once the scattered current is obtained, the scattered field is obtained by

$$\overline{J}_S = 2\hat{n} \times \overline{H}^i \qquad (2.44)$$

and

$$E = \frac{(\overline{\nabla} \times \overline{H})}{(\sigma - j\omega\epsilon)}, \quad \sigma = \text{surface electrical conductivity} \qquad (2.45)$$

(Knott and others, 1985:68; Newman, 1985:4). The scattered field is obtained by using Eq (2.34). Finally, the RCS is obtained by Eq (2.1).

III. Measurement Procedure

The Avionics Laboratory Far-Field Radar Cross Section
(RCS) Measurement Chamber was used to perform the
experimental measurements. In this chapter, the measurement
procedure will be explained using documents provided by AFWAL
for their reports (Simpson, 1985).

The chamber is an indoor "far-field" RCS measurement
facility. The far-field criteria is given by

$$R > \frac{2 D_1 D_2}{\lambda} \tag{3.1}$$

where R is the distance between the target and the radar, D_1
is the maximum dimension of the transmit antenna, D_2 is the
maximum transverse width of the target measured, and   is the
wavelength of operation. Thus, accurate measurements are
limited to targets whose sizes satisfy Eq (3.1). A block
diagram of the system is provided in Fig 3.1. Fig 3.1 shows
that, the measurement system consists of a source, transmit
and receive antennas, and a computer to control the
operation. The system performs the RCS measurements and then
records it as azimuth angle (θ) versus the target's RCS.
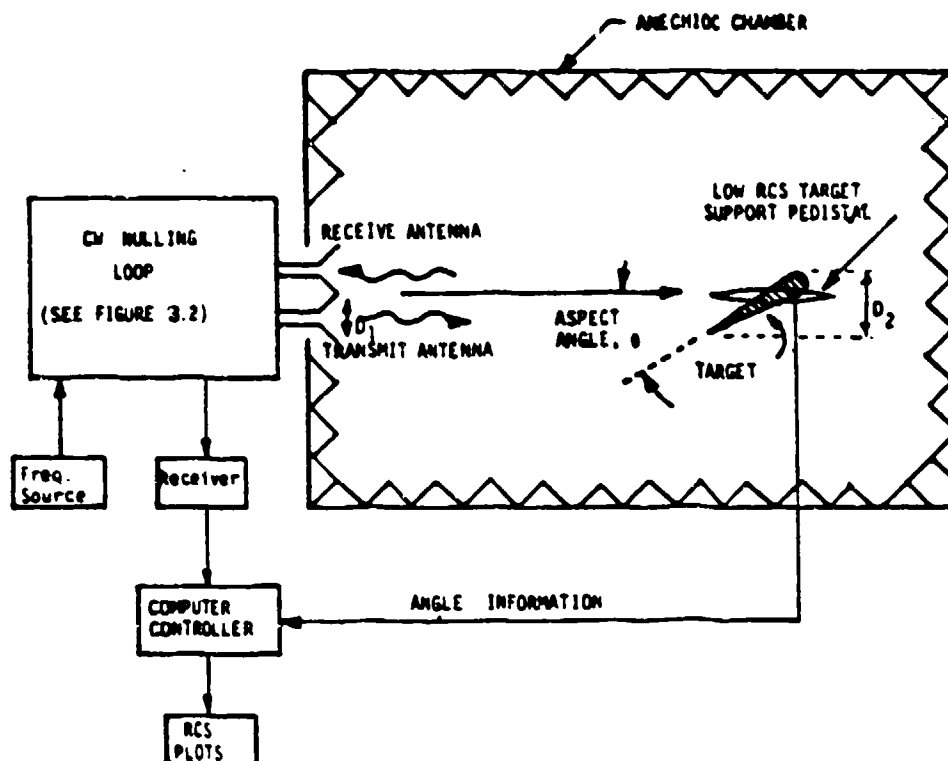
3-1

Fig 3.1.   AFWAL far-field RCS measurement facility
(Simpson, 1985:17)
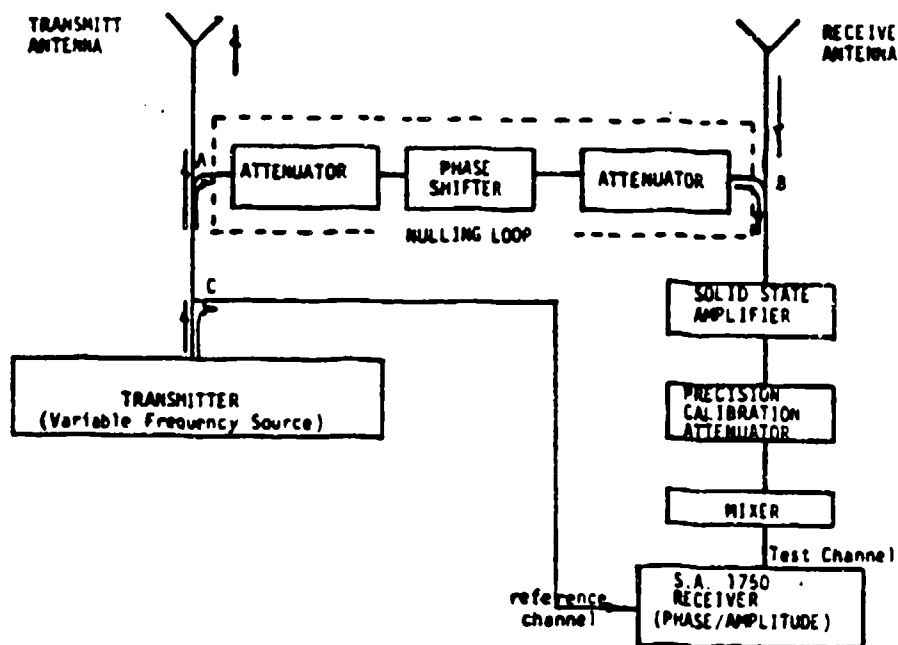
Fig 3.2.   Block diagram of "CW-Nulling Loop" RCS Measurement
System (Simpson, 1985:17)

The measurements are accomplished by using a continuous wave (CW) radar equipped with a nulling loop. The concept of "CW-nulling" is illustrated in Fig 3.2. The source is a Backward Wave Oscillator (BWO) which produces a stable signal. This low power signal is generated at a frequency within the microwave band (2-18 GHz). The frequency used for the investigation was 10 GHz (3 cm wavelength). Most of it is used by the transmit antenna which transmits it to the chamber. The transmit power is split into two parts. One portion is sent to the "reference channel" of a Scientific Atlanta 1750 series phase/amplitude microwave receiver (see point C in Fig 3.2). This reference signal is used to provide a phase reference when the test channel phase is recorded. Once this is done, the test channel can perform accurate amplitude and phase measurements. This portion of the transmit signal also provides the receiver with a signal.

The second portion of the transmit signal is sent to the microwave "nulling loop" (point A in Fig 3.2). The nulling is accomplished by adjusting the nulling loop attenuators and phase shifter. As a result, the receive signal is cancelled at point "B" (see Fig 3.2) by the output of the nulling loop, which is equal in amplitude but opposite in phase to the receive signal. Thus, the test channel signal level is reduced to the noise level of the receiver.

The target is then mounted on a low frontal RCS support pole. The targets used were flat plates. The plates were measured from edge to broadside (-45° to 45°) as can be seen

in Fig 3.3.
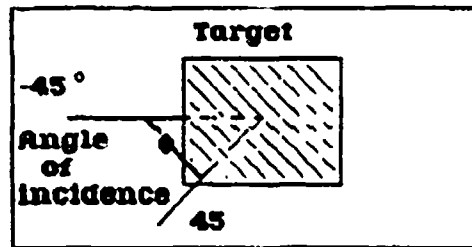
Fig 3.3.   Angle of Incidence on Target

The measurements were taken for $-45° \leq \theta \leq 45°$ (edge to broadside) because the computer software used only can function for angles ranging from negative to positive (or $-A \leq \theta \leq +A$). This is equivalent to taking the incidence angle as going from $0°$ to $90°$ (edge to broadside).

The size of the plates ranged from half a wavelength (1.5 cm) to 6.5 wavelengths (19.5 cm) in increments of half a wavelength. Also, a plate of 3/4 of a wavelength (2.25 cm) was considered. The uncalibrated RCS of the targets are measured as the targets rotate on the mount. These results are then stored in the computer.

The receiver amplitude is calibrated next. This is accomplished by rotating the target to the angle which produces the greatest backscatter RCS. In the case of a square flat plate, this would be the broadside. Once the maximum RCS is obtained, a precision calibration attenuator (in the test channel of the receiver) is adjusted in 5 dB steps from 0 to -60 dB. The computer stores these results and calibrates the raw RCS pattern of the target.

The target is then removed and a calibration sphere is positioned on the mount. Recording the test level with the sphere on the support column establishes an absolute RCS level. If the target's broadside RCS is greater than the sphere's RCS, the target is left in the support. The computer then assigns an absolute RCS scale to the original target pattern. This is a source of calibration error if the plate is not properly located on the mount. The plate's broadside must be perpendicular to the incident wave to avoid this source of error. The final result is given by the computer in decibels per square meter (dBsm).

Vertical polarization (V.P.) measurements are not as accurate as horizontal polarization measurements (H.P.). This is due to the low RCS mount which provides a higher RCS contribution at V.P. than H.P. This RCS contribution is very low but it is more noticeable at V.P. than H.P.

IV. Comparison of Results

In this chapter, the five computational methods used will be compared against each other and against the measurements. The computational methods were Physical Optics (PO), the Physical Theory of Diffraction (PTD), the Geometrical Theory of Diffraction (GTD), the Uniform Theory of Diffraction (UTD), and the Moment Method (MM).

Vertical Polarization

Half a Wavelength. This was the smallest size measured in the range. The RCS pattern of this plate has a null at approximately 45° (see Fig 4.1).
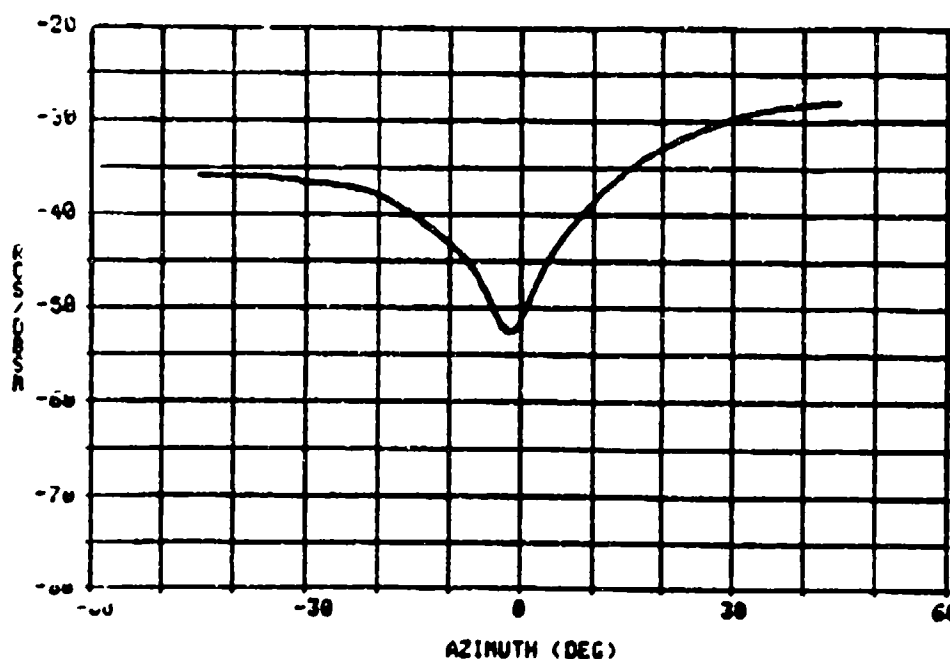
Fig 4.1. RCS measurement of 0.5 wavelength (1.5 cm) plate (V.P.)
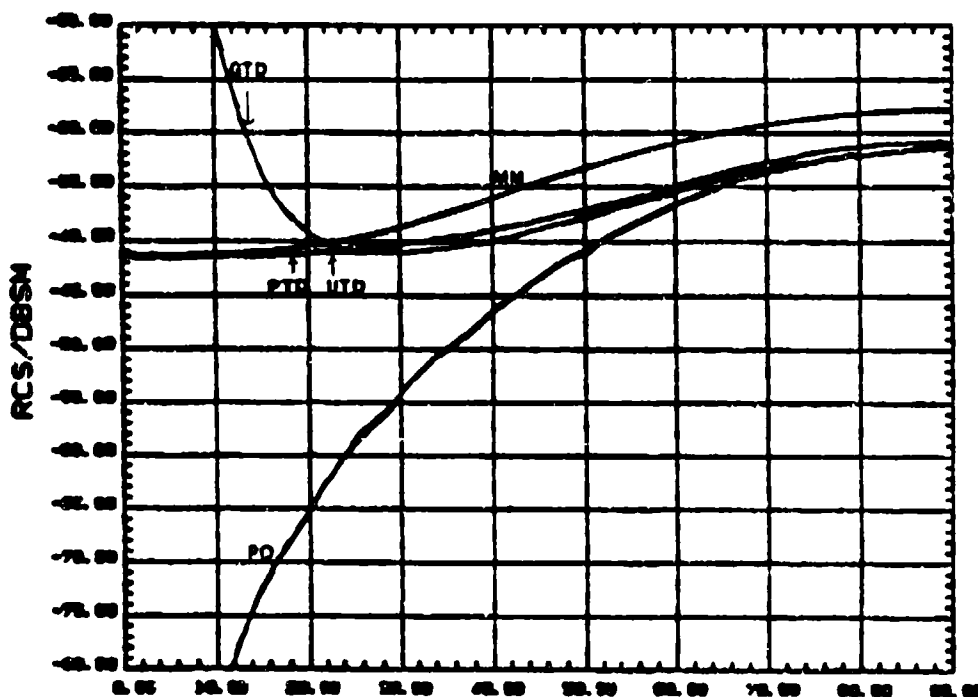
Fig 4.2.   Calculated RCS for 0.5 wavelength (1.5 cm) plate
(V.P.)

None of the computational methods predict this null (see Fig
4.2).   This null may be a result of the small size of the
plate.   The plate is approximately equivalent to two dipoles
which are half a wavelength apart.   It is possible that both
dipoles have the same magnitude but opposite phases, such
that they cancel each other out at an azimuth angle of $45°$.
It is also possible that the range can not accurately
describe the RCS pattern for this plate at this polarization
because of its small size (see p. 5 in Chapter 3).   Other
measurements were performed on the same plate at various
times providing different results.   The most stable
measurement was the one shown in Fig 4.1.

Table 4.1

Comparison of RCS of Half Wavelength Plate (V.P)

	Peak (dBsm)	Grazing Incidence (dBsm)	CPU Time (sec)
PO	-31.5	-100.0	1.8
PTD	-31.5	-41.3	6.6
GTD	-31.0	159.7	100.1
UTD	-31.9	-41.3	135.0
MM	-28.0	-41.2	51.6
Measurement	-28.0	-36.0	N/A

From Fig 4.2 it can be seen that PTD and UTD have approximately the same RCS pattern. This is what Marhefka predicted for this polarization (Marhefka, 1981:Ch 2,11,15). Also by comparing PTD and UTD to Fig 4.1, it is evident that MM is the only computational method to accurately predict the specular peak of the plate's RCS (see Table 4.1). MM also accurately predicts the RCS of the plate near and at broadside ($65° \leq \theta \leq 90°$). The value measured for this plate as grazing incidence differs by 5 dBsm from MM. This may be due to the mounting plataform used in the measurements.

The RCS predicted by GTD increases as the azimuth angle approaches grazing incidence ($0°$). This should be expected because the reflection boundary for this particular situation occurs at grazing incidence (see Fig 4.3).
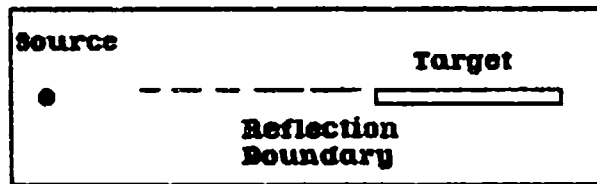
Fig 4.3. Reflection Boundary on Flat Plate (Monostatic RCS)

The Moment method is the most accurate computational method to calculate the RCS of a plate that is small with respect to wavelength.

Table 4.1 shows the accuracy of the methods at specular (broadside) and grazing (edge) incidence. Also, the CPU time is included for comparison purposes. Again, MM is the most accurate prediction method for the half wavelength plate at this polarization. The MM CPU time is small when compared to the UTD time. Thus, MM is the preferred computational method for a target of this size using vertical polarization.

The rest of the graphs and tables will be presented in Appendix A and B respectively.

Three Quarters of a Wavelength. In this case the measured RCS pattern and the RCS pattern predicted by the Moment Method are in agreement for a longer range of azimuth angle ($15° \leq \theta \leq 90°$) (see Fig A.3 in App. A). MM differs by approximately 1 dBsm when compared to the actual measurements (see Table B.2 in App. B). This difference can be attributed to measurement calibration error. This calibration error accounts for the difference between the levels.

The Moment Method is again the most accurate prediction

method. Also, the CPU time required for computing the MM has increased (see Table B.2 in App. B). Thus, the CPU time will increase as the size of the plate increases.

Again, UTD and PTD predict the same RCS pattern (see Fig A.4 in App. A). GTD increases as it approaches grazing incidence, and PO continues to predict a small return from the edge.

The PO, PTD, GTD, and UTD predictions for the specular region are closer to those of MM. All the computational methods are in close agreement with the measurements for $70° \leq \theta \leq 90°$ (see Fig A.3 and A.4 in App. A).

One Wavelength. For this case, MM provides the most accurate representation of the RCS. It is very accurate in the range of $35° \leq \theta \leq 90°$ (see Fig A.5 and A.6 in App. A).

PO, PTD, GTD, and UTD predict a higher specular peak than MM (see Fig A.6). In fact, the four methods agree in the range of $68° \leq \theta \leq 90°$. Thus, the plate's size is too small to be modeled by those four computational methods.

The CPU time required to model this plate with MM is greater than the time required for the other plates (see Table B.3 in App. B). The Moment Method is the most accurate computational method for this plate size. Its CPU time is smaller than UTD's CPU time. Thus, MM is still the preferred method for a plate of this size.

One and a Half Wavelengths. The RCS pattern for this plate has 3 nulls and peaks (see Fig A.7 in App. A). Thus,

as the size of the plate increases (in wavelengths), the
number of nulls and peaks also increases.

MM very accurately predicts the shape of the RCS pattern
of this plate (see Fig A.8 in App. A). The levels of the
first 2 peaks computed by MM are approximately equal to the
measured peaks (see Fig A.7 and A.8).

As can be seen from Table B.4 in App. B, MM is the
longest running computational method used for this plate.
Also, PO, PTD, GTD and UTD are more accurate in the specular
region for a plate of this size. For these four
computational methods, the CPU time remains the same
regardless of the size of the plate.

All the methods converge within the range of $74° \leq \phi \leq 85°$
. For larger sized plates (in wavelengths), the five
computational methods will all converge near the specular
region.

Two Wavelengths. MM predicts the shape of the RCS of
this target very accurately (see Fig A.9 and A.10 in App. A).
The five computational methods converge near the specular
region as expected $(76° \leq \phi \leq 90°)$. A summary of the most
important findings is given in Table B.5 in App. B.

Two and a Half Wavelengths. As mentioned before the
peaks and nulls have increased because of the increase in the
size of the plate (see Fig A.11 in App. A). Again, MM is the
most accurate prediction method. Also, PTD, GTD, and UTD are
more accurate than they were for the smaller plates (for 37°

4-6

$\leq \phi \leq 90°$) (see Fig A.11 and A.12 in App. A). Thus, as the size of the plate increases, the accuracy of PTD, GTD, and UTD increases. All five computational methods converge between 78° and 90°.

Again, Table B.6 in App. B summarizes some of the most important aspects of the comparisons.

Three Wavelengths. As expected, MM provides the most accurate RCS pattern for this plate (see Fig A.13 and A.14 in App. A). All methods converge accurately near the specular region (82° $\leq \phi \leq$ 90°). PO is good for predicting the sidelobe peaks from 65° to 90°. As expected, PTD, GTD, UTD, and MM converge for an azimuth angle from 36° to 90°.

As mentioned before, the number of peaks and nulls increase as the plate size increases. Note, that the CPU time to implement the Moment Method has increased again. Also note that MM is not very accurate near the edge (see Table B.7 in App. B).

Three and a Half Wavelengths. MM is again the most accurate RCS prediction method (see Fig A.15 and A.16 in App. A). All the computational methods converge for a greater range of azimuth angle (70° $\leq \phi \leq$ 90°) (see Fig A.16). Note the increasing accuracy of PTD, GTD, and UTD. Also, PO is good near the specular region.

Note again that the computational methods require the same CPU time, and MM still requires the most time (see Table B.8 in App. B).

4-7

Four Wavelengths. MM is the most accurate computational method for this plate size. All methods converge for an azimuth angle ranging from 76° to 90° (see Fig A.17 and A.18 in App. A).

The difference between the measured and the computed specular levels (see Table B.9 in App. B) is caused by measurement calibration error.

The rest of the cases follow the same pattern for vertical polarization. The reader is referred to Appendix A where the rest of the cases are plotted. Appendix B contains the rest of the tables.

Horizontal Polarization

Half a Wavelength. Because of the boundary conditions, the edge RCS is lower than it was for the vertical polarization case (see Fig A.1 and A.19 in App. A). The incident E field is now perpendicular to the edge of the plate. Thus, when the azimuth angle is zero the radar "sees" the minimum RCS return possible from that plate. This is the same for any size plate at this polarization. Note that the measurements near $\theta = 0°$ are unstable. This is due to the chamber's limited ability for measuring an RCS of less than -60 dBsm.

For a plate of this size, the only accurate prediction method is the Moment Method (see Fig A.19 and A.20 of Appendix A. The CPU time for MM is very short in this case (see Table B.1 in App. B). All the computational methods

take the same amount of CPU time for a given plate size regardless of the polarization. Note that PO, PTD, GTD, and UTD are not good for predicting the RCS of a target of this size regardless of the polarization.

For horizontal polarization, PTD and UTD do not predict the same RCS for the same target. This is because UTD's second order diffraction solution is used when the E field is perpendicular to the edge of diffraction. For vertical polarization the boundary conditions are such that double diffraction of the E fields is small. Thus, the contribution of double diffraction to the UTD solution is negligible (Marhefka, 1981:Ch2, 15). The PTD solution, which has only first order diffraction built into it, is not as accurate.

The tables in Appendix B provide the values of the specular peak and CPU time for both vertical and horizontal polarization.

Three Quarters of a Wavelength. Again, MM is the most accurate prediction method (see Fig A.17 and A.18 in App. A). However, PO, PTD, GTD, and UTD seem to converge better near the specular region ($81^{\circ} \leq \theta \leq 90^{\circ}$).

One Wavelength. MM is the only computational method to accurately predict the specular peak level (see Table B.12 in App. B). GTD is more accurate than PO, PTD, and UTD. This can be attributed to the fact that the GTD solution has a third order diffraction term added to it (see Fig A.19 and A.20 in App. A).

4-9

MM is not "exact" because to use it, the user must take
into account the limitations of the computer system itself.
The VAX 11/780 is a powerful computer system but it is much
slower than a Cray computer.   In order to speed up the
computing process the user has to reduce the number of modes
as the size of the plate increases (see pp. 20-26 in Ch. 2).
Also, if the number of modes is too large, the computer
cannot handle all the modes. This explains why MM is not
"exact" when compared to the measurements.

One and a Half Wavelengths. As the size of the plate
becomes larger than the operating wavelength, PO, PTD, GTD,
and UTD start to converge within the specular and near
specular regions ($71° \leq \theta \leq 90°$) (see Fig A.21 and A.22 in
App. A). MM is still the most accurate RCS prediction
method. As in the vertical polarization case, the number of
peaks and nulls increase as the plate size.

Two Wavelengths. MM is the most accurate prediction
method (see Fig A.23 and A.24 in App. A). GTD is more
accurate than UTD because GTD has a third order diffraction
term included in the solution (see Fig 4.4). This third
order term accounts for triple (edge to edge to edge)
bounces. The UTD solution includes only the first and second
order diffraction terms in the solution. Note that GTD
predicts a large RCS as it approaches the edge whereas UTD
does not. If a third order diffraction term were added to
the UTD solution, UTD would more accurately compute the RCS

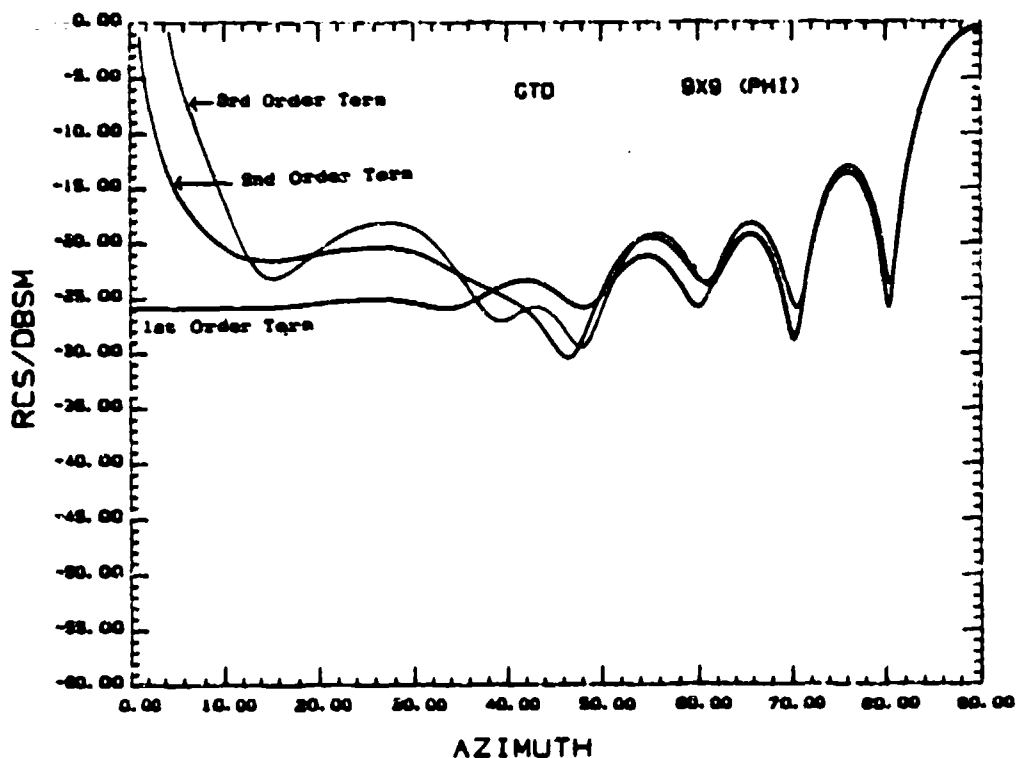of a large target at horizontal polarization.

Fig 4.4.   GTD RCS with first, second, and third order
diffraction terms.

Two and a Half Wavelengths.   PTD, GTD, UTD, and MM all

converge for an azimuth angle of 55° .   The convergence is

excellent for all five methods from 78° to 90°.

The RCS computations have the same type of behavior for

the rest of the plates.   The reader is referred to both

appendices A and B for the results obtained for the rest of

the targets.

General Results

Pattern Complexity.   One of the results found in the

investigation is that the number of peaks and nulls increase

with plate size (see App. A).   This agrees with Ross' results

(Ross, 1966:332). As a result, the complexity of the RCS

pattern increases as the plate size increases.

Polarization Dependence. Another important result is

that the RCS measurements of the plates exhibit polarization

dependence for $\phi <$ 60°. For horizontal polarization the edge

RCS has a much smaller value than the edge RCS of the same

plate for vertical polarization. GTD, UTD, and MM are the

only computational methods that were polarization dependent

in the investigation. The polarization dependence of these

computational methods also occurs when   is less than

60°.

PTD has only a first order diffraction term built into

its solution. Thus, the RCS appears to be the same for the

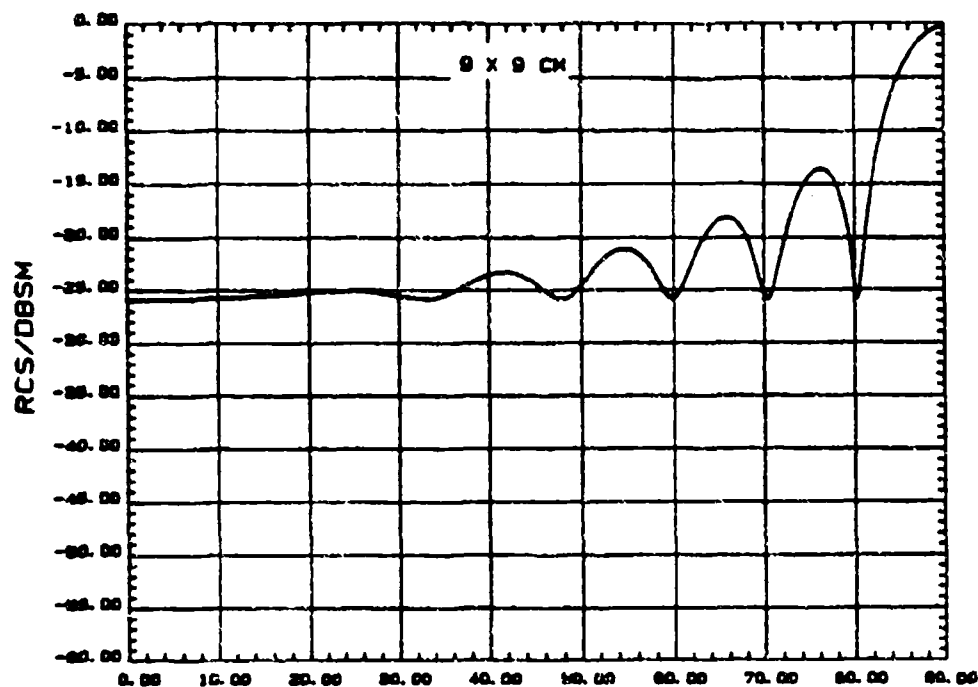same plate at either polarization (see Fig 4.5).

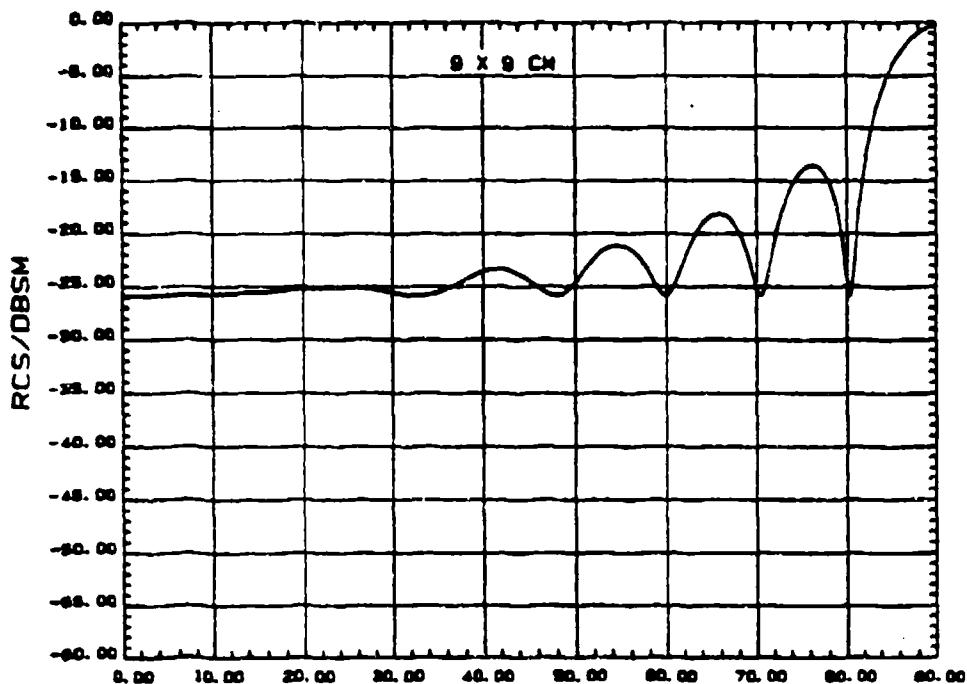Fig 4.5a.   PTD RCS (Vertical Polarization)

Fig 4.5b. PTD RCS (Horizontal Polarization)

If a second order diffraction term is added to the PTD

solution, the PTD RCS pattern would be polarization

dependent. Thus, this implementation of PTD is not a viable

computational method for more complex targets. Higher order

diffraction terms are needed to make this solution more

accurate.

PO produces the same result for either polarization.

Thus, PO is independent of polarization for any plate size

(Ross, 1966:332).

Specular Region. MM is the most accurate prediction

method in the specular region (broadside) (see Table 4.2).

At 2.5 wavelengths (7.5 cm), the plates are much larger than

the wavelength. This situation leads to High-Frequency

scattering (Knott and others, 1985:57).

4-13

Table 4.2

Specular RCS (broadisde)

Size (wave.)	PO (dBsm)	PTD (dBsm)	GTD (dBsm)	UTD (dBsm)	MM (dBsm)
0.5	-31.5	-31.5	-31.0	-31.9	-28.0
0.75	-24.6	-24.6	-24.2	-24.2	-23.9
1.0	-19.5	-19.5	-19.3	-19.3	-20.3
1.5	-12.4	-12.4	-11.9	-12.4	-12.5
2.0	-7.4	-7.4	-7.4	-7.4	-7.4
2.5	-3.5	-3.5	-3.6	-3.9	-3.7
3.0	-0.4	-0.4	-0.4	-0.4	-0.4
3.5	2.3	2.3	2.3	2.3	2.3
4.0	4.6	4.6	4.6	4.6	4.6
4.5	6.7	6.7	6.7	6.7	6.7
5.0	8.5	8.5	8.5	8.5	8.5
5.5	10.2	10.2	10.2	10.2	10.2
6.0	11.7	11.7	11.7	11.7	11.7
6.5	13.1	13.1	13.1	13.1	13.1

Table 4.3
CPU Time

Size (wave.)	PO (sec)	PTD (sec)	GTD (sec)	UTD (sec)	MM (sec)
0.5	1.8	6.6	100.1	135.0	51.6
0.75	1.8	6.6	100.1	135.0	76.9
1.0	1.8	6.6	100.1	135.0	116.4
1.5	1.8	6.6	100.1	135.0	163.4
2.0	1.8	6.6	100.1	135.0	199.4
2.5	1.8	6.6	100.1	135.0	263.7
3.0	1.8	6.6	100.1	135.0	386.7
3.5	1.8	6.6	100.1	135.0	606.0
4.0	1.8	6.6	100.1	135.0	829.3
4.5	1.8	6.6	100.1	135.0	1646.9
5.0	1.8	6.6	100.1	135.0	2219.9
5.5	1.8	6.6	100.1	135.0	3002.4
6.0	1.8	6.6	100.1	135.0	4018.6
6.5	1.8	6.6	100.1	135.0	4032.6

For this type of scattering, the detailed geometry of the target is important to the scattering process. GTD, UTD, PO, and PTD are all high-frequency computational methods. Thus, their accuracy is considerably better in the high-frequency region (Knott, 1985:57). All the computational methods are highly accurate in the specular region from 2.5 wavelengths to 6.5 wavelengths (19.5 cm). Note that MM differs by 1 to 2 dBsm from the measurements because of measurement calibration error (see p. 5 in Ch. 3).

CPU Time. The CPU time was estimated thru the use of a subroutine used by RCSBSC and ESP for this purpose (Newman, 1985:60). The GTD time was an estimate taken over a period of time by the author. Also, the GTD program works only for rectangular flat plates. Therefore, the CPU time is not as accurate as the others. As previously mentioned, MM computation time increases as the size of the plate increases (see Table 4.3). The other computational methods take the same CPU time regardless of the plate size. UTD's CPU time for a 2.5 wavelength plate is 135 sec. MM's CPU time for a plate of the same size is 263.70. MM is still much more accurate than the other computational methods, but one must take into account that 4018.5 sec (1 hour and 7 minutes) of CPU time is required to calculate the RCS of a 6 wavelengths (18 cm) square flat plate.

UTD takes more CPU time than GTD because its RCS solution is more complex than GTD's solution.

Overall Accuracy. MM is the most accurate RCS computational method. It accurately predicts the RCS pattern for almost all of the plates. The levels of the measurements may differ in some cases (measurement calibration error) but the shape of the pattern predicted by MM is correct. MM is more accurate at vertical polarization than at horizontal polarization. This is because higher order terms that occur at horizontal polarization are more difficult to model than the first order terms that occur at vertical polarization. Also, accuracy is achieved at the expense of CPU time. If a 2.0 wavelength square flat plate is modeled using 0.2 wavelength increments, the CPU time would be 1181.3 sec. If a 0.4 wavelength increment is used, the CPU time required by MM is 114.4 sec. The former case is more accurate than the latter case. Thus, the accuracy of an MM model is directly related to the size of the increments or samples.

On the other hand, the accuracy cf PTD, GTD, and UTD generally depends on the higher order terms added to the solution. GTD is very accurate because of the addition of second and third order terms to the RCS solution. As mentioned before, the higher order terms only affect the horizontal polarization case. Unfortunately, GTD fails at grazing incidence where the predicted RCS approaches infinity. UTD and GTD have a better convergence (predict the same result) for vertical polarization than horizontal polarization (see Table 4.4), because the higher order diffraction terms are negligible on vertical polarization.

Table 4.4

UTD Versus GTD Convergence

Size (wave.)	V.P. (degrees)	H.P. (degrees)
0.5	60 - 90	0
0.75	66 - 90	73 - 90
1.0	35 - 90	72 - 90
1.5	12 - 90	76 - 90
2.0	8 - 90	78 - 90
2.5	6 - 90	71 - 90
3.0	6 - 90	71 - 90
3.5	6 - 90	66 - 90
4.0	5 - 90	61 - 90
4.5	5 - 90	63 - 90
5.0	5 - 90	68 - 90
5.5	5 - 90	69 - 90
6.0	4 - 90	65 - 90
6.5	4 - 90	65 - 90

UTD also is not very accurate at grazing incidence. However, the RCS it predicts there does not approach infinity. UTD's accuracy could be improved if higher order diffraction terms were added.
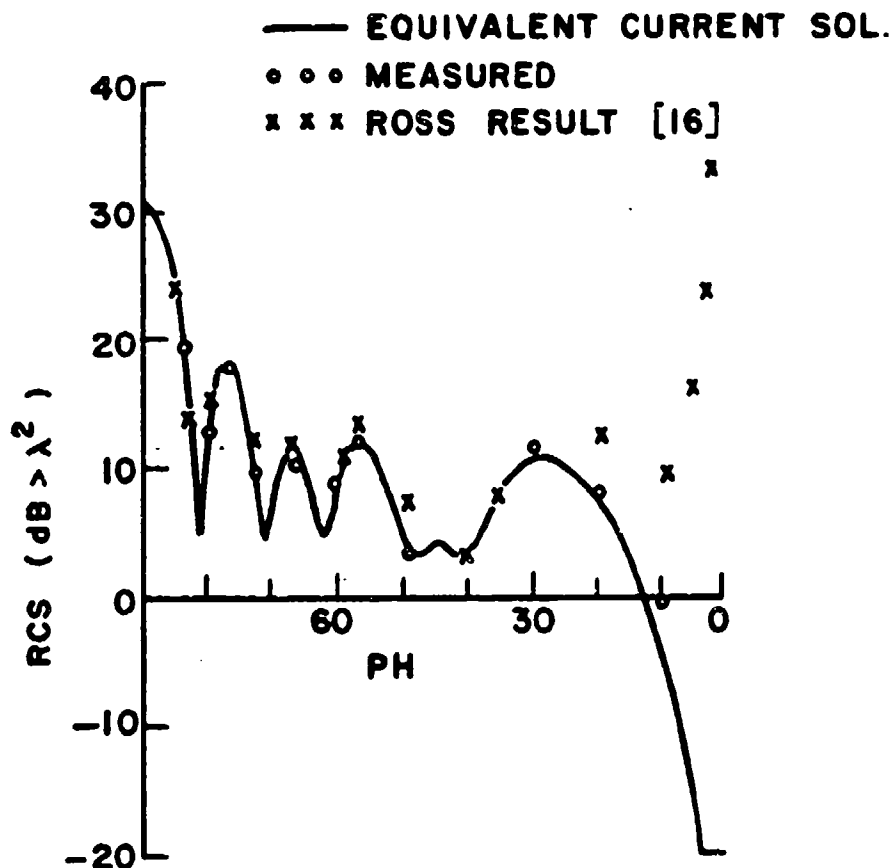
Fig 4.6.   RCS of a 4 x 4 inch Plate at 9.227 GHz
(Marhefka, 1981:Ch5, 12)

In Fig 4.6, the RCS of a 4 in square flat plate at 9.227 GHz is compared against Ross' GTD calculations and against the UTD with third order diffraction terms (Marhefka, 1981:Ch5, 11-12). UTD is much more accurate than GTD for this example. Thus, UTD's accuracy can be enhanced with the addition of higher order terms.

PTD is more accurate at vertical polarization than
horizontal polarization. This is because the PTD solution
has only a first order diffraction term in it. Thus, the PTD
solution does not take into account the multiple bounces that
occur at the horizontal polarization.

PO is the least accurate of all the computational methods
investigated. However, PO is very good for predicting the
RCS at the near specular region (approximately $70° \leq \phi \leq 90°$)
in a relatively small amount of CPU time for plates that are
2.5 wavelengths or larger.

V.   Conclusions and Recommendations

Conclusions

The Moment Method is the most accurate RCS computational technique of the five investigated. MM accounts for polarization dependence, pattern complexity, and the specular peak of a plate which is small with respect to wavelength (smaller than 2 wavelengths). MM is also highly accurate for larger plates (larger than 2 wavelengths), but its CPU time increases as the size of the plate increases. Thus, MM is a poor choice of RCS computation method for plates that are larger than 2.0 wavelengths due to the CPU time required.

The Geometrical Theory of Diffraction does not predict an accurate RCS for plates that are smaller than 2.5 wavelengths on a side. GTD provides a more accurate solution for plates whose size is 2.5 wavelength or larger. It is very accurate for horizontal polarization because of its second and third order diffraction terms. For a given type of target, GTD's CPU time remains the same as the plate size increases. Unfortunately, GTD fails to predict the RCS near and at the edge of the plate (the reflection boundary of the target).

The Uniform Theory of Diffraction is accurate for plates that are larger than 2.0 wavelengths, but it is less accurate than GTD. However, UTD, unlike GTD, does not give infinite results at the edge. If a third diffraction coefficient was added to the solution, UTD would be more accurate than GTD. UTD's CPU time is greater than GTD's CPU time. This is due

to the complexity of the UTD mathematical expressions. Also, the GTD solution was derived specifically only for rectangular flat plates. However, the UTD solution used for this investigation can model more complex shapes than flat plates. Fortunately, UTD's CPU time remains the same as the plate size increases.

The Physical Theory of Diffraction is not as accurate as MM, GTD, and UTD. This is because the PTD solution only takes into account the first order diffraction term. Thus, PTD is not very accurate at horizontal polarization where the higher order terms are more important. Therefore, PTD predicts the same result for a given plate at either polarization.

The Physical Optics approximation is the least accurate of the five computational methods investigated. Also, PO is independent of polarization. Thus, PO predicts the same RCS for either polarization. PO is accurate near and at the specular region. The CPU time required to implement this method is the shortest of the five investigated.

Although MM is the most accurate computational method for a perfectly conducting flat plate, it takes too much CPU time to use. Since CPU time is expensive, MM is the most expensive to use of the five methods. Also, as the size of the target increases, MM requires more CPU time. Thus, for a large (when compared to wavelength) perfectly conducting target, MM results can be very expensive. In general, UTD is a better choice for predicting the RCS of a perfectly

conducting flat plate with a side dimension of at least 2.5 wavelengths. UTD is quick and accurate for computing the RCS of a target. Finally, PO is a good choice for calculating the RCS of large targets near and in the specular region because of its speed and accuracy.

Recommendations

There are more computational methods that could be investigated. Among these are the original form of UTD developed by Kouyoumjian and Pathak (Kouyoumjian and Pathak, 1974), the Uniform Asymptotic Theory (Knott and others, 1985:134), and the Spectral Theory of Diffraction (Kouyoumjian, 1985:6). Hybrid techniques like MM-GTD and UTD-PTD could also be investigated. In addition, the UTD and PTD solutions could include higher order terms.

The 0.5 wavelength flat plate should be analyzed at a different frequency to observe if the RCS pattern varies from the measurements obtained in this investigation.

Other types of targets (besides square flat plates) could be analyzed in future investigations using the same five computational methods.

VI. Appendix

Appendix A. RCS Graphs
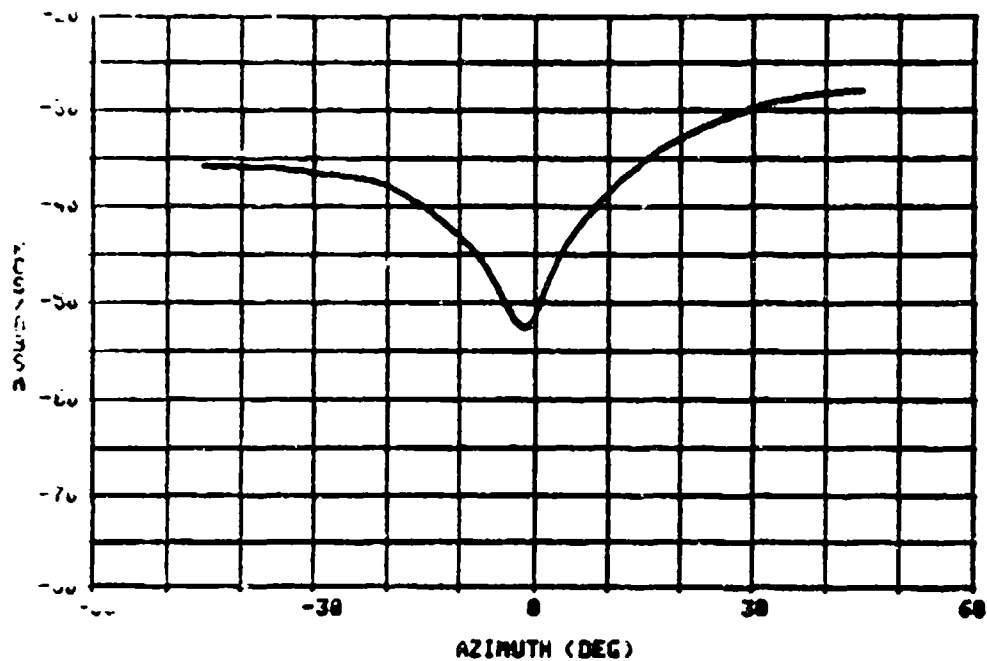
Fig A.1. RCS measurement of 0.5 wavelength (1.5 cm) plate (V.P.)
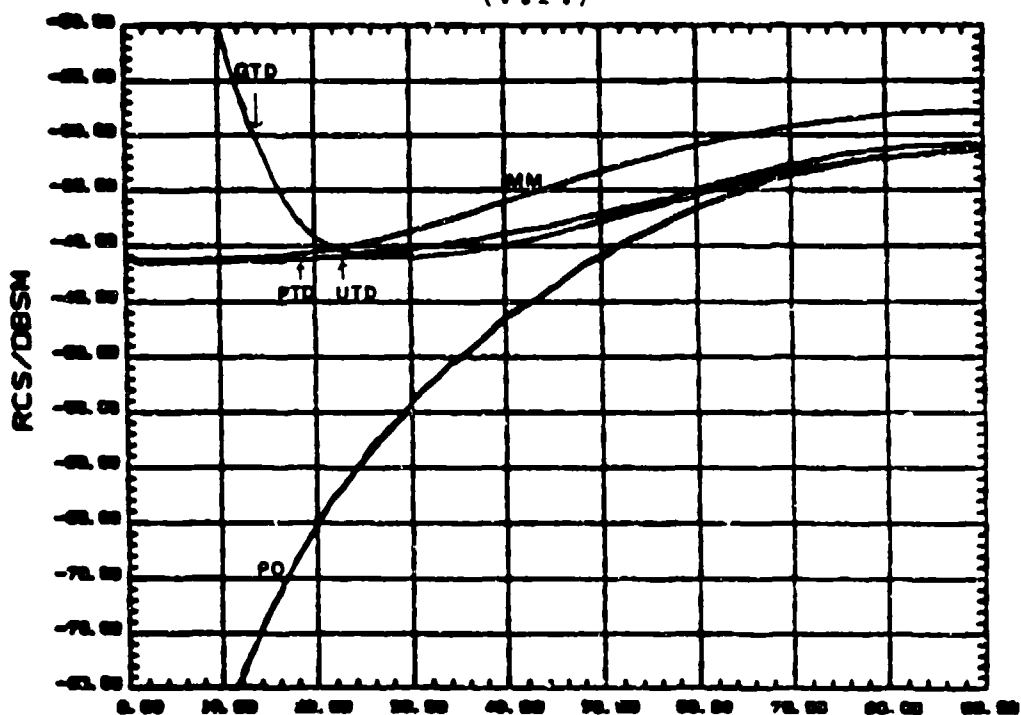
Fig A.2. RCS for 0.5 wavelength (1.5 cm) plate (V.P.)
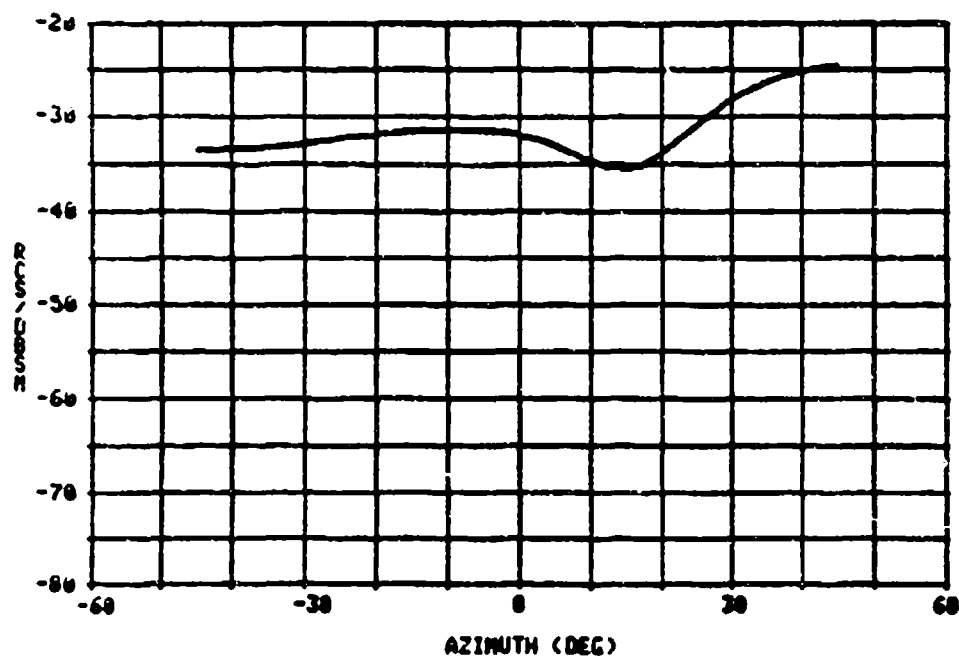
Fig A.3. RCS measurement of 0.75 wavelength (2.25 cm) plate
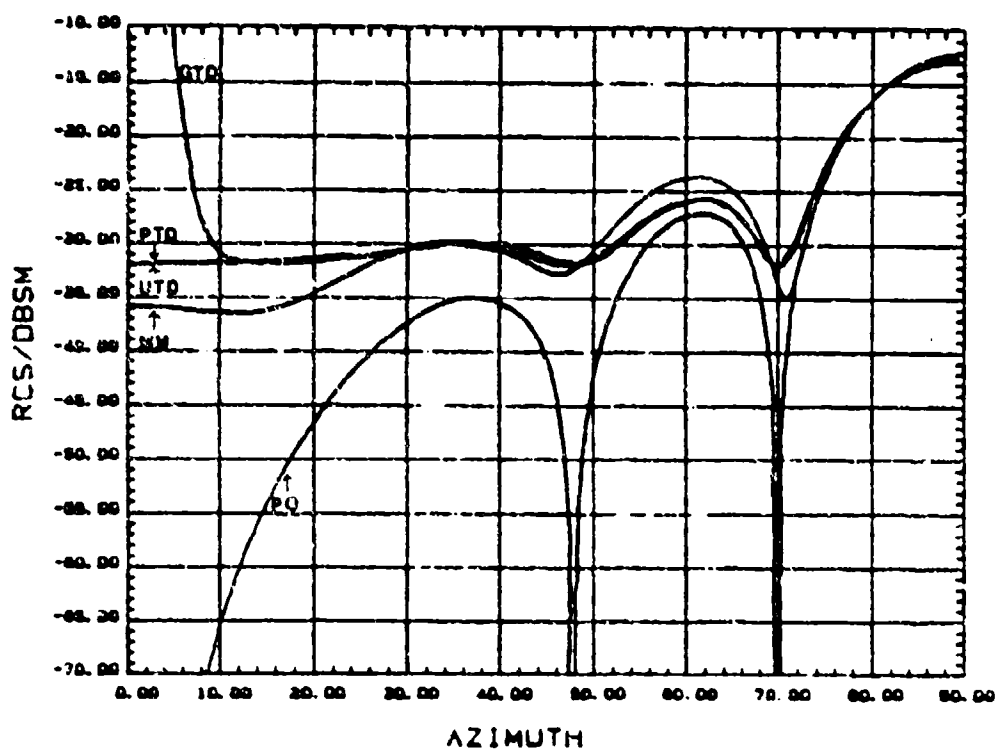(V.P.)
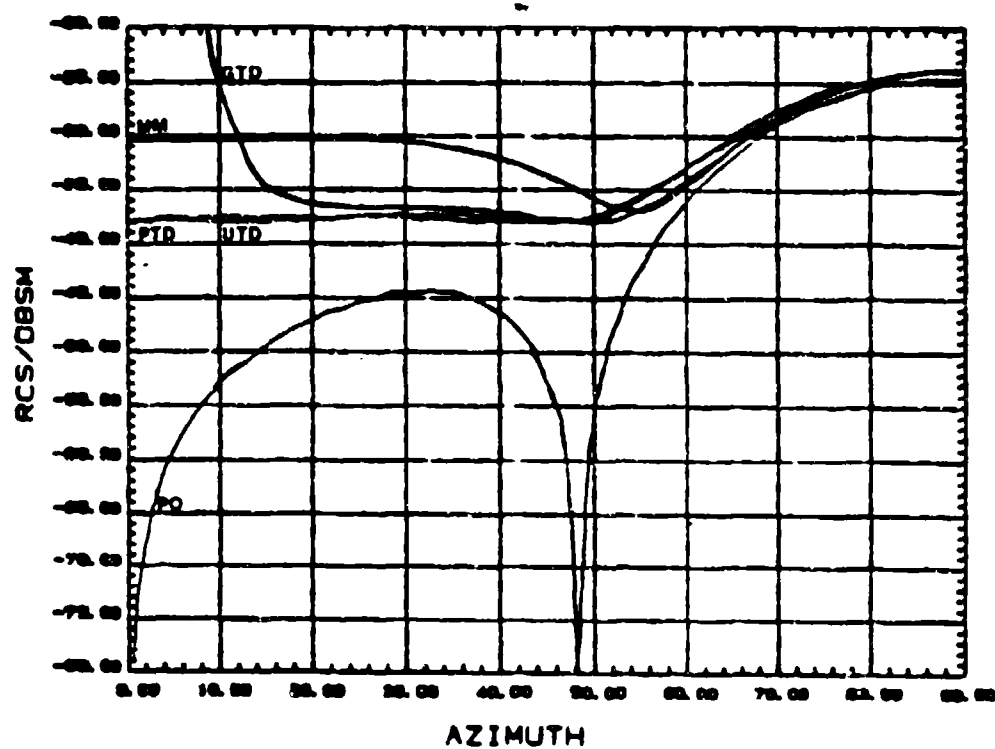
Fig A.4. Calculated RCS for 0.75 wavelength (2.25 cm) plate
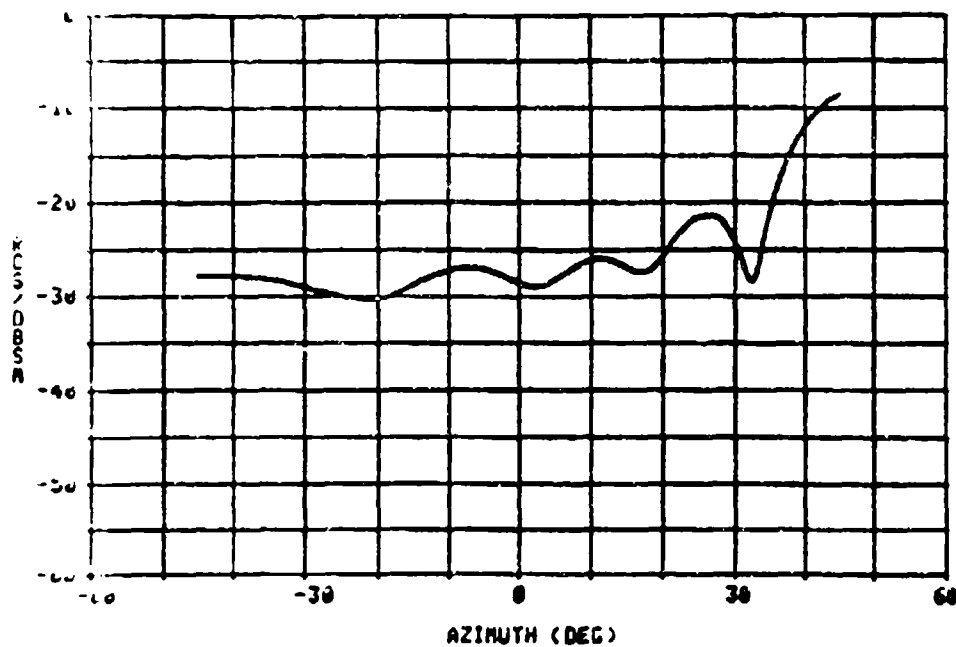(V.P.)

A-2
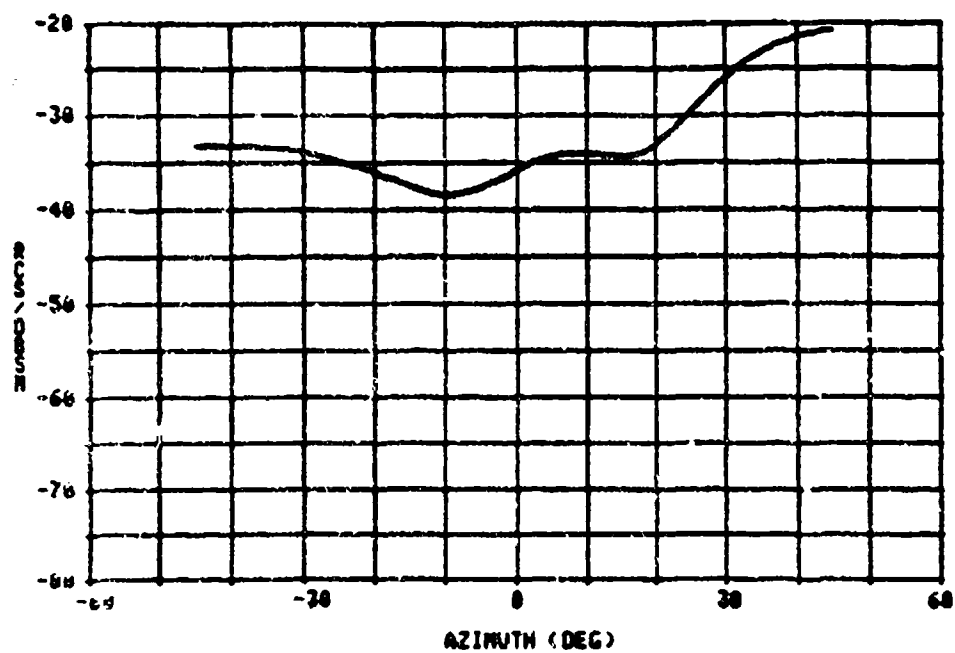
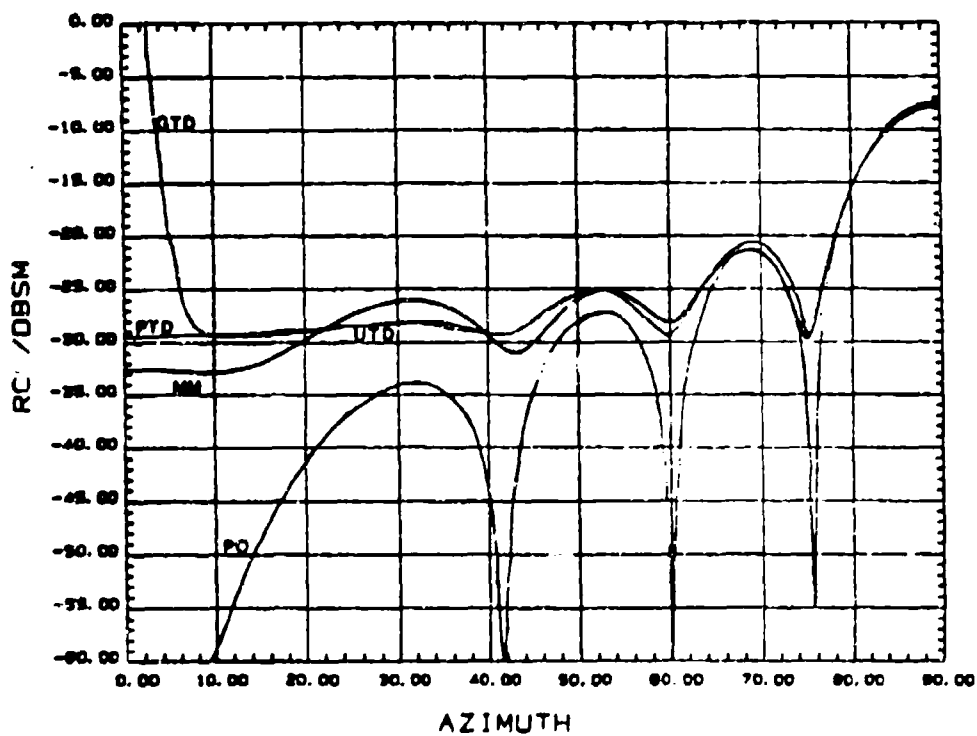Fig A.5. RCS measurement of 1.0 wavelength (3.0 cm) plate
(V.P.)
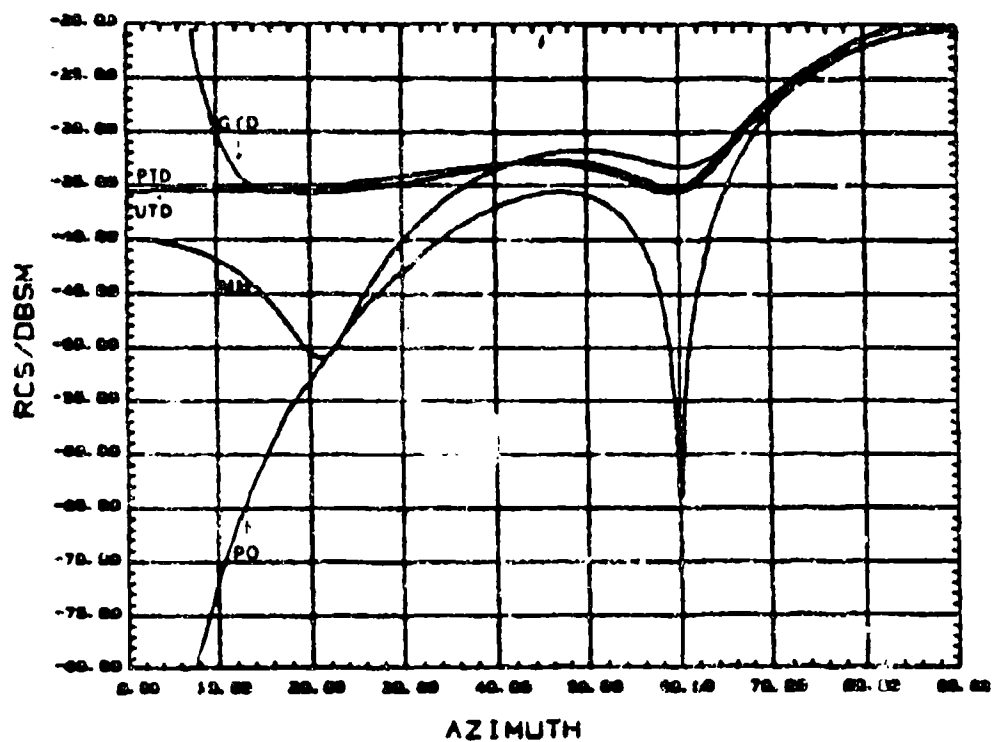
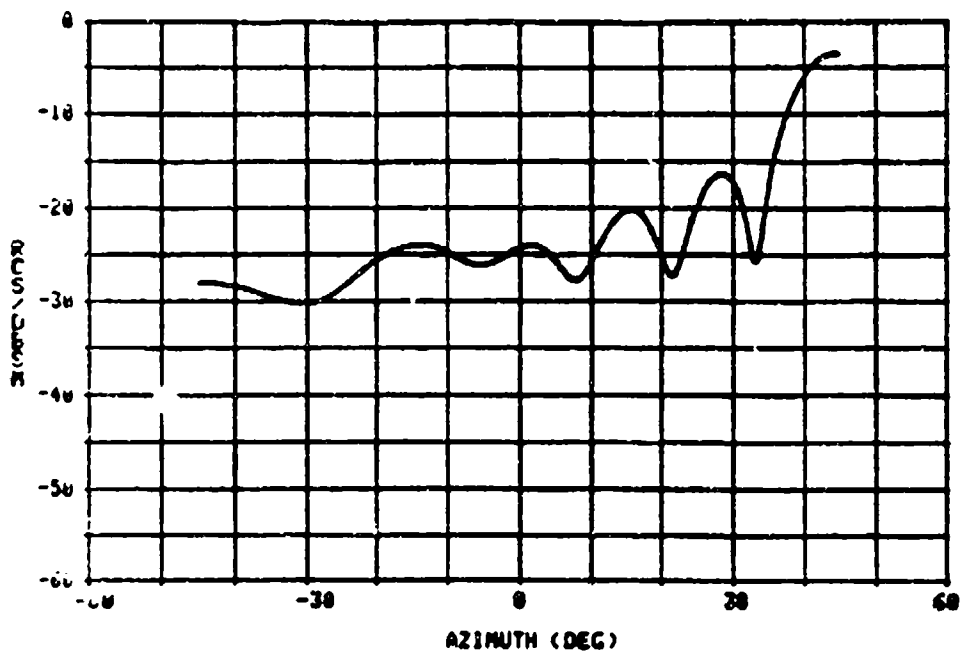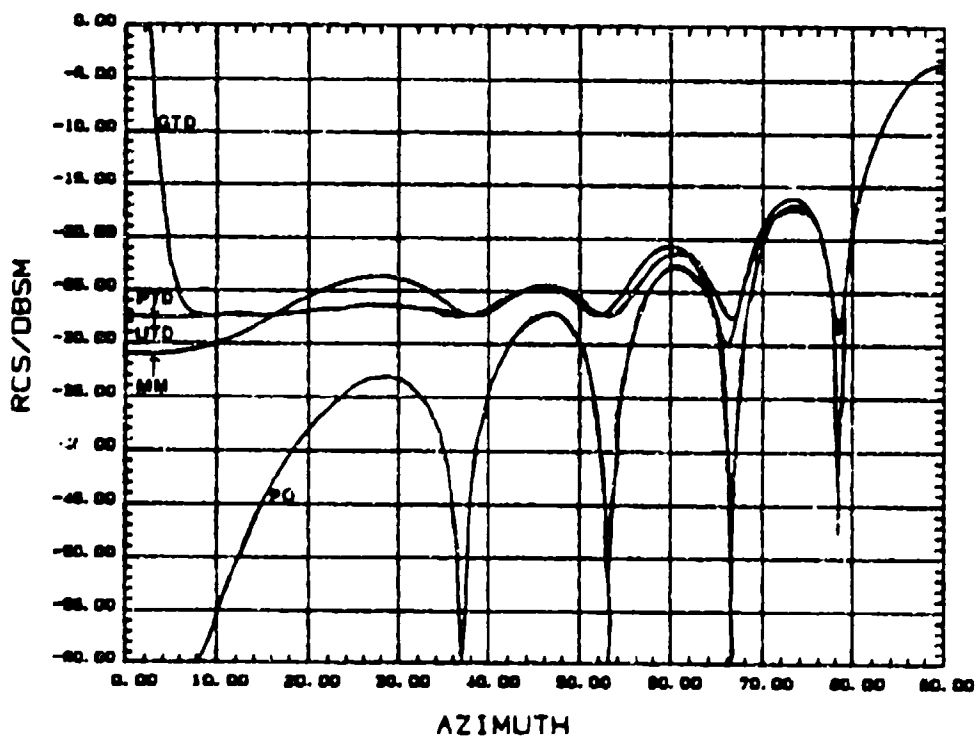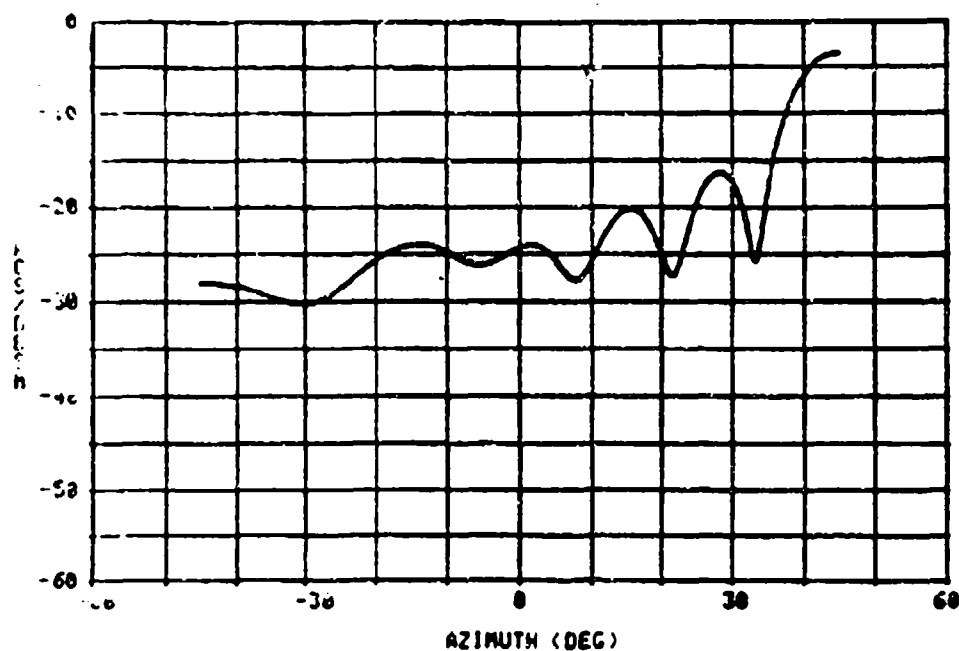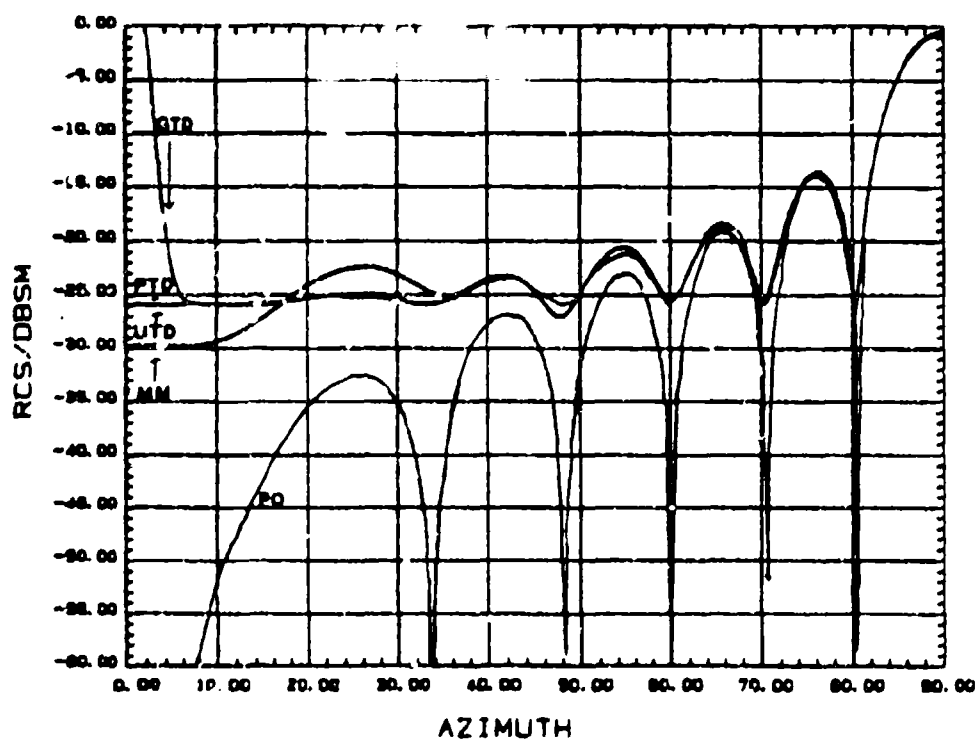Fig A.6. Calculated RCS for 1.0 wavelength (3.0 cm) plate
(V.P.)

A-3
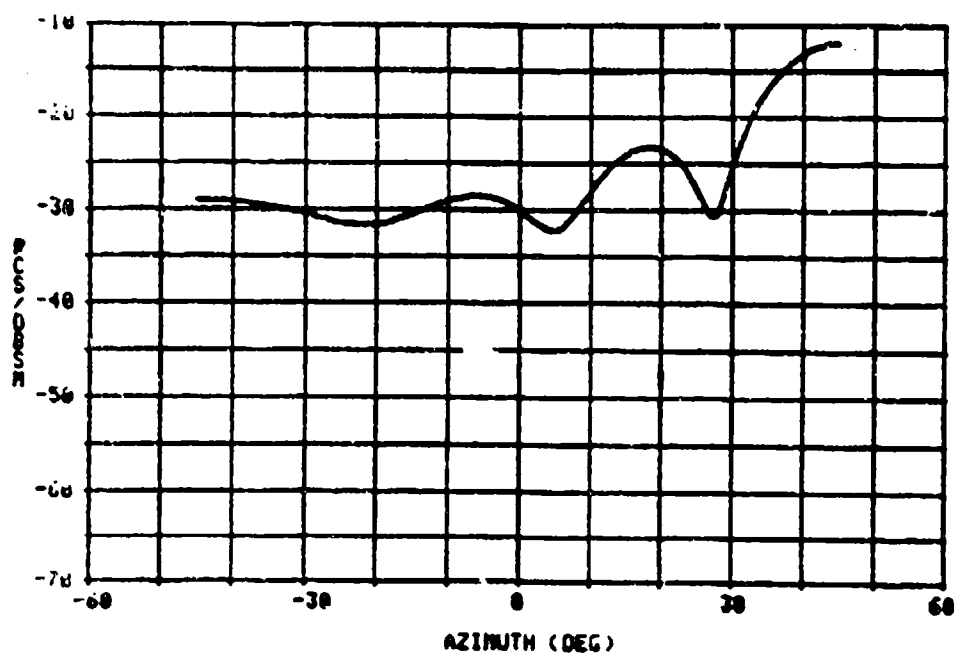
Fig A.7. RCS measurement of 1.5 wavelength (4.5 cm) plate (V.P.)

Fig A.8. Calculated RCS for 1.5 wavelength (4.5 cm) plate (V.P.)

A-4

Fig A.9.   RCS measurement of 2.0 wavelength (6.0 cm) plate
(V.P.)

Fig A.10.   Calculated RCS for 2.0 wavelength (6.0 cm) plate
(V.P.)

A-5

Fig A.11. RCS measurement of 2.5 wavelength (7.5 cm) plate
(V.P.)

Fig A.12. Calculated RCS for 2.5 wavelength (7.5 cm) plate
(V.P.)

Fig A.13. RCS measurement of 3.0 wavelength (9.0 cm) plate
(V.P.)

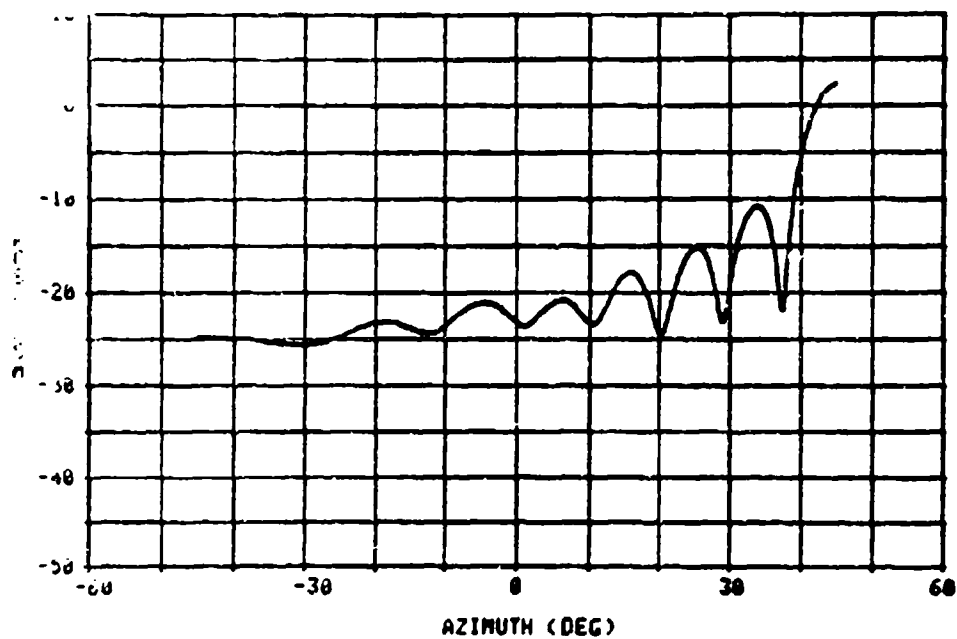Fig A.14. Calculated RCS for 3.0 wavelength (9.0 cm) plate
(V.P.)

A-7

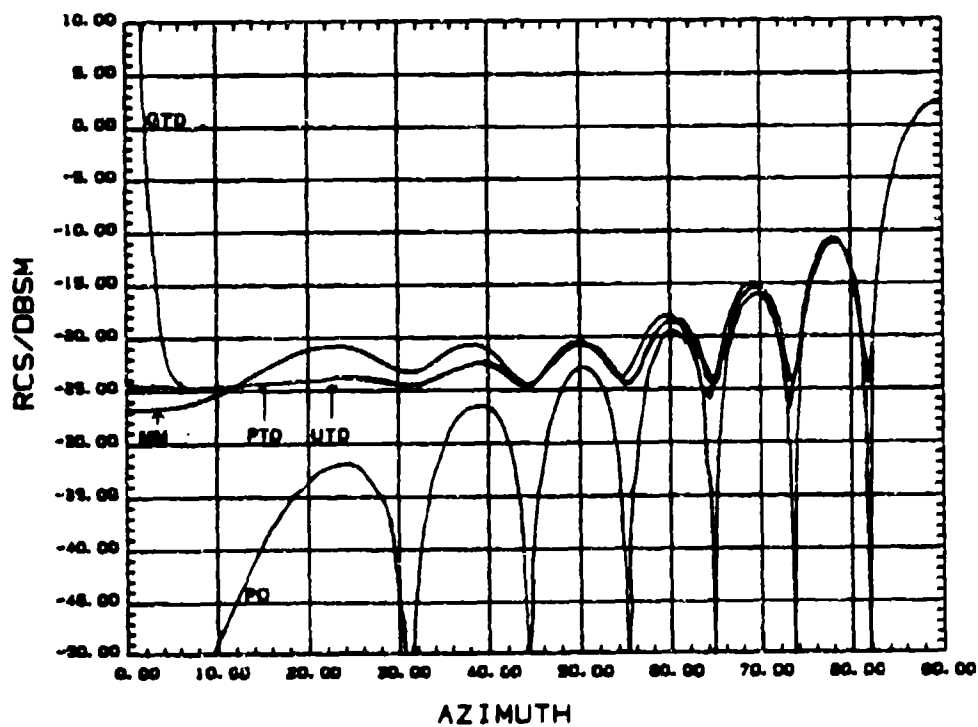Fig A.15.   RCS measurement of 3.5 wavelength (10.5 cm) plate
(V.P.)

Fig A.16.   Calculated RCS for 3.5 wavelength (10.5 cm) plate
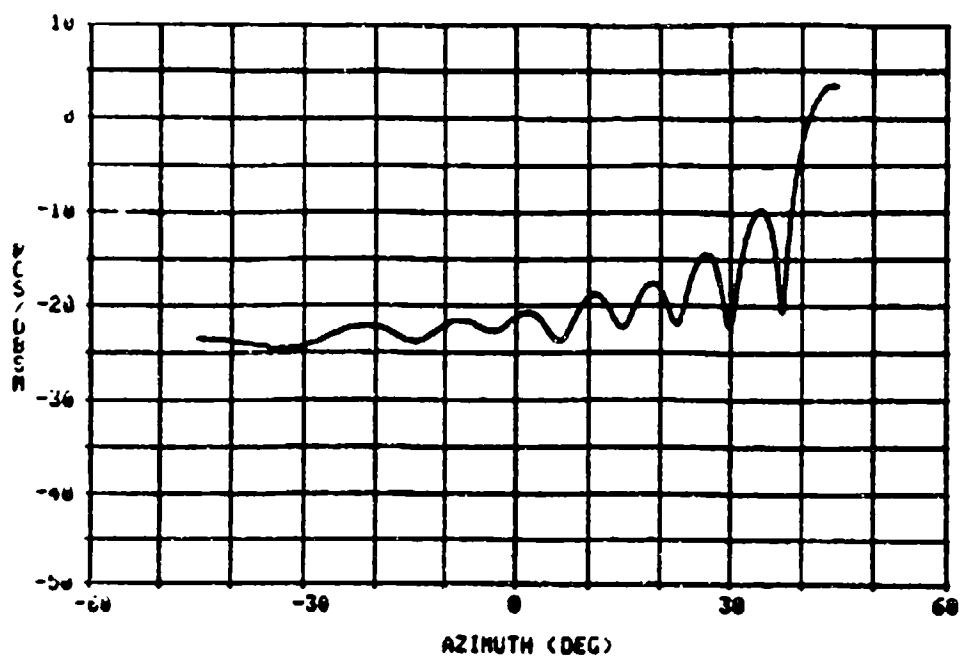(V.P.)

A-8

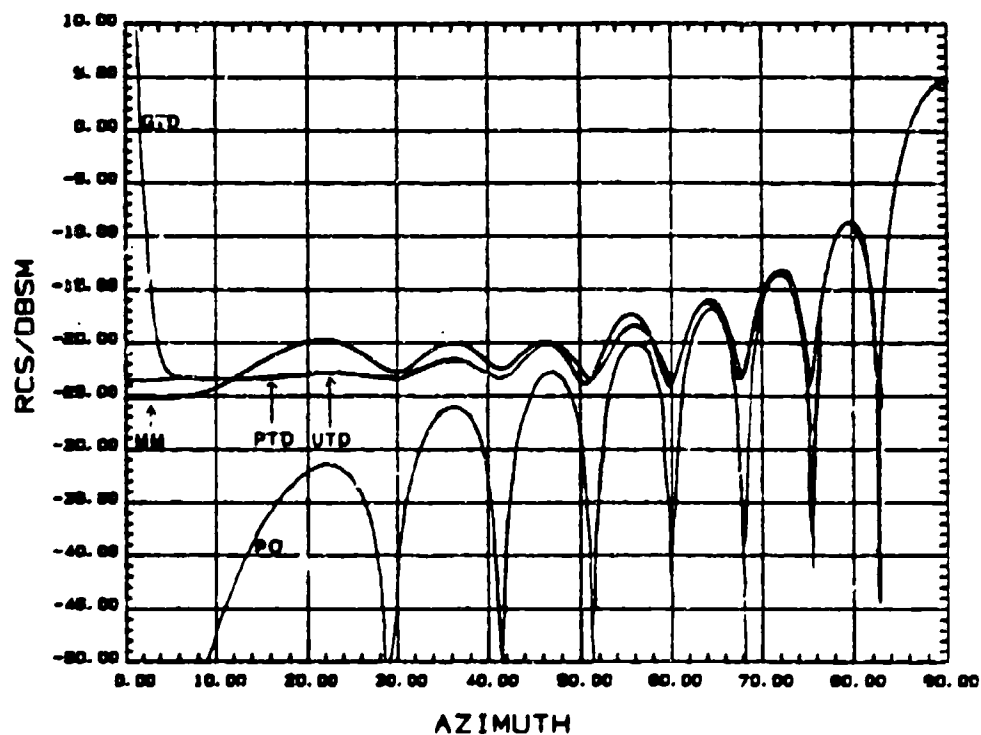Fig A.17.   RCS measurement of 4.0 wavelength (12.0 cm) plate
(V.P.)

Fig A.18.   Calculated RCS for 4.0 wavelength (12.0 cm) plate
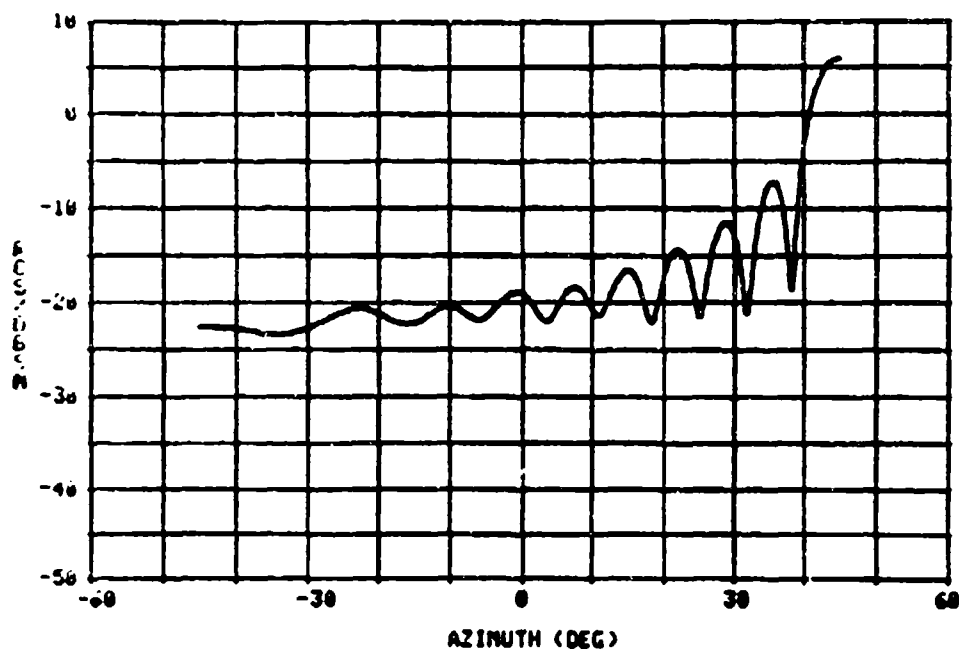(V.P.)

A-9

Fig A.19. RCS measurement of 4.5 wavelength (13.5 cm) plate
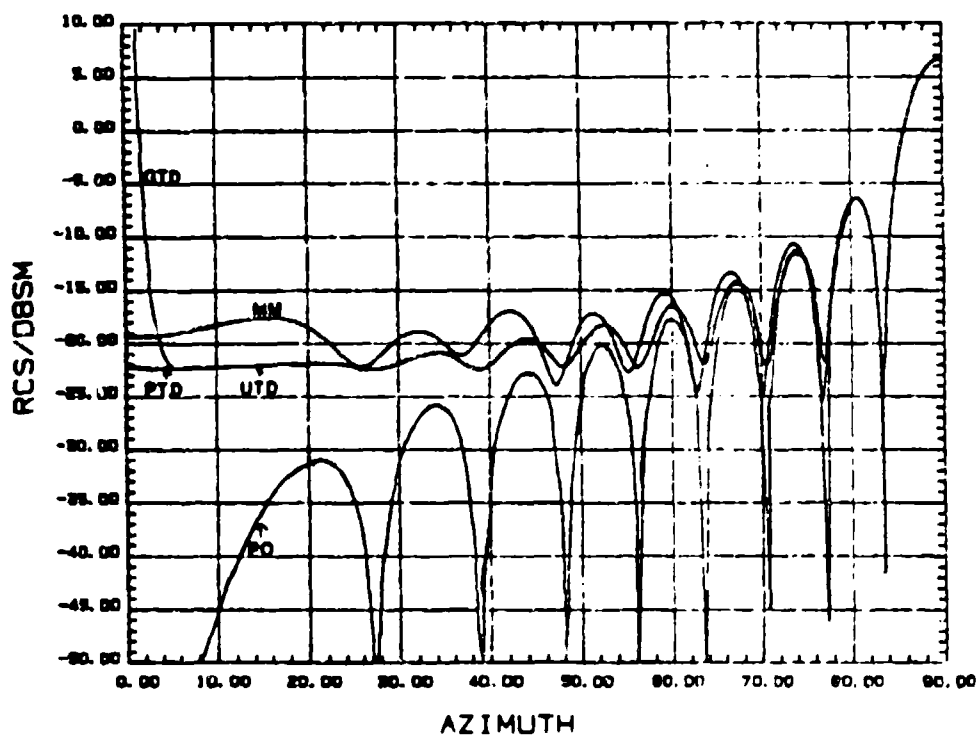(V.P.)

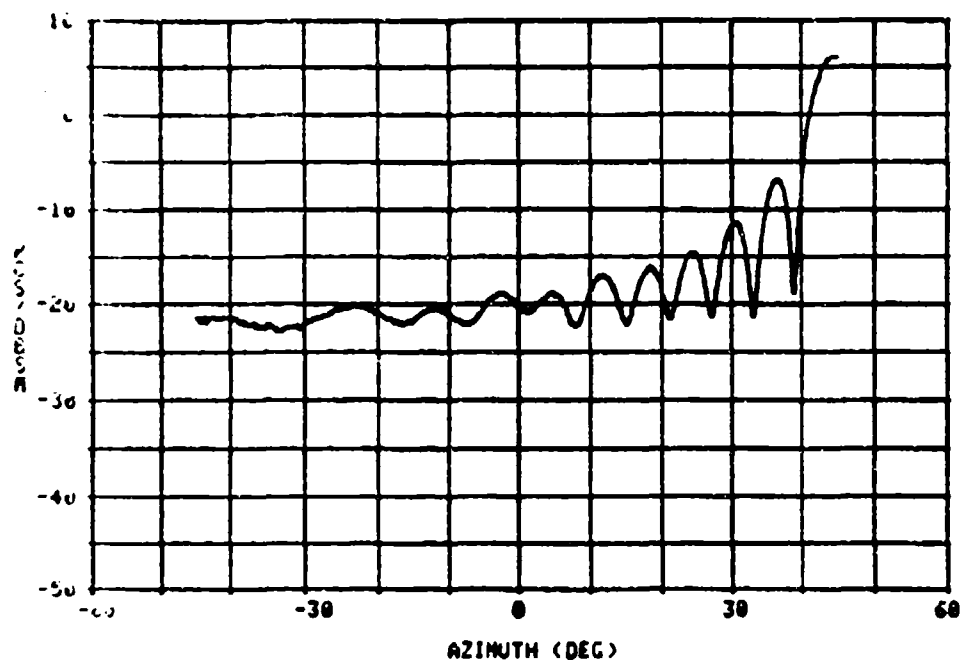Fig A.20. Calculated RCS for 4.5 wavelength (13.5 cm) plate
(V.P.)

Fig A.21.   RCS measurement of 5.0 wavelength (15.0 cm) plate
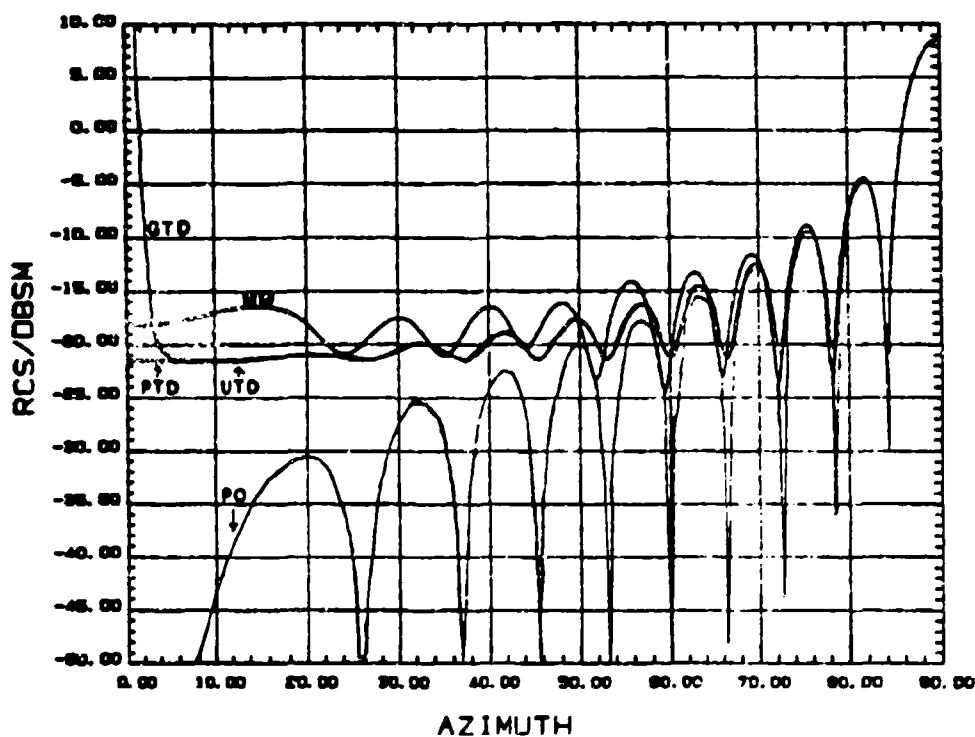(V.P.)

Fig A.22.   Calculated RCS for 5.0 wavelength (15.0 cm) plate
(V.P.)

Fig A.23.   RCS measurement of 5.5 wavelength (16.5 cm) plate
(V.P.)

Fig A.24.   Calculated RCS for 5.5 wavelength (16.5 cm) plate
(V.P.)

A-12

Fig A.25. RCS measurement of 6.0 wavelength (18.0 cm) plate
(V.P.)

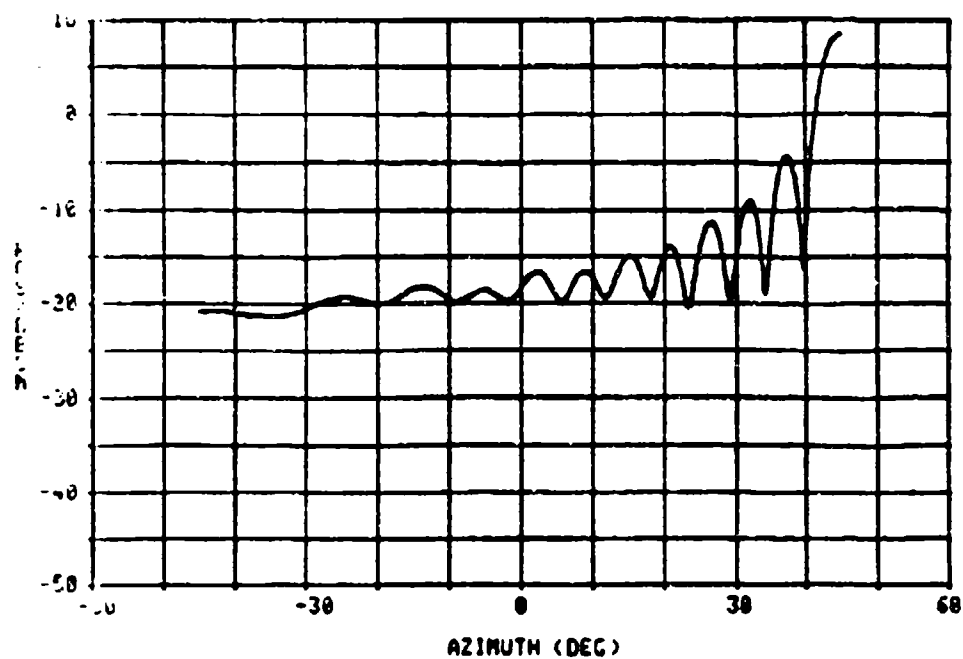Fig A.26. Calculated RCS for 6.0 wavelength (18.0 cm) plate
(V.P.)

A-13
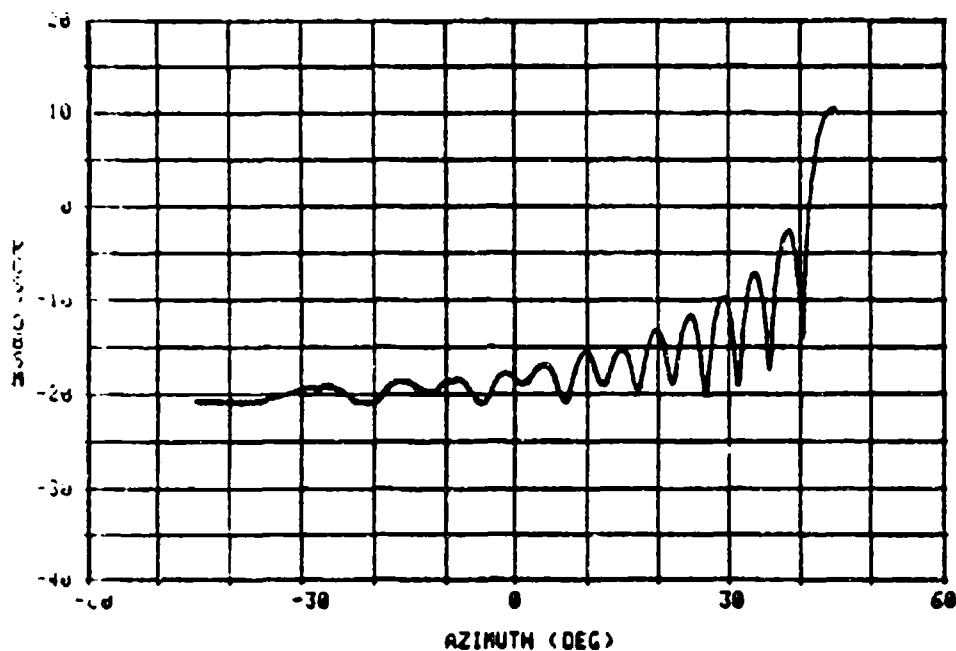
Fig A.27. RCS measurement of 6.5 wavelength (19.5 cm) plate (V.P.)

Fig A.28. Calculated RCS for 6.5 wavelength (19.5 cm) plate (V.P.)

A-14

Fig A.29. RCS measurement of 0.5 wavelength (1.5 cm) plate
(H.P.)
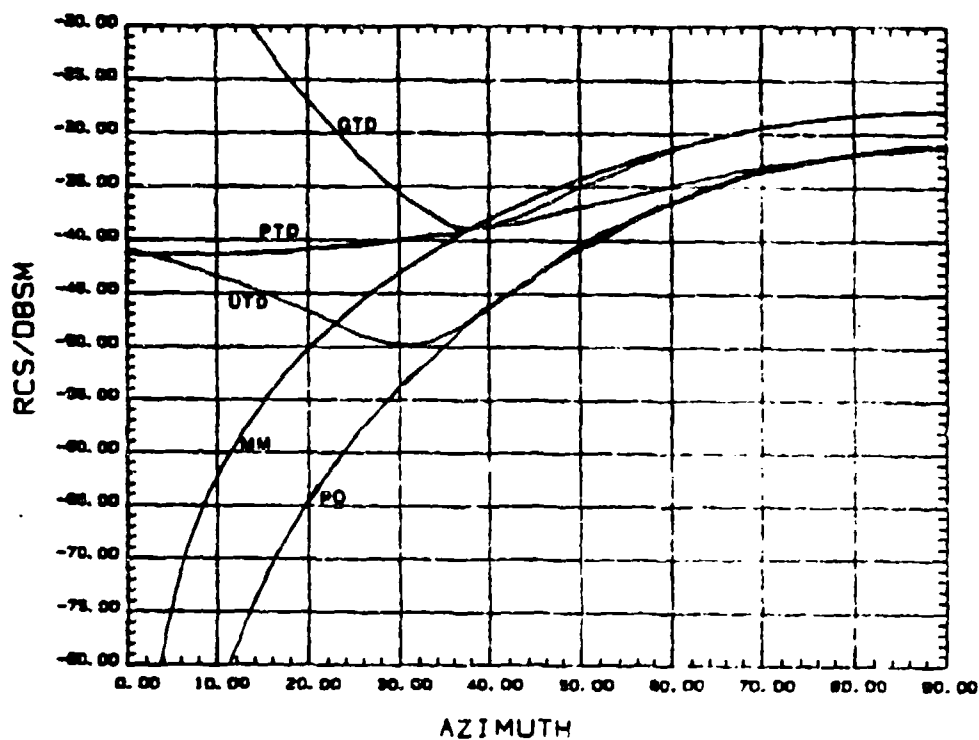
Fig A.30. Calculated RCS for 0.5 wavelength (1.5 cm) plate
(H.P.)

A-15

Fig A.31.   RCS measurement of 0.75 wavelength (2.25 cm) plate
(H.P.)

Fig A.32.   Calculated RCS for 0.75 wavelength (2.25 cm) plate
(H.P.)

A-16
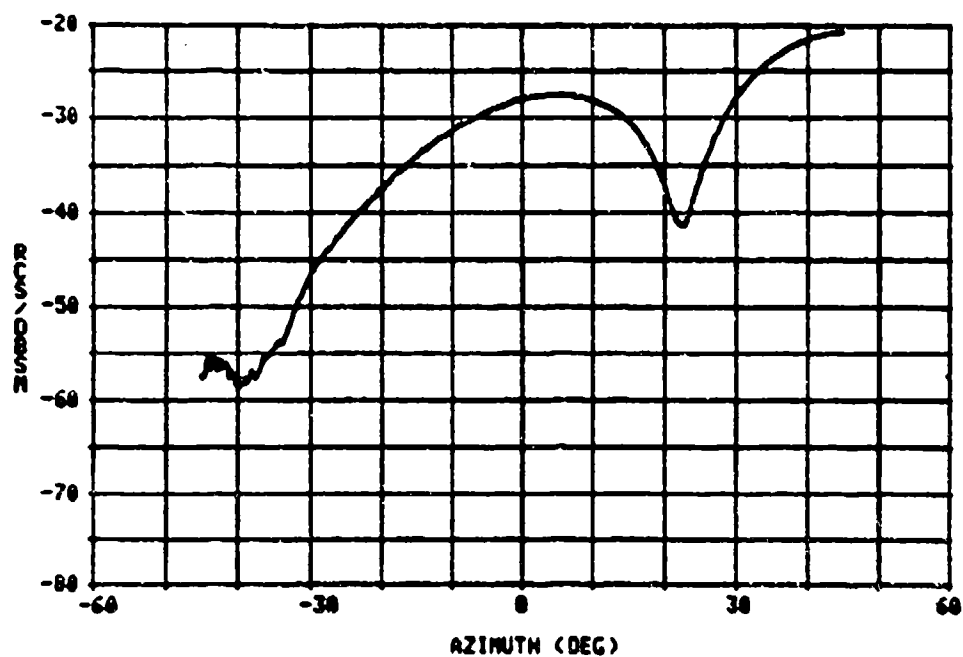
Fig A.33.   RCS measurement of 1.0 wavelength (3.0 cm) plate
(H.P.)
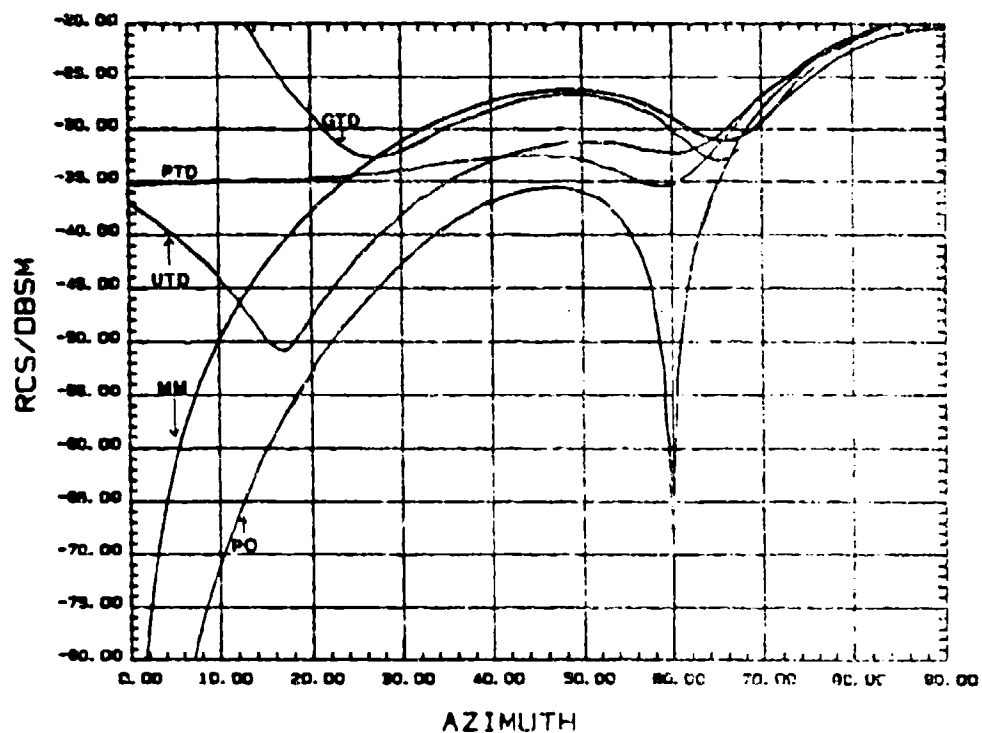
Fig A.34.   Calculated RCS for 1.0 wavelength (3.0 cm) plate
(H.P.)

A-17

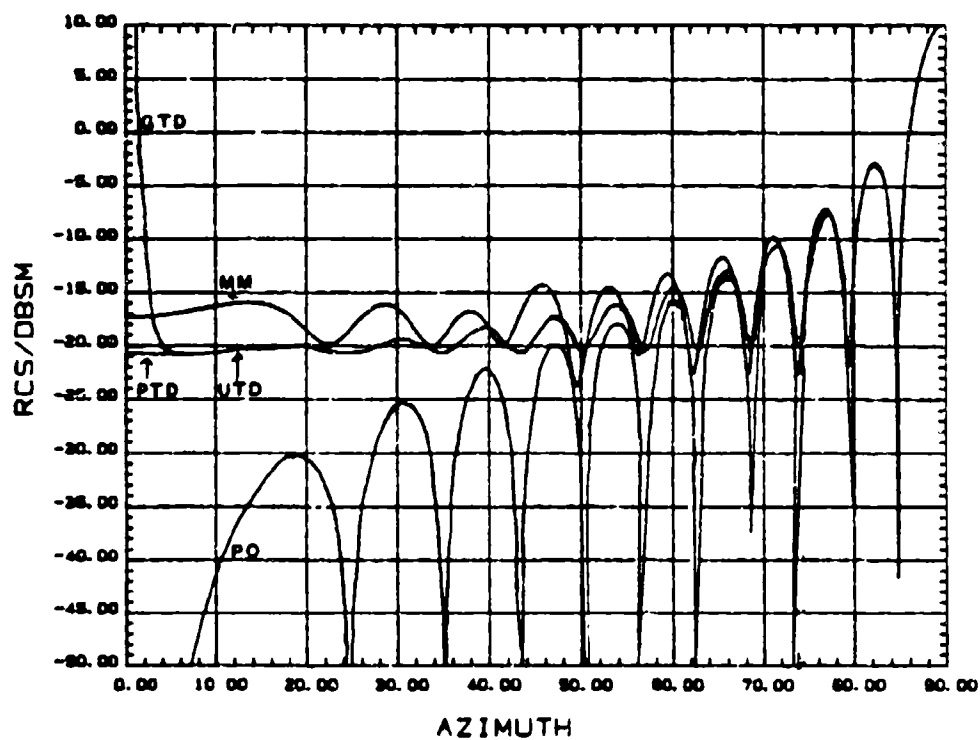Fig A.35. RCS measurement of 1.5 wavelength (4.5 cm) plate
(H.P.)

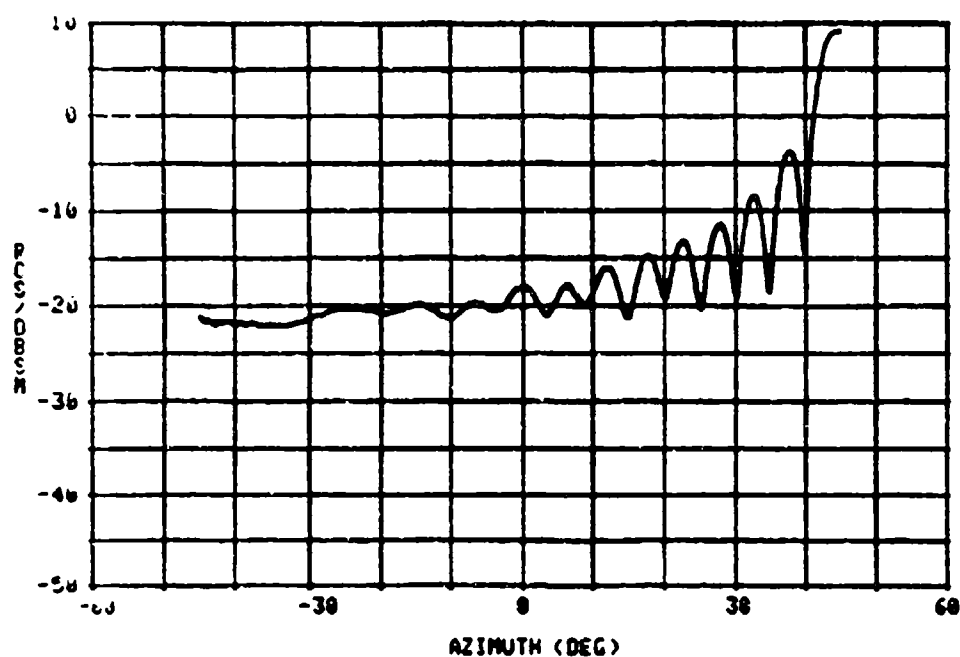Fig A.36. Calculated RCS for 1.5 wavelength (4.5 cm) plate
(H.P.)

A-18

Fig A.37.   RCS measurement of 2.0 wavelength (6.0 cm) plate
(H.P.)

Fig A.38.   Calculated RCS for 2.0 wavelength (6.0 cm) plate
(H.P.)

A-19
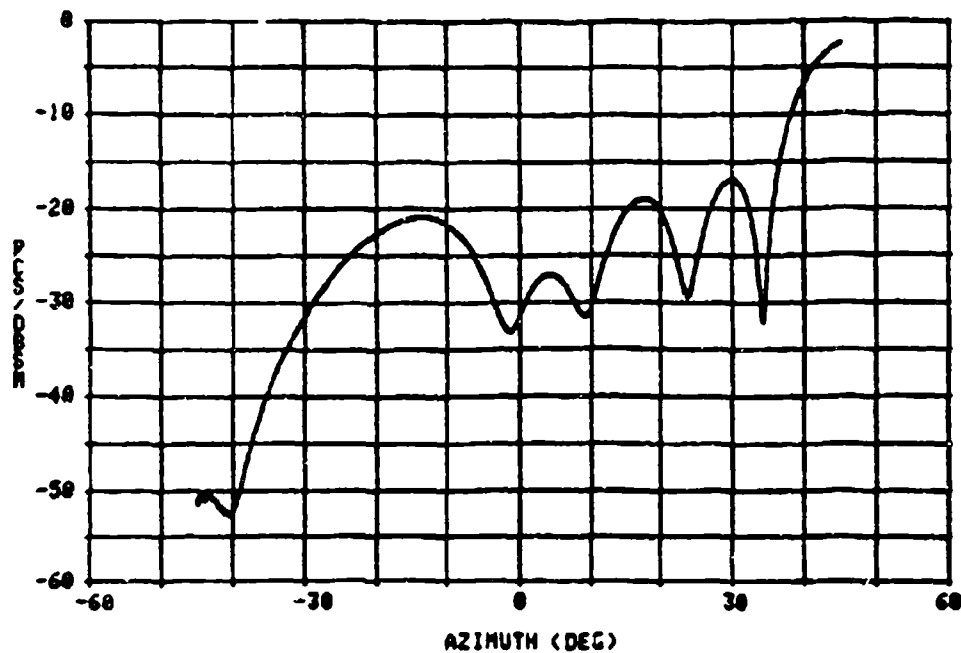
Fig A.39. RCS measurement of 2.5 wavelength (7.5 cm) plate
(H.P.)
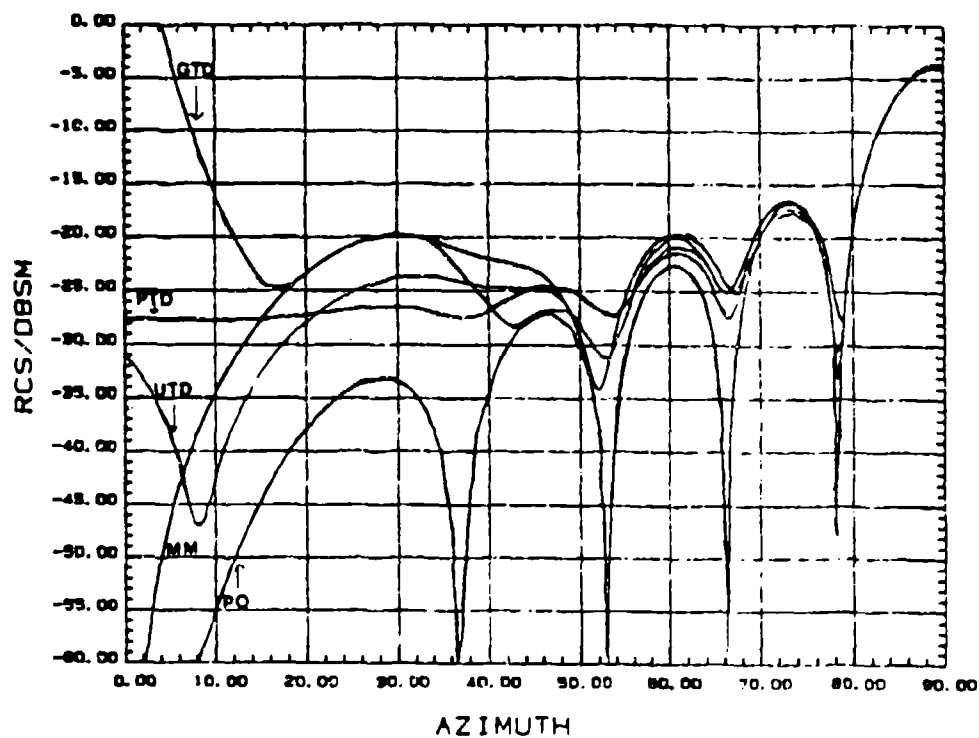
Fig A.40. Calculated RCS for 2.5 wavelength (7.5 cm) plate
(H.P.)
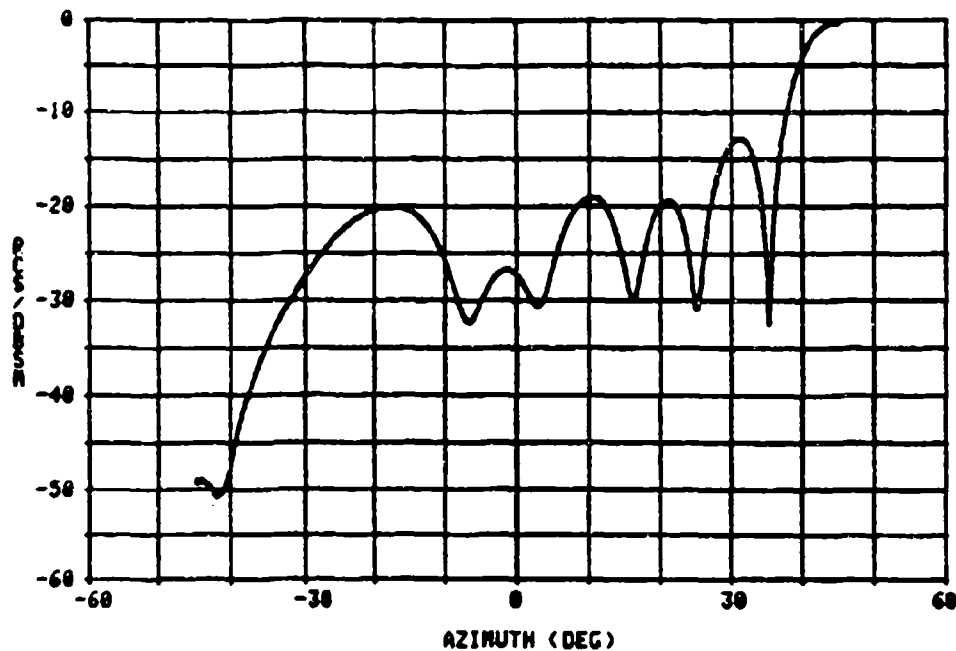
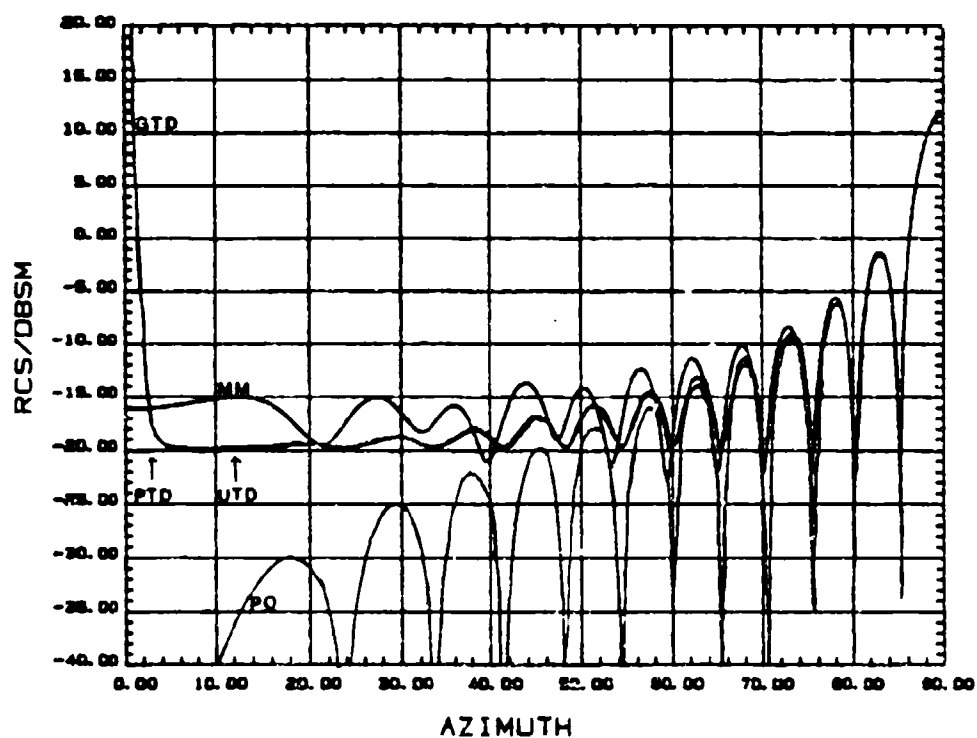Fig A.41. RCS measurement of 3.0 wavelength (9.0 cm) plate
(H.P.)
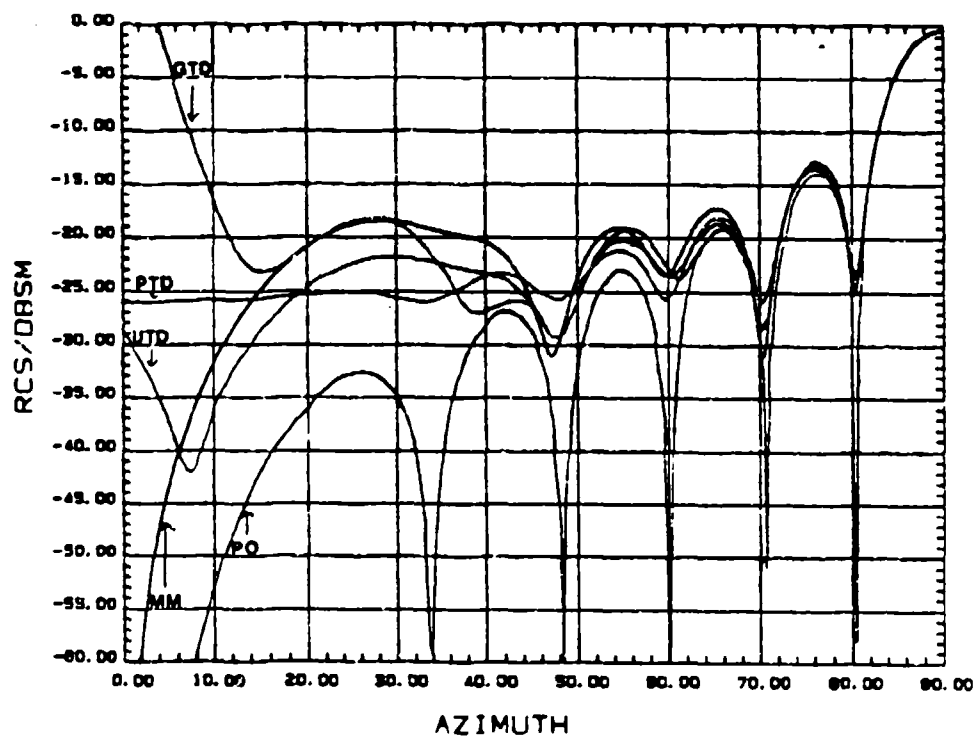
Fig A.42. Calculated RCS for 3.0 wavelength (9.0 cm) plate
(H.P.)
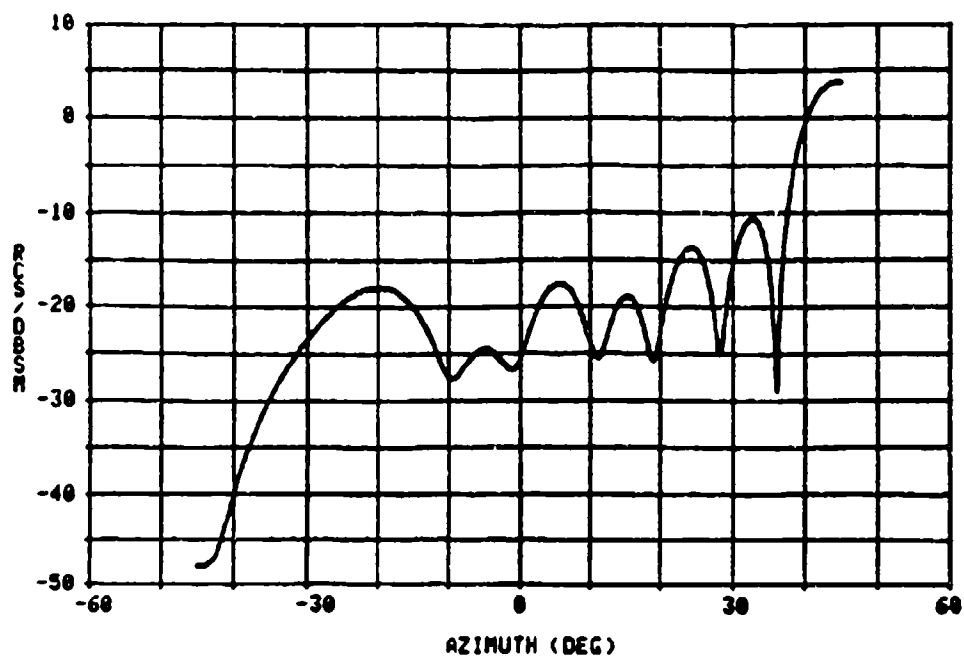
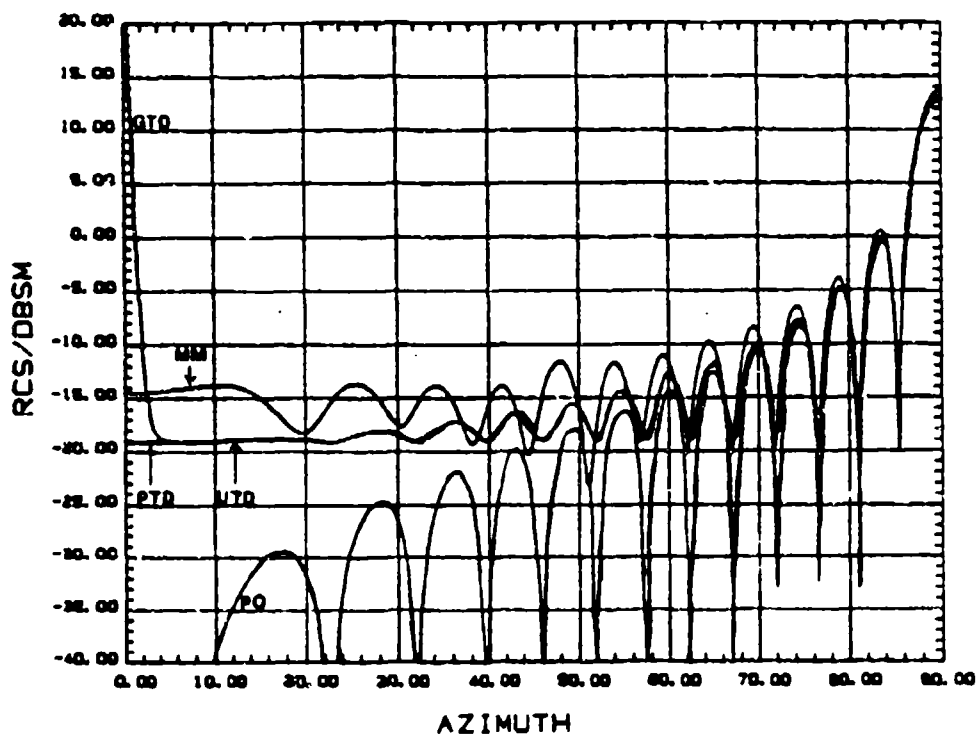Fig A.43.   RCS measurement of 3.5 wavelength (10.5 cm) plate
(H.P.)

AZIMUTH
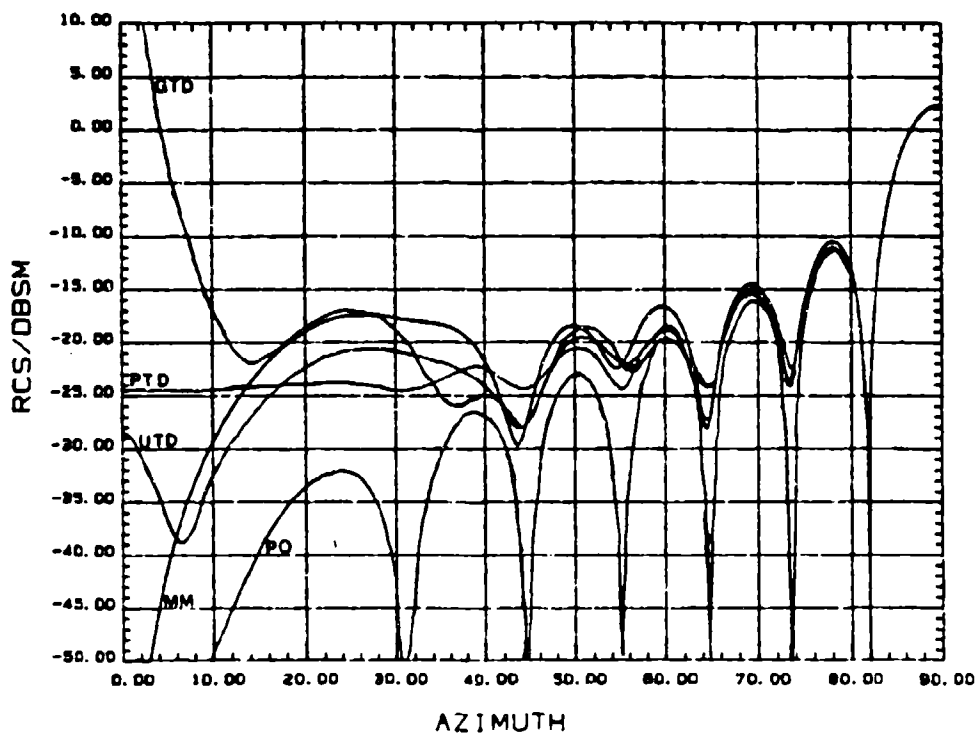
Fig A.44.   Calculated RCS for 3.5 wavelength (10.5 cm) plate
(H.P.)

A-22
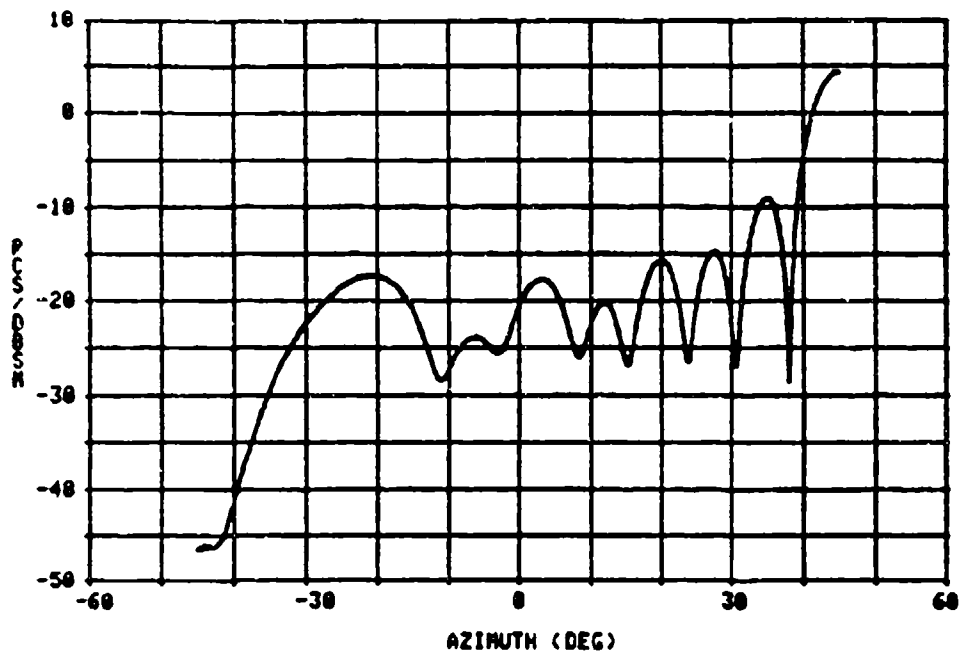
Fig A.45.   RCS measurement of 4.0 wavelength (12.0 cm) plate
(H.P.)
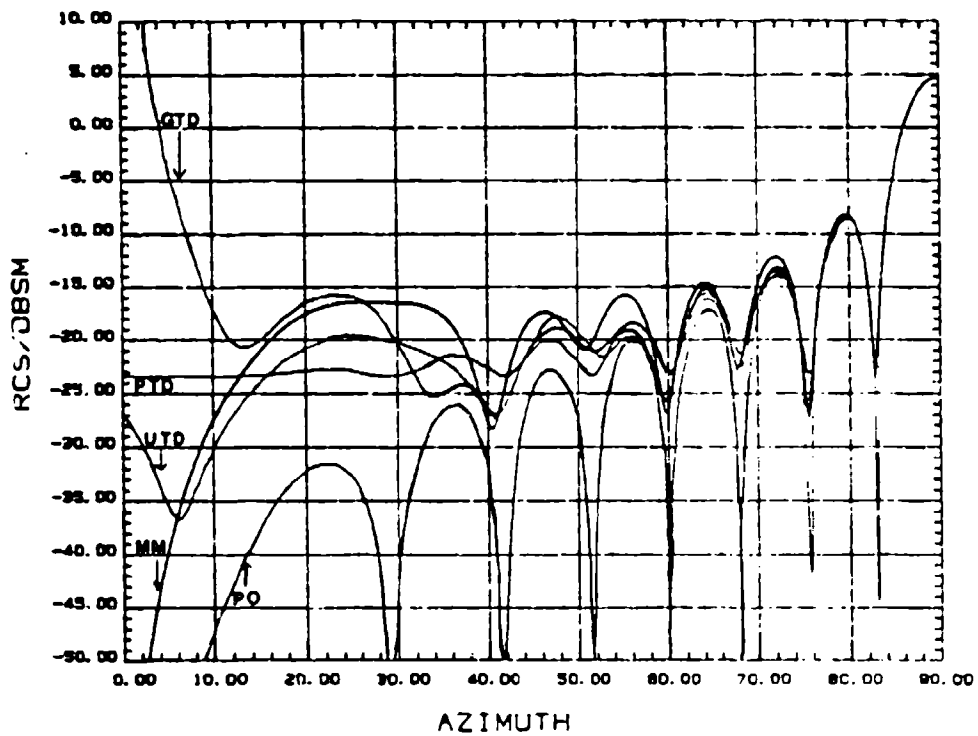
Fig A.46.   Calculated RCS for 4.0 wavelength (12.0 cm) plate
(H.P.)

A-23
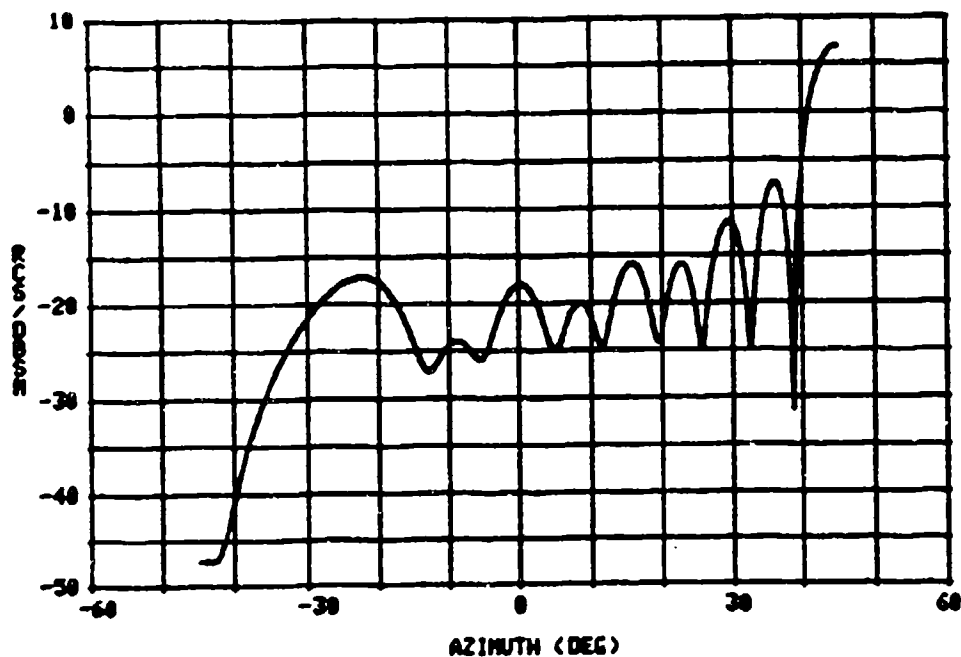
Fig A.47.   RCS measurement of 4.5 wavelength (13.5 cm) plate
(H.P.)
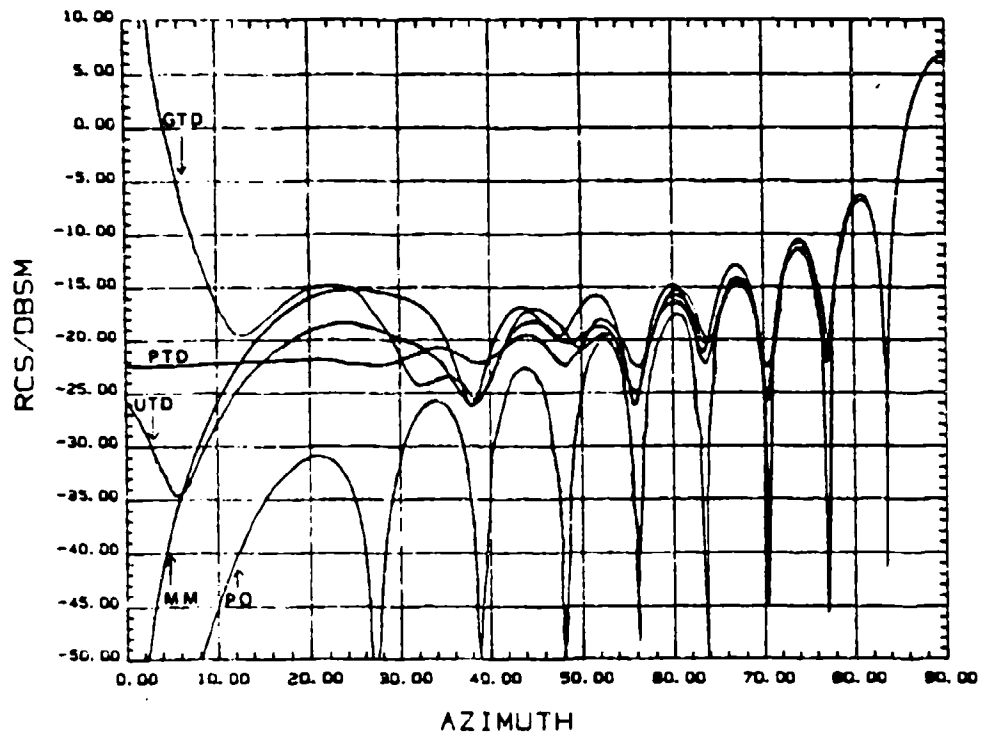
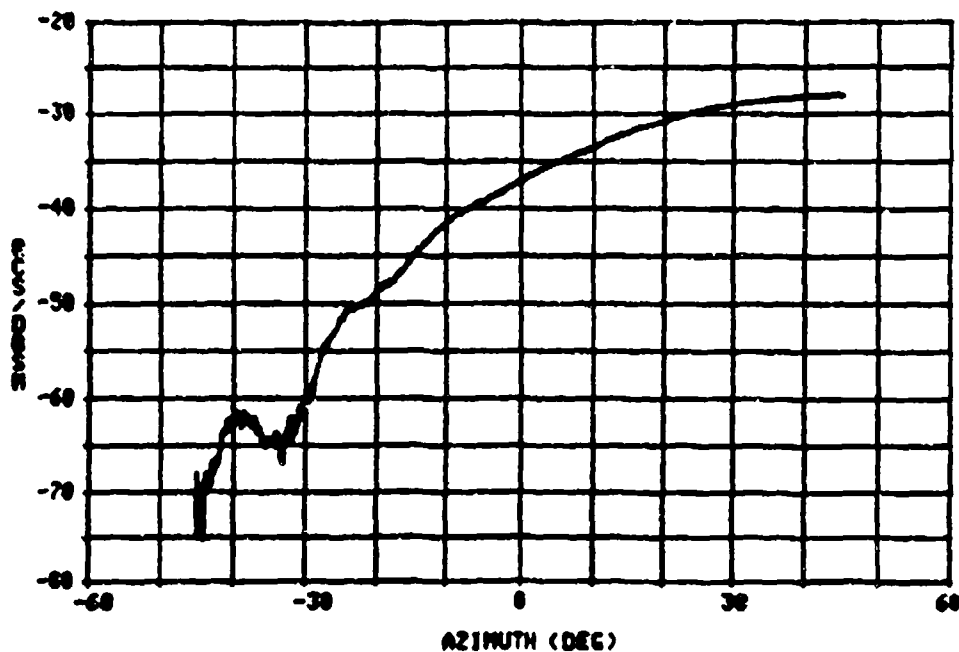Fig A.48.   Calculated RCS for 4.5 wavelength (13.5 cm) plate
(H.P.)

A-24
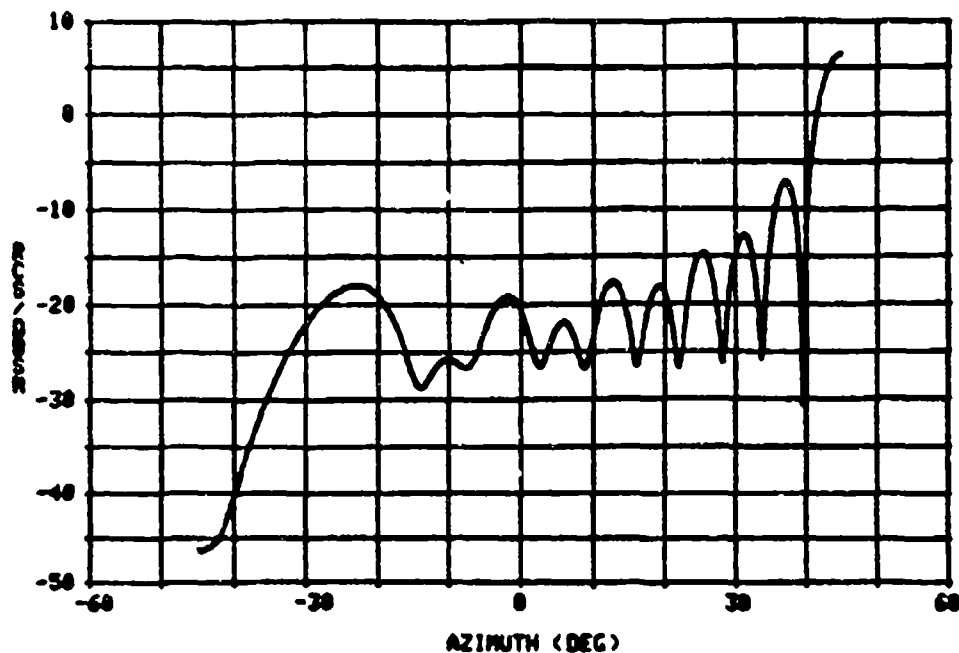
Fig A.49.   RCS measurement of 5.0 wavelength (15.0 cm) plate
(H.P.)
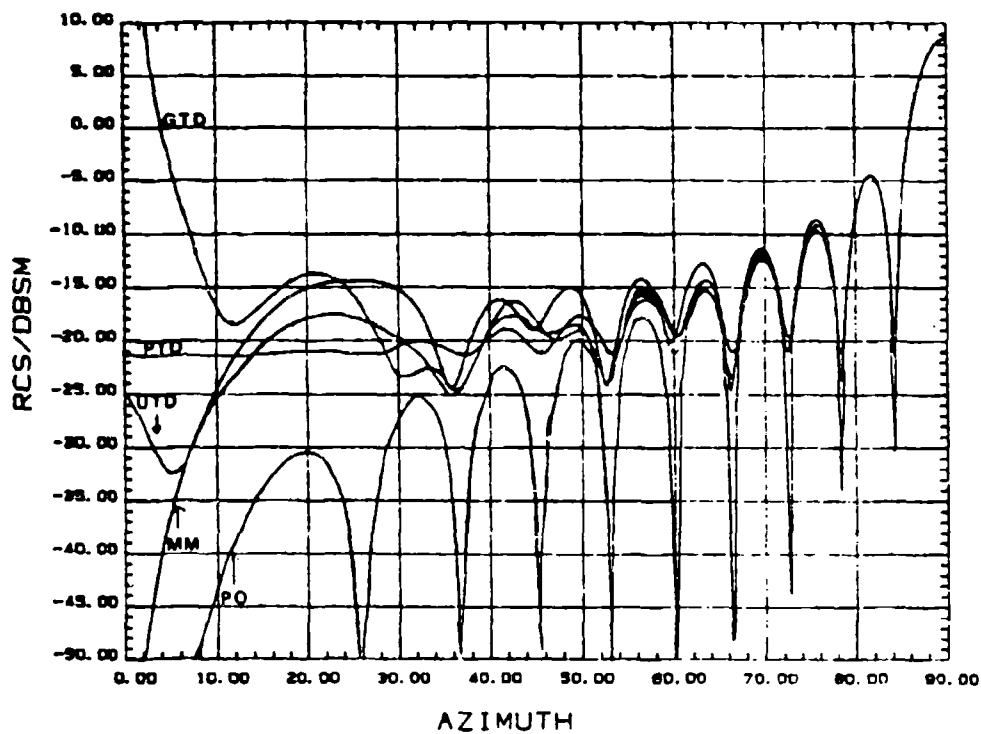
Fig A.50.   Calculated RCS for 5.0 wavelength (15.0 cm) plate
(H.P.)

A-25
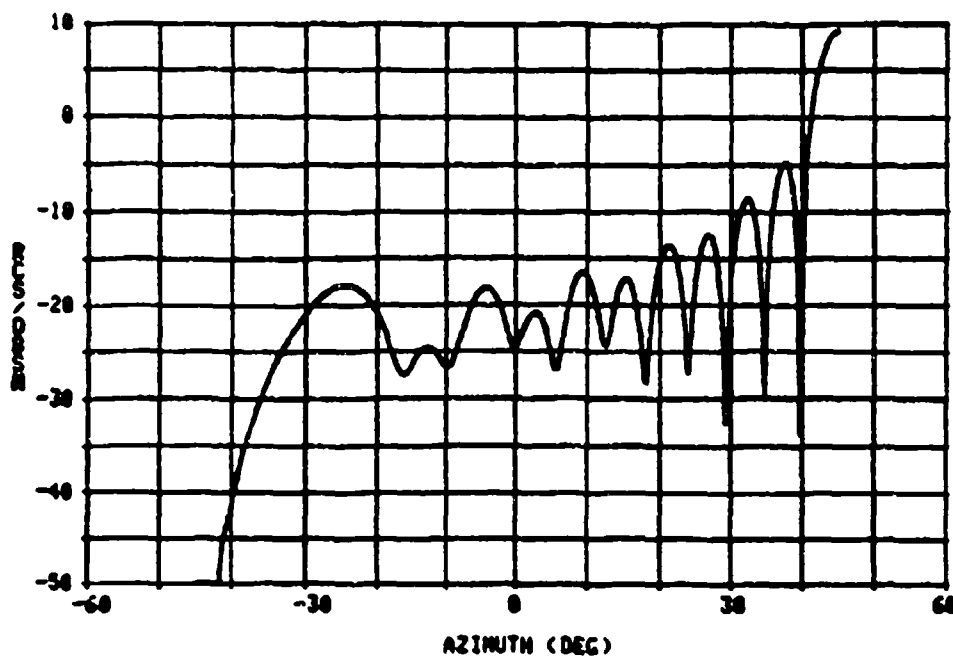
Fig A.51.   RCS measurement of 5.5 wavelength (16.5 cm) plate
(H.P.)
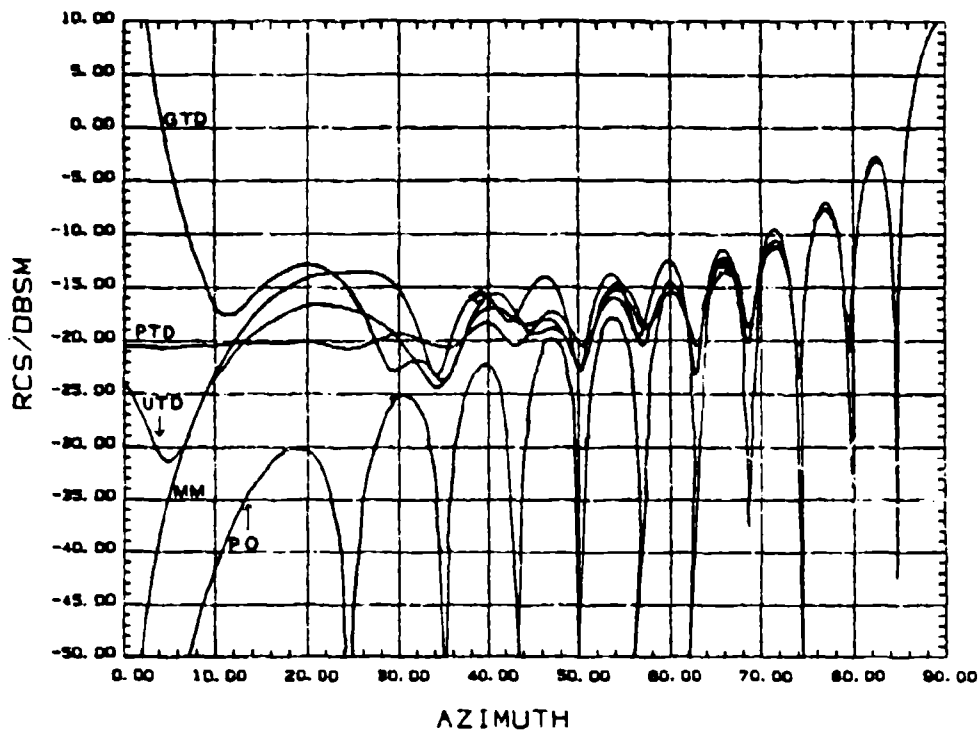
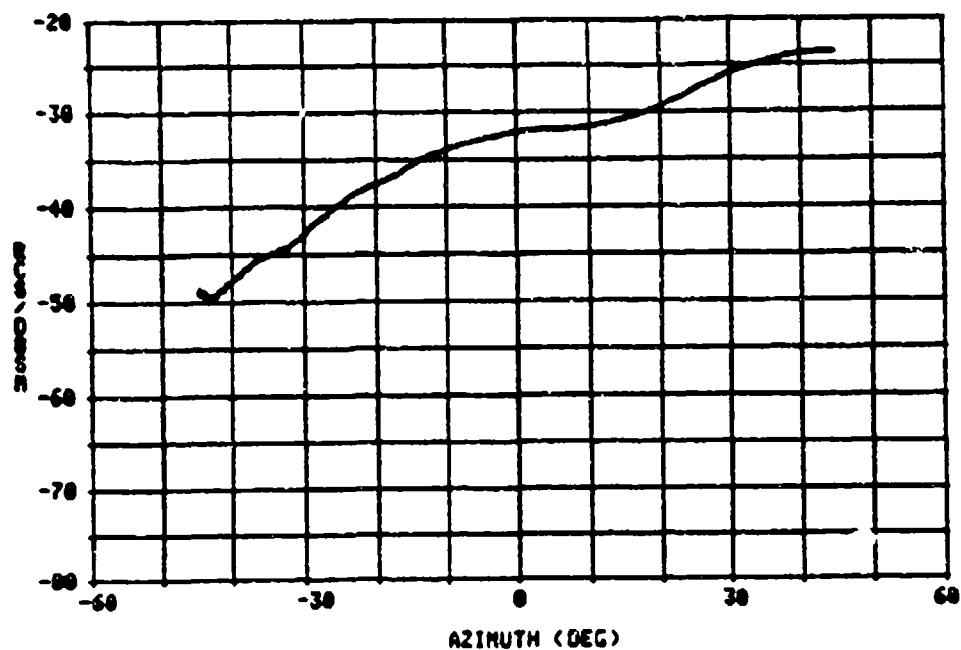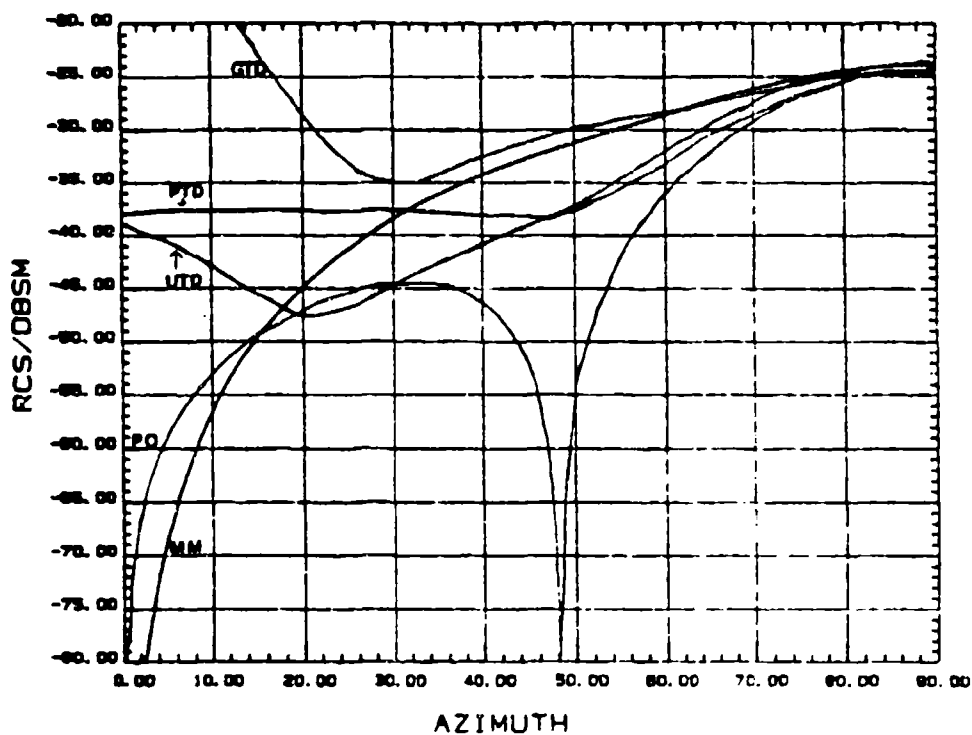Fig A.52.   Calculated RCS for 5.5 wavelength (16.5 cm) plate
(H.P.)

A-26
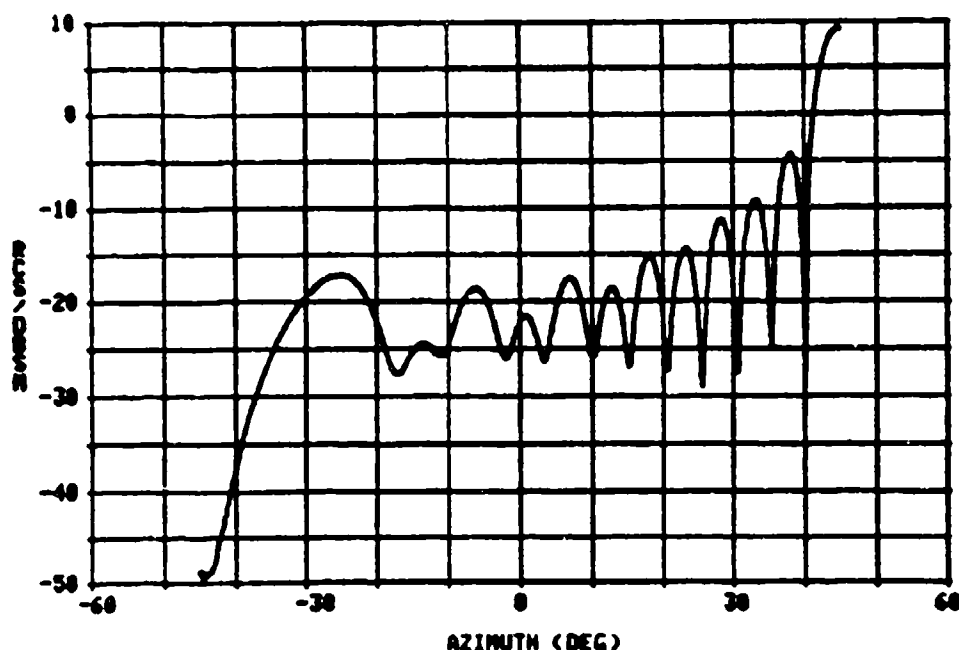
Fig A.53.   RCS measurement of 6.0 wavelength (18.0 cm) plate
(H.P.)
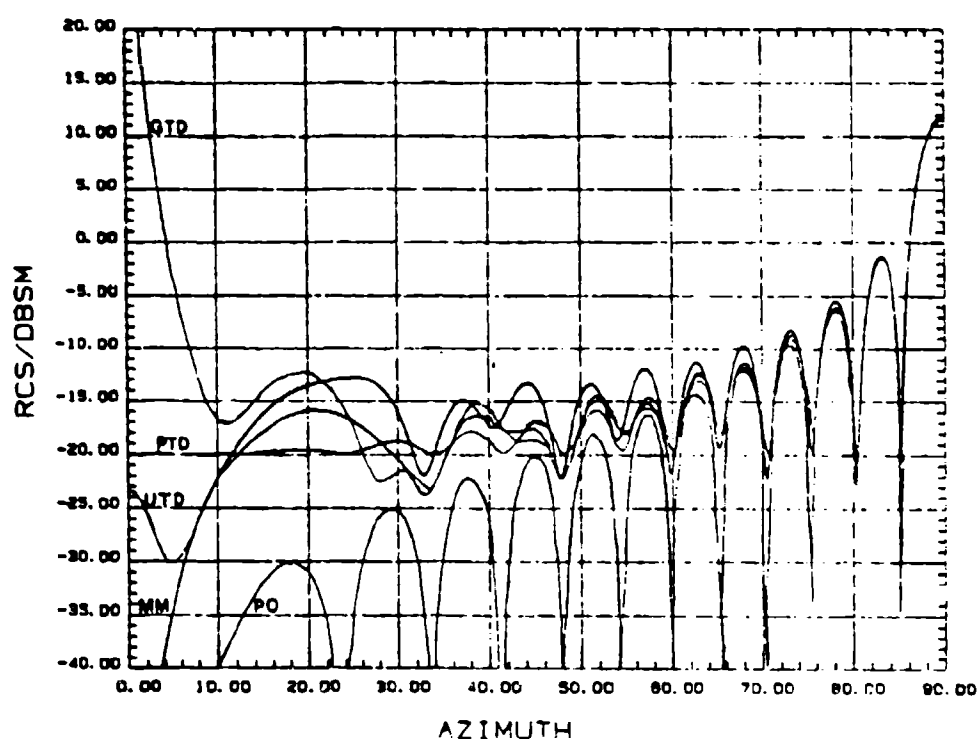
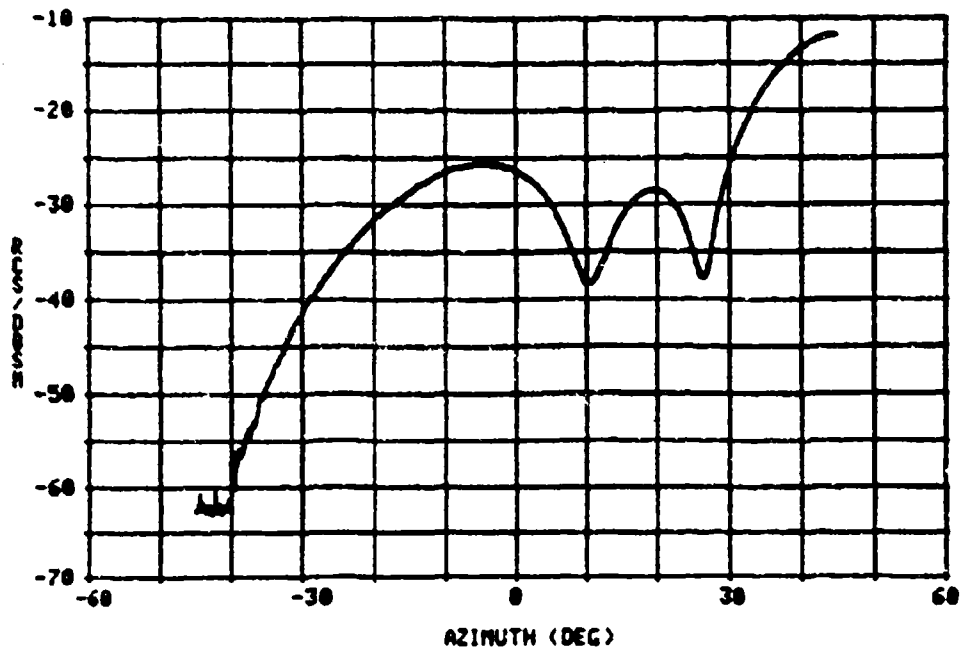Fig A.54.   Calculated RCS for 6.0 wavelength (18.0 cm) plate
(H.P.)

A-27
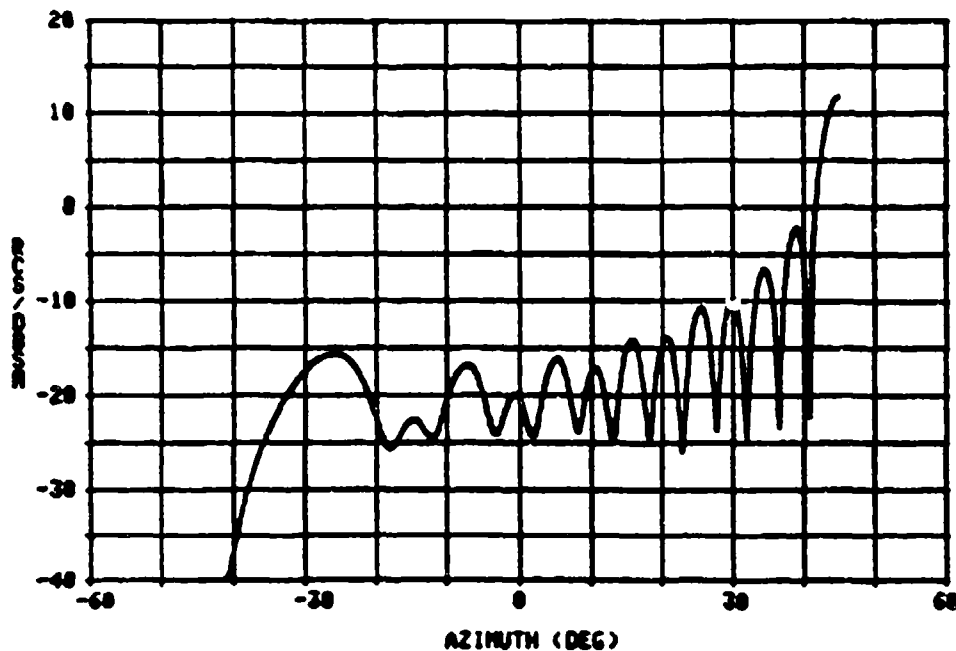
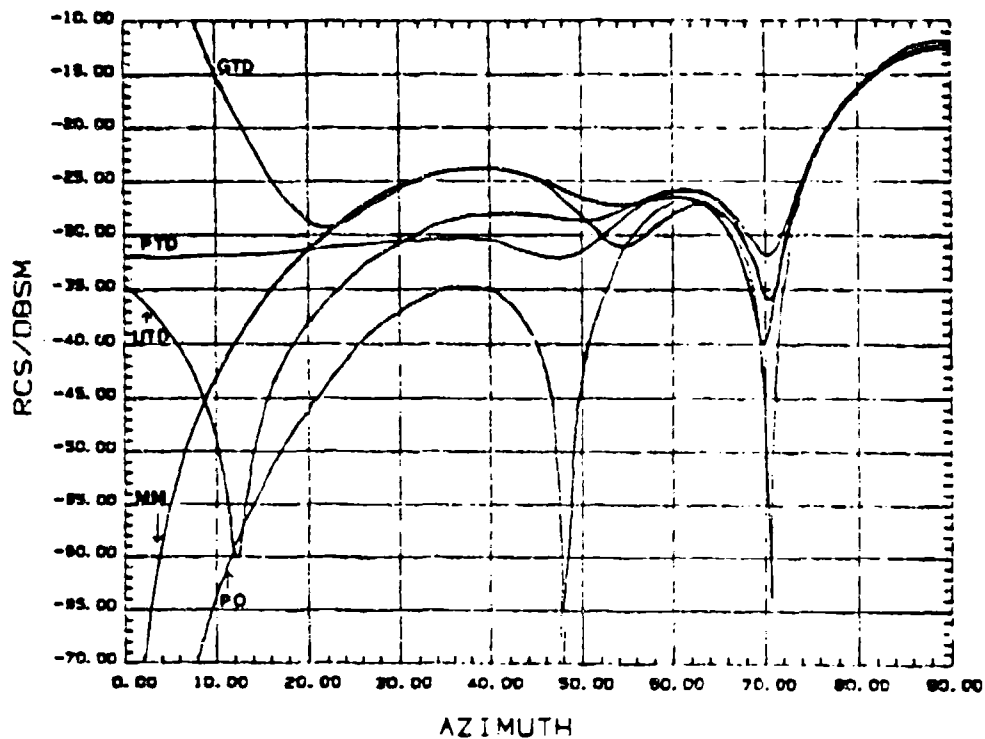Fig A.55.   RCS measurement of 6.5 wavelength (19.5 cm) plate
(H.P.)

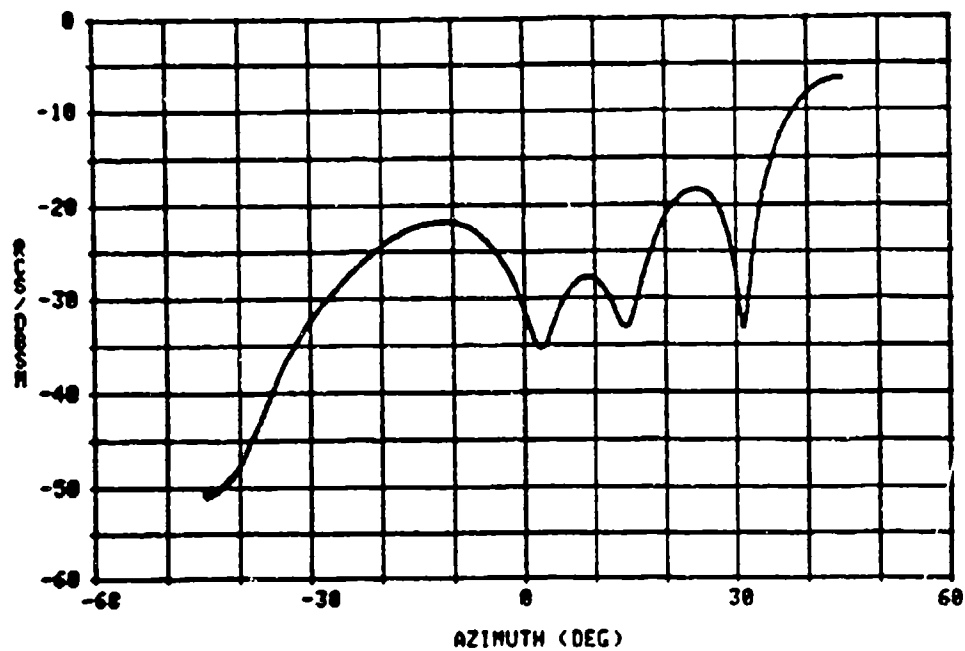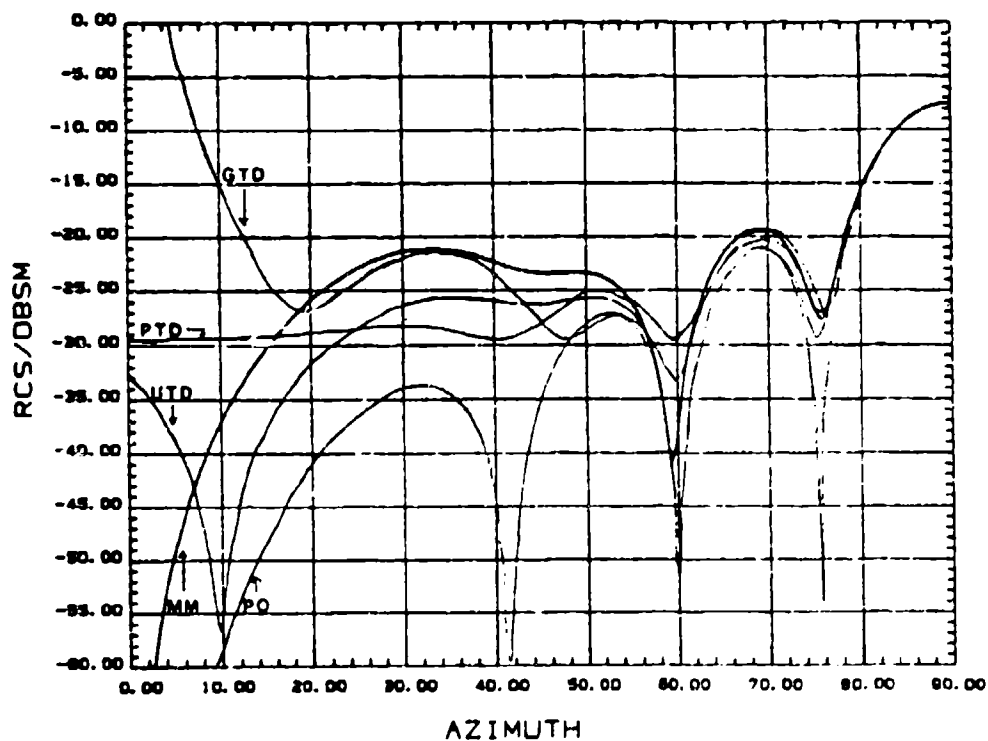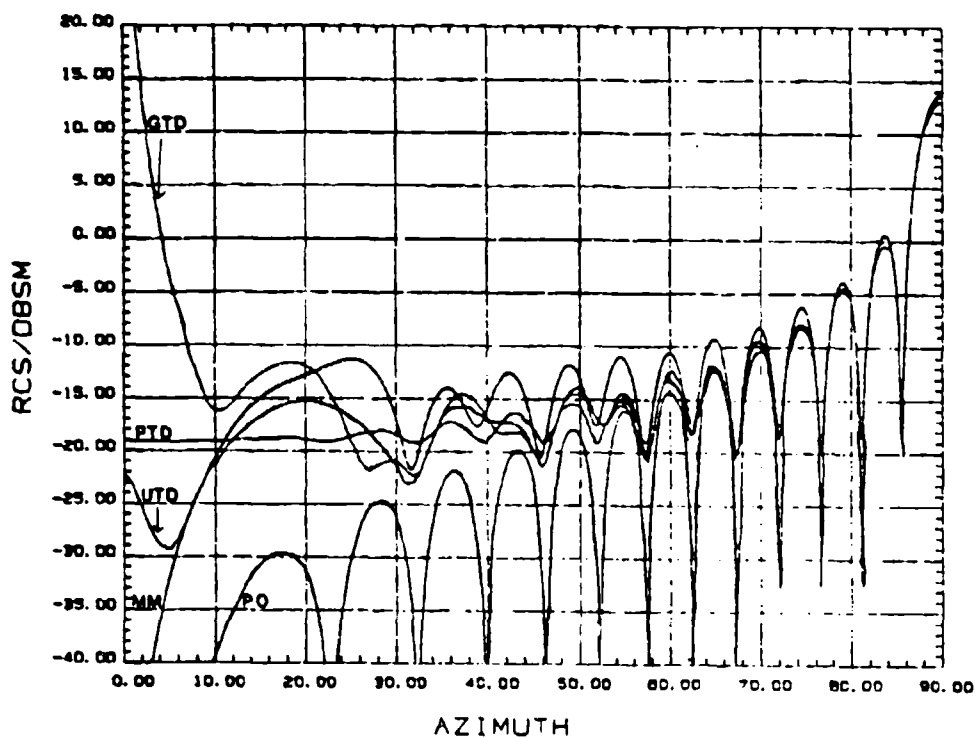Fig A.56.   Calculated RCS for 6.5 wavelength (19.5 cm) plate
(H.P.)

A-28

Appendix B.   Comparison of RCS Computational Methods

Table B.1

Comparison of RCS of Half Wavelength Plate

	Peak (dBsm)	CPU Time (sec)
PO	-31.5	1.8
PTD	-31.5	6.6
GTD	-31.0	100.1
UTD	-31.9	135.0
MM	-28.0	51.6
Measurement	-28.0	N/A

Table B.2

Comparison of RCS of 3/4 Wavelength Plate

	Peak (dBsm)	CPU Time (sec)
PO	-24.6	1.8
PTD	-24.6	6.6
GTD	-24.2	100.1
UTD	-24.2	135.0
MM	-23.9	76.9
Measurement	-24.0	N/A

Table B.3

Comparison of RCS of 1.0 Wavelength Plate

	Peak (dBsm)	CPU Time (sec)
PO	-19.5	1.8
PTD	-19.5	6.6
GTD	-19.3	100.1
UTD	-19.3	135.0
MM	-20.3	116.9
Measurement	-20.3	N/A

Table B.4

Comparison of RCS of 1.5 Wavelength Plate

	Peak (dBsm)	CPU Time (sec)
PO	-12.4	1.8
PTD	-12.4	6.6
GTD	-11.9	100.1
UTD	-12.4	135.0
MM	-12.5	163.4
Measurement	-12.5	N/A

Table B.5

Comparison of RCS of 2.0 Wavelength Plate

	Peak (dBsm)	CPU Time (sec)
PO	-7.4	1.8
PTD	-7.4	6.6
GTD	-7.4	100.1
UTD	-7.4	135.0
MM	-7.4	199.4
Measurement	-7.4	N/A

Table B.6

Comparison of RCS of 2.5 Wavelength Plate

	Peak (dBsm)	CPU Time (sec)
PO	-3.5	1.8
PTD	-3.5	6.6
GTD	-3.6	100.1
UTD	-3.5	135.0
MM	-3.9	263.7
Measurement	-3.7	N/A

Table B.7

Comparison of RCS of 3.0 Wavelength Plate

	Peak (dBsm)	CPU Time (sec)
PO	-0.4	1.8
PTD	-0.4	6.6
GTD	-0.4	100.1
UTD	-0.4	135.0
MM	-0.4	386.7
Measurement	-0.4	N/A

Table B.8

Comparison of RCS of 3.5 Wavelength Plate

	Peak (dBsm)	CPU Time (sec)
PO	2.3	1.8
PTD	2.3	6.6
GTD	2.3	100.1
UTD	2.3	135.0
MM	2.3	606.0
Measurement	2.3	N/A

Table B.9

Comparison of RCS of 4.0 Wavelength Plate

	Peak (dBsm)	CPU Time (sec)
PO	4.6	1.8
PTD	4.6	6.6
GTD	4.6	100.1
UTD	4.6	135.0
MM	4.6	829.3
Measurement	4.5	N/A

Table B.10

Comparison of RCS of 4.5 Wavelength Plate

	Peak (dBsm)	CPU Time (sec)
PO	6.7	1.8
PTD	6.7	6.6
GTD	6.7	100.1
UTD	6.7	135.0
MM	6.7	1646.9
Measurement	6.7	N/A

Table B.11

Comparison of RCS of 5.0 Wavelength Plate

	Peak (dBsm)	CPU Time (sec)
PO	8.5	1.8
PTD	8.5	6.6
GTD	8.5	100.1
UTD	8.5	135.0
MM	8.5	2219.9
Measurement	7.5	N/A

Table B.12

Comparison of RCS of 5.5 Wavelength Plate

	Peak (dBsm)	CPU Time (sec)
PO	10.2	1.8
PTD	10.2	6.6
GTD	10.2	100.1
UTD	10.2	135.0
MM	10.2	3002.4
Measurement	9.2	N/A

Table B.13

Comparison of RCS of 6.0 Wavelength Plate

	Peak (dBsm)	CPU Time (sec)
PO	11.7	1.8
PTD	11.7	6.6
GTD	11.7	100.1
UTD	11.7	135.0
MM	11.7	4018.6
Measurement	9.8	N/A

Table B.14

Comparison of RCS of 6.5 Wavelength Plate

	Peak (dBsm)	CPU Time (sec)
PO	13.1	1.8
PTD	13.1	6.6
GTD	13.1	100.1
UTD	13.1	135.0
MM	13.1	4032.6
Measurement	12.8	N/A

This program was developed from Ross' equations for the RCS of a rectangular flat plate (Ross, 1966:332). The program computes the GTD RCS versus angle of incidence for a square flat plate at 10 GHz. The size of the plate and the degree increments are specified in Logical Unit 5. The program is written in FORTRAN/77, and the output file is written in Logical Unit 6. A data file for plotting is provided in Logical Unit 1.

The Output is given in three columns: angle of incidence in degrees, vertical polarization RCS in dBsm, and horizontal polarization RCS in dBsm.

```
C       THIS PROGRAM IS BASED ON ROSS FORMULAS FOR
C       A RECTANGULAR FLAT PLATE
C         BY 2D LT ULICE J. MACIAS,  AFIT
C A=SIDE OF SQUARE FLAT PLATE
C     F=FREQUENCY OF PLATE= 10 GHz
        COMPLEX CMEAT,SD,DD,TD,DD1,DD2,DD3,DD4
        COMPLEX HMEAT,HSD,HDD,HTD,HDD1,HDD2,HDD3,HDD4
        OPEN(UNIT=1,FILE='GTDPLOT.DAT',STATUS='NEW',
        FORM='UNFORMATTED')
        READ(5,*) A
C***    F= FREQUENCY OF OPERATION
        F=10E9
        W=3E8/F
        PI=3.14159265
        K=2*PI/W
        SQ=SQRT(2*PI)
        HRT=SQ*(K*A)**0.5
        RT=SQ*(K*A)**1.5
C***    RI=INCREMENTS OF THETA(THE)
        READ(5,*)RI
        DO 100 THETA=0,90,RI
        II=THETA
        THE=THETA*PI/180-PI/2
        IF(THE.EQ.0)THE=0.005
        IF(THE.EQ.-PI*.5)THE=-(PI/2-.001)
        RTA=K*A*SIN(THE)
```

```fortran
        HDD11=K*A+PI/4
        DD11=K*A-PI/4
        HDD1=4*CEXP(CMPLX(0.,HDD11))/HRT
        DD1=CEXP(CMPLX(0.,DD11))/RT
        HDD2=HDD1/2
        DD2=DD1/4
        HDD3=(CEXP(CMPLX(0.,-RTA))/(1-SIN(THE)))

DD3=(1+SIN(THE))/((1-SIN(THE))**2)*CEXP(CMPLX(0.,-RTA))
        HDD4=(CEXP(CMPLX(0.,RTA))/(1+SIN(THE)))

DD4=(1-SIN(THE))/((1+SIN(THE))**2)*CEXP(CMPLX(0.,RTA))
        HDD=HDD1*(1/COS(THE)-HDD2*(HDD3+HDD4))
        DD=DD1*(1/COS(THE)+DD2*(DD3+DD4))
        HTD=(1-CEXP(CMPLX(0.,2*HDD11))/(2*PI*K*A))**(-1)
        TD=(1-(CEXP(CMPLX(0.,2*DD11))/(8*PI*(K*A)**3)))**(-1)
        RSD=COS(RTA)
        CSD=-SIN(RTA)/SIN(THE)
        HSD=CMPLX(RSD,-CSD)
        SD=CMPLX(RSD,CSD)
        HMEAT=HSD-HDD*HTD
        CMEAT=SD-DD*TD
        HREAT=CABS(HMEAT)
        RMEAT=CABS(CMEAT)
        SIH=1/PI*((HREAT*A)**2)
        SIV=1/PI*((RMEAT*A)**2)
        SIHDB=10*ALOG10(SIH)
        SIVDB=10*ALOG10(SIV)
C***    WRITE AZIMUTH ANGLE, V.P. AND H.P. RCS
        WRITE(6,1)THETA,SIVDB,SIHDB
1       FORMAT(1X,F7.2,F7.2,F7.2)
C****   WRITE DATA FOR PLOTS
        WRITE(1)II,THETA,SIVDB,SIHDB
100     CONTINUE
        STOP
        END
```

Bibliography

Blacksmith, P. and others. "Introduction to Radar Cross Section Measurements", Proceedings of the IEEE, 53: 901-920 (August 1985).

Johnson, Capt Thomas W. Introduction to Radar Cross Section for Non-Electrical Engineers Class Notes, Department of Electrical Engineering, Air Force Institute of Technology (AU), Wright-Patterson AFB OH, June 1982.

Keller, Joseph B. "Geometrical Theory of Diffraction", Journal of the Optical Society of America, 52:116-130 (February 1962).

Knott, Eugene F. and others. Radar Cross Section Dedham: Artech House, Inc., 1985.

------. "A Progression of High-Frequency RCS Prediction Techniques", Proceedings of the IEEE, 73: 252-264 (February 1985).

Kouyoumjian, R. G. Lecture materials on Short Course on the Modern Geometrical Theory of Diffraction. ElectroScience Laboratory, Ohio State University, OH, September 1985.

Kouyoumjian, R. G. and P. H. Pathak. "The Dyadic Diffraction Coefficient for a Curved Edge." Technical Report NASA CR-2401, Contract No. NGR 36-008-144 with National Aeronautics and Space Administration. Ohio State University, OH, June 1974.

------. "Asymptotic High-Frequency Methods", Proceedings of the IEEE, 53: 864-876 (August 1965).

Marhefka, R. J. "Computer Code for Radar Cross Section of Convex Plate and Cone Frustrum Structure: Final Report." Ohio State University, OH, December 1981.

Newman, E. H. "A User's Manual for Electromagnetic Surface Patch (ESP) Code: Version II - Polygonal Plates

and Wires." Technical Report 717067-4, Contract
No. N00014-78-C-0049 with Office of Naval Research. Ohio
State University, OH, May 1985.

Peters, Leon and W. D. Burnside. "Equivalent Currents with
application to Finite Edges Caustics and corners", Class
lecture material on the Modern Theory of Geometrical
Diffraction, vol 1. Electroscience Laboratory, Ohio
State University, OH, September, 1985.

Ross, R. A. "Radar Cross Section of Rectangular Flat Plates
as a Function of Aspect Angle", IEEE Transactions on
Antennas and Propagation, AP-14: 329-335 (May 1966).

Ruck, George T. and others. Radar Cross Section
Handbook, Vol. 1 & 2. New York: Plenum Press, 1970.

Simpson, 1Lt Robert G. Comparison of Background
Characteristics of an RCS Measurement Range Using a
CW-Nulling Method and Pulse-Gated Method. MS thesis.
School of Engineering, Air Force Institute of Technology
(AU), Wright-Patterson AFB OH, Dec 1985.

Skinner, 1Lt Paul. A Survey of Several Classical Methods
for Prediction of Electromagnetic Scattering,
AFWAL/AAWP-3, Wright-Patterson AFB OH, December 1985.

Skolnik, Merrill I. Introduction to Radar Systems.
New York: McGraw-Hill Book Co., 1980.

Stutzman, Warren L. and Gary A. Thiele. Antenna Theory
and Design. New York: John Wiley & Sons, 1981.

Wilton, D. R. and others. "Electromagnetic Scattering by
Surfaces of Arbitrary Shape",Lectures on Computational
Methods in Electromagnetics. St. Cloud: The SCEEE Press,
1981.

Young, Hugh D. Fundamentals of Waves, Optics, and
Modern Physics. New York: McGraw-Hill Book Company,
1976.

Ulice J. Macias was born on July 25, 1962 in Glen Cove, New York. He graduated from Jose C. Alegria High School in Dorado, Puerto Rico, in 1980. He then attended the University of Puerto Rico at Mayaguez in a five year Electrical Engineering program. In 1981, he was awarded a 4-year ROTC scholarship. He graduated Magna Cum Laude in May, 1985 receiving the degree of Bachelor of Science in Electrical Engineering. At that time he received a commission in the United States Air Force through the ROTC program.

After graduation, his first active duty assignment was to the Air Force Institute of Technology in May, 1985.

        Permanent address: Ruta Rural Guarisco #4,
                            Espinosa, Dorado
                            Puerto Rico   00646

A177718

REPORT DOCUMENTATION PAGE		Form Approved OMB No. 0704-0188

1a. REPORT SECURITY CLASSIFICATION UNCLASSIFIED	1b. RESTRICTIVE MARKINGS

2a. SECURITY CLASSIFICATION AUTHORITY	3. DISTRIBUTION/AVAILABILITY OF REPORT
2b. DECLASSIFICATION/DOWNGRADING SCHEDULE	Approved for public release; distribution unlimited.

4. PERFORMING ORGANIZATION REPORT NUMBER(S) AFIT/GE/ENG/86D-13	5. MONITORING ORGANIZATION REPORT NUMBER(S)

6a. NAME OF PERFORMING ORGANIZATION School of Engineering	6b. OFFICE SYMBOL (If applicable) AFIT/ENG	7a. NAME OF MONITORING ORGANIZATION

6c. ADDRESS (City, State, and ZIP Code) Air Force Institute of Technology Wright-Patterson AFB, Ohio 45433-6583	7b. ADDRESS (City, State, and ZIP Code)

8a. NAME OF FUNDING/SPONSORING ORGANIZATION Avionics Laboratory	8b. OFFICE SYMBOL (If applicable) AFWAL/AAWP-3	9. PROCUREMENT INSTRUMENT IDENTIFICATION NUMBER

8c. ADDRESS (City, State, and ZIP Code) Air Force Wright Aeronautical Labs. Wright-Patterson AFB, Ohio 45433-6523	10. SOURCE OF FUNDING NUMBERS			
	PROGRAM ELEMENT NO. 62204F	PROJECT NO. 7633	TASK NO. 13	WORK UNIT ACCESSION NO. 09

11. TITLE (Include Security Classification)

See Box 19

12. PERSONAL AUTHOR(S)

Alice J. Macias, B.S.E.E., 2 Lt, USAF

13a. TYPE OF REPORT MS Thesis	13b. TIME COVERED FROM_____ TO_____	14. DATE OF REPORT (Year, Month, Day) 1986 December	15. PAGE COUNT 119

16. SUPPLEMENTARY NOTATION

17. COSATI CODES			18. SUBJECT TERMS (Continue on reverse if necessary and identify by block number)
FIELD	GROUP	SUB-GROUP	Radar Cross Section (RCS), RCS Prediction Methods, Physical Optics, Moment Method, Physical Theory of Diffraction. (see back)
17	03		

19. ABSTRACT (Continue on reverse if necessary and identify by block number)

Title: A COMPARISON OF COMPUTATIONAL ELECTROMAGNETIC METHODS
          FOR THE PREDICTION OF RADAR CROSS SECTION

Thesis Chairman: Andrew J. Terzuoli
                    Assistant Professor of Electrical Engineering

Approved for public release: IAW AFR 190-1/.
LYNN E. WOLAVER   8 Dec 86
Dean for Research and Professional Development
Air Force Institute of Technology (AFCT)
Wright-Patterson AFB OH 45433

20. DISTRIBUTION/AVAILABILITY OF ABSTRACT ☒ UNCLASSIFIED/UNLIMITED ☐ SAME AS RPT. ☐ DTIC USERS	21. ABSTRACT SECURITY CLASSIFICATION UNCLASSIFIED	
22a. NAME OF RESPONSIBLE INDIVIDUAL Andrew J. Terzuoli	22b. TELEPHONE (Include Area Code) 513-255-6913	22c. OFFICE SYMBOL AFIT/ENG

DD Form 1473, JUN 86   Previous editions are obsolete.   SECURITY CLASSIFICATION OF THIS PAGE

18. Continued
Geometrical Theory of Diffraction, Uniform Theory of Diffraction

19. Continued
The effectiveness of the various Radar Cross Section (RCS) prediction techniques was investigated. The RCS of square flat plates was analyzed using the Physical Optics approximation, the Physical Theory of Diffraction, the Geometrical Theory of Diffraction, the Uniform Theory of Diffraction, and the Moment Method or Method of Moments. The RCS predicted by the computational methods was compared to measurements performed in an anechoic RCS measurement chamber. Also, the five computational methods were compared to each other in terms of plate size (in wavelengths), computer (CPU) time required for computation, and angular regions of computational integrity.

It was found that although the Moment Method is the most accurate RCS prediction method, it takes too much CPU time for large plates (over 2.5 wavelengths). The Uniform Theory of Diffraction, on the other hand, is accurate for large plates and takes less CPU time than the Moment Method. The Geometric Theory of Diffraction is also accurate but fails near the edge of the plate. Finally, the Physical Theory of Diffraction and the Physical Optics approximation are relatively inaccurate.